Department of Aerospace Engineering
University of Maryland
College Park, Maryland 20742

CENTER FOR ROTORCRAFT EDUCATION AND RESEARCH

Progress Report on Army Research Office
Contract No. DAAL03-88-C-0002 and
DAAHO4-94-G-0074
"Rotorcraft Center of Excellence"

Final Report

DISTRIBUTION STATEMENT A
Approved for public release
Distribution Unlimited

REPORT DOCUMENTATION PAGE

Form Approved
OMB NO. 0704-0188

Public reporting burden for this collection of information is estimated to average 1 hour per response, including the time for reviewing instructions, searching existing data sources, gathering and maintaining the data needed, and completing and reviewing the collection of information. Send comment regarding this burden estimates or any other aspect of this collection of information, including suggestions for reducing this burden, to Washington Headquarters Services, Directorate for information Operations and Reports, 1215 Jefferson Davis Highway, Suite 1204, Arlington, VA 22202-4302, and to the Office of Management and Budget, Paperwork Reduction Project (0704-0188), Washington, DC 20503.

1. AGENCY USE ONLY *(Leave blank)*	2. REPORT DATE	3. REPORT TYPE AND DATES COVERED
	September 15, 1997	Final Report 1 Jul 94 - 10 Jul 96

4. TITLE AND SUBTITLE
Center for Rotorcraft Education and Research
The University of Maryland

5. FUNDING NUMBERS
DAAH04-94-G-0074

6. AUTHOR(S)
I. Chopra, R. Celi, J.G. Leishman, A.J. Vizzini
J. Baeder and N.M. Wereley

7. PERFORMING ORGANIZATION NAMES(S) AND ADDRESS(ES)
University of Maryland
Department of Aerospace Engineering
College Park, MD 20742

8. PERFORMING ORGANIZATION REPORT NUMBER

9. SPONSORING / MONITORING AGENCY NAME(S) AND ADDRESS(ES)
U.S. Army Research Office
P.O. Box 12211
Research Triangle Park, NC 27709-2211

10. SPONSORING / MONITORING AGENCY REPORT NUMBER

11. SUPPLEMENTARY NOTES
The views, opinions and/or findings contained in this report are those of the author(s) and should not be construed as an official Department of the Army position, policy or decision, unless so designated by other documentation.

12a. DISTRIBUTION / AVAILABILITY STATEMENT
Approved for public release; distribution unlimited.

12 b. DISTRIBUTION CODE

13. ABSTRACT *(Maximum 200 words)*
The status of a number of rotorcraft research tasks supported under the Army Research Office "Center of Excellence" program is reported herein. The tasks are grouped under the disciplinary headings of dynamics, flight dynamics, aerodynamics, composite structures, and computational fluid dynamics. For each task an attempt is made to describe the objective of the work, the approach being taken, the status of the work in terms of recent results, problems or changes in approach or objective, and pertinent abstracts of journal articles or conference papers coming out of the task.

14. SUBJECT TERMS

15. NUMBER IF PAGES

16. PRICE CODE

17. SECURITY CLASSIFICATION OR REPORT	18. SECURITY CLASSIFICATION OF THIS PAGE	19. SECURITY CLASSIFICATION OF ABSTRACT	20. LIMITATION OF ABSTRACT
UNCLASSIFIED	UNCLASSIFIED	UNCLASSIFIED	UL

CENTER FOR ROTORCRAFT EDUCATION AND RESEARCH

Progress Report on Army Research Office
Contract No. DAAL03-88-C-0002 and
DAAHO4-94-G-0074
"Rotorcraft Center of Excellence"

Final Report

DTIC QUALITY INSPECTED 2

19971203 063

Center for Rotorcraft Education and Research

Progress Report on Army Research Office
Contract No. DAAL03-88-C-0002 and
DAAHO4-94-G-0074
"Rotorcraft Center of Excellence"

Final Report

The status of a number of rotorcraft research tasks supported under the Army Research Office "Center of Excellence" program is reported herein. Dr. Thomas Doligalski is the Technical Monitor for the project.

The tasks are grouped under the disciplinary headings of dynamics, flight dynamics, aerodynamics, composite structures, and computational fluid dynamics. For each task, an attempt is made to describe the objective of the work, the approach being taken, the status of the work in terms of recent results, problems or changes in approach or objective, and pertinent abstracts of journal articles or conference papers coming out of the task. Inquiries are invited on any aspect of the report, and may be addressed to the undersigned or to the disciplinary group leaders as follows:

Dynamics	Inderjit Chopra	tel (301) 405-1122
Flight Dynamics	Roberto Celi	tel (301) 405-1132
Aerodynamics	J. Gordon Leishman	tel (301) 405-1126
Composite Structures	Anthony J. Vizzini	tel (301) 405-1123
Computational Fluid Dynamics	James Baeder	tel (301) 405-1107

Inderjit Chopra, Director
Alfred Gessow Rotorcraft Center
(301) 405-1122

FACULTY

Inderjit Chopra — Professor and Director of CRER
James Baeder — Assistant Professor
Roberto Celi — Associate Professor
Alfred Gessow — Professor Emeritus
J. Gordon Leishman — Associate Professor
Anthony J. Vizzini — Associate Professor
Norman Wereley — Assistant Professor

ASSISTANT RESEARCH SCIENTIST

Ramesh Chandra

RESEARCH ASSOCIATES

Ashish Bagai
Ranjan Ganguli

RESEARCH ENGINEERS

William R. Pogue, III
Mark O'Connor

DEGREES AWARDED FOR PERIOD
Final Report

Ph.D.

Napei Bi, Ph.D., 6/91 -- Advanced Technllogies Inc.
Ki C. Kim, Ph.D., 6/91 -- U.S. Army - Aberdeen
J.W. Wang, Ph.D. 11/91 -- Sikorsky Aircraft
Gilbert Crowse, Ph.D., 6/92 -- SSN Systems & Technologies
E.C. Smith, Ph.D. 8/92 -- Pennsylvania State University
M.W. Nixon, Ph.D. 12/93 -- U.S. Army, NASA Langley Research Center
Anne Spence, Ph.D., 6/94 -- Lecturer, University of Maryland
R. Ganguli, Ph.D. 8/94 -- GE Engine
David Fleming, Ph.D. 8/95 -- Florida Institute of Technology
F. Gandhi, Ph.D. 9/95 -- Pennsylvania State University
Ashish Bagai, Ph.D., 9/95 -- Boeing Helicopter
V. Srinivas, Ph.D. 12/95 -- Ford Motor Company
Vineet Sahasrabudhe, Ph.D., 6/96 -- System Technology, Inc.
Stephen Turnour, Ph.D., 6/96 -- Australian Aircraft Company
P.C. Chen, Ph.D. 9/96 -- Systems Planning and Analysis, Inc.
A.L. Tracy, Ph.D. 9/96 -- Pratt & Whitney
J.H. Milgram, Ph.D. 10/96 -- Research Associate, University of Maryland
Sunghwan Hwang, Ph.D., 2/97 -- Agency for Defense Development Korea
Christopher Jones, Ph.D., 3/97 -- Sikorsky Aircraft

M.S. (Thesis)

R.M. Barrett, M.S. 5/90 -- Auburn University
Greg Agnes, M.S., 6/91, U.S. Air Force
Anthony Botting, M.S., 6/91 -- Structured Research & Analysis Inc.
Terrence Ghee, M.S., 6/91 -- Navy Patuxent River
Carl Ockier, M.S., 6/91 -- DLR Germany
Joe Tyler, M.S. 5/91 -- NASA Goddard
Agnes Wozniak, M.S., 6/91 -- Boeing
Bernard Van der Wall, M.S., 6/91 -- DLR
Steve Ingle, M.S., 6/92 -- Boeing Helicopters
P.Y. Ouillet, M.S. 6/92 -- Ministry of Defense, France
P. Picavet, M.S. 9/92 -- France
Mark Daghir, M.S., 6/93 -- Boeing Helicopter
Joseph Ruddy, MS 5/95 -- Dyncorp
Ajay Divekar, M.S., 6/95 -- Aerostructures
Keith Robinson, M.S., 6/95 -- U.S. Army Pentagon
Stephen Teager, M.S., 6/95 -- FAA Headquarters
B.T. Spencer, M.S. 8/95 -- US Air Force
Megan McCluer, M.S., 9/95 -- NASA Ames

Vasudev Parameswaran, M.S., 9/95 -- Ph.D.
Burtis Spencer, M.S., 9/95 -- US Air Force
Andy Baker, M.S., 12/95 -- Navy Patuxent River, Test Pilot School
Scott Kuczma, MS 12/95 -- Applied Physics Laboratory
Jennifer Knack, MS 5/96 -- CSC, Inc.
Alan Coyne, M.S., 5/97 -- Raytheon

M.S. (Without Thesis)

C. Brunner, M.S. (1990) -- Navy Patuxent River
E.C. Smith, M.S. 1990 -- Ph.D.
S. Dirlik, M.S. 6/90 -- David Taylor R&D Center
N. Kimata, M.S. 1990 -- U.S. Army
R. Ganguli, M.S. 1991 -- Ph.D.
A. Tracy, M.S. 1991 -- Ph.D.
D. Shaffer, M.S., 1991 -- US Army
W.P. Chan, M.S. 1991 -- Ph.D.
David Arterburn, M.S., 6/92 -- US Army, Ft. Rucker
Ashish Bagai, M.S., 6/92 -- Ph.D.
Robert Bupp, M.S., 6/92 -- Ph.D.
Vineet Saharabudhe, M.S., 6/92 -- Ph.D.
J. Milgram, M.S. 1992 - Ph.D.
V. Srinivasan, M.S. 1992 -- Ph.D.
J. Smith, M.S. 1992 -- Ph.D.
Peter Chen, M.S. 1993 -- Ph.D.
David Platz, M.S., 6/93 -- Bell Helicopter
S. Vellaichamy, M.S. 1993 -- West Virginia University
Chris Niggemeier, M.S. 1993 -- Learjet Aircraft
Andy Bernhard, M.S. 1994 -- Ph.D.
Mike Bothwell, M.S. 1994 -- Bell Helicopter Company
Curtis Walz, M.S. 1994 -- Boeing Helicopter Company
Jeanette Epps, M.S. 1994 -- Ph.D.
Lazar Alon, M.S. 1995 -- Israel Air Force
Oren Ben-Zeev, M.s. 1995 -- NAVAIR
Luc Renoil, M.S. 1995 -- France
Gopal Kamath, M.S., 6/95 -- Ph.D.
Erwin Moedersheim, M.S., 6/95 -- IBM, Paris
Ih-Cheng Shih, M.S., 6/95
Clifford Smith, M.S., 12/95 -- Ph.D.
Melanie Hurt, M.S., 6/96 -- Bell Helicopter
Sudha Veeramani, M.S., 3/97 -- Cessna Aircraft
Subhobroto Nath, M.S., 8/97 -- American Network Systems Inc.
Brian Harkless, M.S., 8/97 -- Gascon Secondary School

AERODYNAMICS

AERODYNAMICS

J. Gordon Leishman

Task 1

1.1 Investigation of Rotor/Body/Lifting Surface Interactional Aerodynamics

The objectives of this work were to experimentally investigate the highly significant aerodynamic interference effects that exist between a helicopter rotor and its airframe. Because of design trends toward increasing rotor disk loadings and decreasing clearances between the main rotor and the fuselage, interactional aerodynamic effects on helicopters have been identified as an area where a limited and insufficient understanding exists. Work on this problem at Maryland has been specifically focused toward an improved understanding rotor/empennage/tailplane (lifting surface) interactions.

The wake of a helicopter main rotor is by nature an energetic, highly unsteady flow regime. As the wake passes near a lifting surface, such as a horizontal tail plane, a mutual interaction takes place which induces high unsteady airloads on the surface and also distorts the wake. The frequencies of excitation cover a wide range, often falling near the natural frequencies of the helicopter empennage. These variations in the loading on the tail and the resulting changes in pitching moment also interfere with the handling qualities of the aircraft, and can even cause loss of control. Unfortunately, because this problem is poorly understood, it is often difficult to design the empennage assembly. For example, after the initial prototypes of the AH-64 Apache had been built, the placement of the horizontal tail surface was dramatically altered twice due to unacceptable handling qualities.

The interactional aerodynamics between a helicopter main rotor and a horizontal tailplane have been studied in detail during tests in the Glenn L. Martin Wind Tunnel. The model used in the experiment consisted of a 4-blade, fully articulated rotor (65 inches in diameter) and a fuselage with an internally supported horizontal lifting surface in T-tail configuration (see figure). The basic rotor/fuselage configuration is an AGARD test case for CFD validation. The tail used for the present tests was a T-tail configuration similar to the RAH-66 Comanche. The horizontal tail had a chord of 8 inches and an aspect ratio of 2.5. The vertical position of the tail was adjustable by varying the length of the vertical support and fairing.

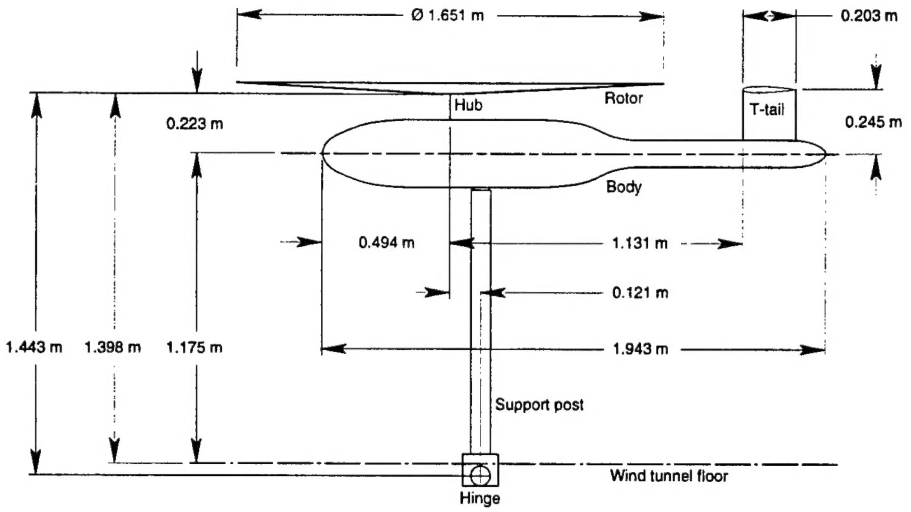

Figure showing experimental set-up for rotor/tail interaction studies

The horizontal stabilizer was instrumented to measure time-dependent pressures using 16 pressure transducers located at four chordwise positions on the upper and lower surface of the tail. These measurements were made using a completely updated and refined data acquisition and analysis system using LabVIEW software specifically developed for these experiments. The system interfaces a Macintosh Quadra 950 computer to a CAMAC crate, and is capable of simultaneously sampling up to 64 time-varying analog signals at up to 150kHz per channel. Time-averaged pressures were also measured at 32 locations along the leading and trailing edges of the tail model. The rotor wake boundary relative to the empennage was documented using wide-field shadowgraphy, and converted into quantitative measurements of wake location as functions of rotor azimuth position and flight condition. An example of the unsteady measurements are shown below.

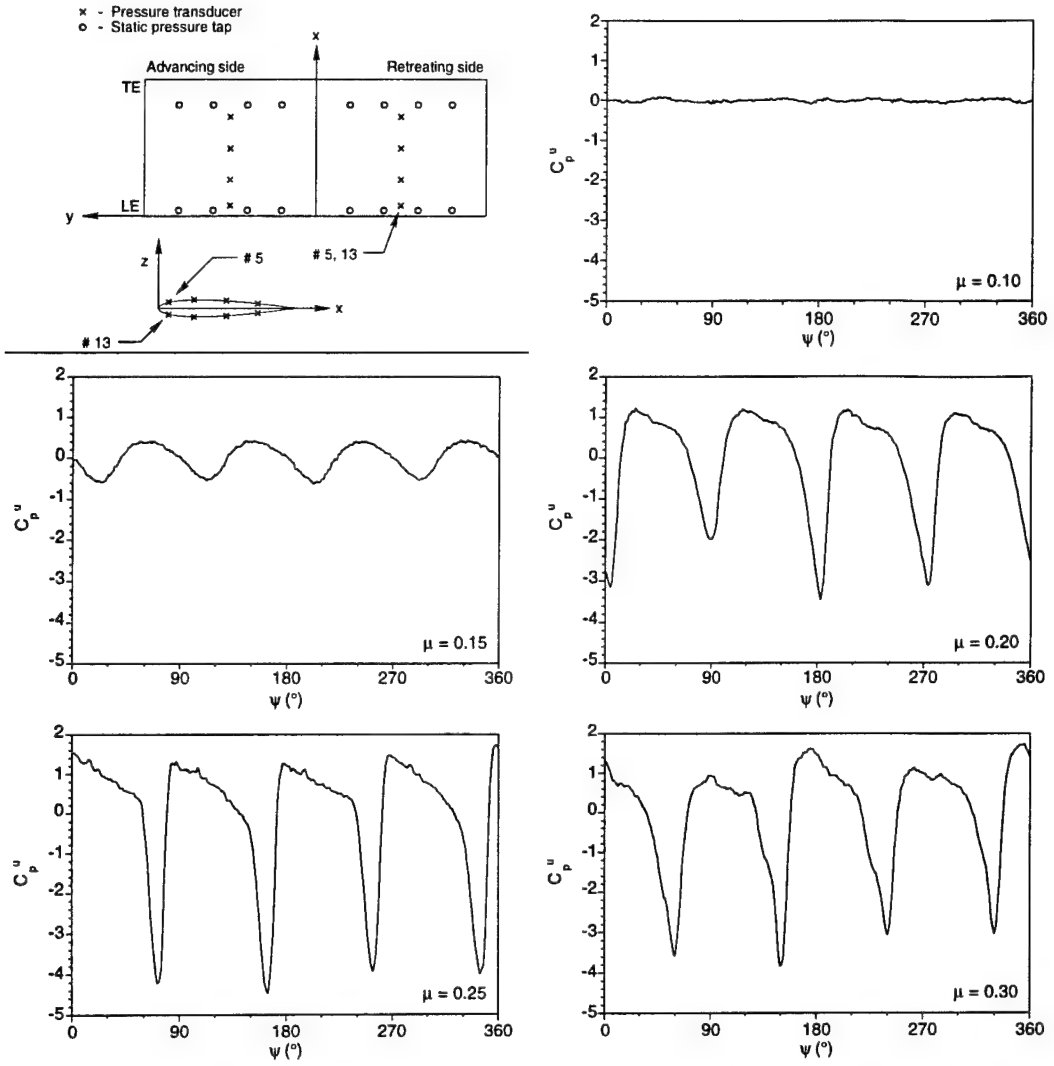

Figure 1: typical unsteady pressure responses on the tail

Several papers on this work have been prepared:

Leishman, J. G., Nai-pei Bi, "Experimental Data on the Aerodynamic Interactions Between a Helicopter Rotor and an Airframe," AGARD-AR-303 - A Selection of Experimental Test Cases for the Validation of CFD Codes, Vol. 1, August 1994.

Modersheim, E., Leishman, J.G., "Investigation of Aerodynamic Interactions Between a Rotor and a T-Tail Empennage," Proceedings of the 2nd International Aeromechanics Specialists' Conference, Bridgeport, CT, Oct. 11-13, 1995.

Leishman, J.G., Modersheim, E., "Experimental Investigation of Rotor/Tail Interactions," Proceedings of the 22nd European Rotorcraft Forum, Brighton, U.K., Sept. 17-19, 1996.

Modersheim, E., Leishman, J.G., "Investigation of Aerodynamic Interactions Between a Rotor and a T-Tail Empennage," Accepted for publication in the Journal of the American Helicopter Society. To appear in 1997.

1.2 Experimental and Numerical Rotor Wake Studies

Considerable progress has been made on this task, particularly in regard to the computational aspects of rotor wake modeling and validation with experimental measurements of wake geometries, and induced velocity fields. Experimental work has centered around the use of a 3-dimensional laser Doppler velocimetry system.

On the numerical side, the development of a pseudo-implicit predictor-corrector relaxation algorithm with five point central differencing in space has been completed. The scheme is used to predict the locations of the wake trailed by the rotor blades in hover and forward flight, and to predict the rotor induced velocity field. The free-wake problem is governed by the vorticity transport equation, which in essence states that vorticity trailed behind the rotor blades is convected downstream of the rotor at its local velocity. For the rotor problem, this may be written as

$$\frac{\partial \bar{r}(\psi,\zeta)}{\partial \psi} + \frac{\partial \bar{r}(\psi,\zeta)}{\partial \zeta} = \bar{V}\left(\bar{r}(\psi,\zeta)\right)$$

where from the figure below it is clear that the vector **r** is the position vector of an element on a tip vortex filament trailed from a rotor blade at azimuth ψ. The variable ζ represents the age of this element relative to the blade from which it was trailed. The term on the right-hand-side represents the local velocity field under which the vortex filaments are convected through the rotor flow field. It is this term that essentially governs the rotor free-wake problem. For the special case that **V** is uniform or constant throughout the flow field, the problem degenerates into a trivial one, and the equation can be solved analytically for the exact solution. In general, however, the local velocity is not uniform because it contains the self- and mutually-induced velocities due to all the vortex filaments in the rotor wake. This results in a highly non-linear function equation which cannot be solved analytically, and numerical means must be adopted to determine a solution.

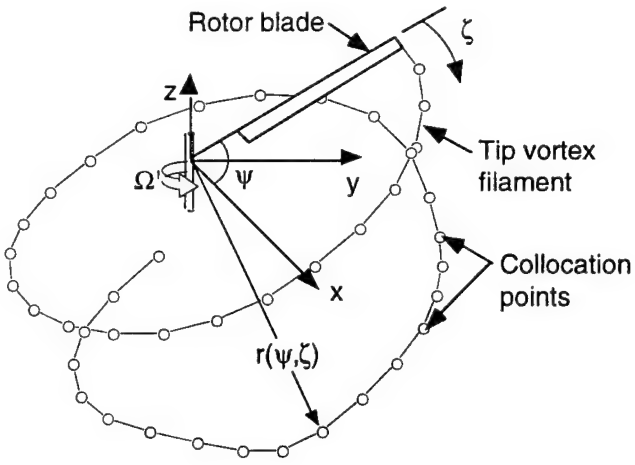

Fig 2: The free-wake problem: Definition of terms

To better understand the problem, the velocity term can be decomposed into two components, namely into the sum of a uniform free-stream velocity and an induced contribution form the interacting vortices trailed behind the blades

$$\bar{V}\left(\bar{r}(\psi,\zeta)\right) = \frac{1}{\Omega}\left(\bar{V}_{\infty} + \bar{V}_{induced}\left(\bar{r}(\psi,\zeta)\right)\right)$$

where the induced velocity component is given by the Biot-Savart law as

$$\bar{V}_{induced}\left(\bar{r}(\psi,\zeta),\bar{r}\left(\psi_j,\zeta\right)\right) = \frac{h^2}{4\pi\sqrt{r_c^4 + h^4}} \int \frac{\Gamma\left(\psi_j,\zeta\right)\partial\zeta_j \times \left(\bar{r}(\psi,\zeta) - \bar{r}\left(\psi_j,\zeta\right)\right)}{\left|\bar{r}(\psi,\zeta) - \bar{r}\left(\psi_j,\zeta\right)\right|^3}$$

Two important modifications have been incorporated into the original Biot-Savart law in the above equation. First, a vortex model with a finite core model has been incorporated to avoid the singularity that results from the potential vortex assumption in the original Biot-Savart law. This is represented by the term outside the integral. Note that the vortex model is different from the model used by Scully, and more faithfully represents measured rotor tip vortex tangential velocity profiles obtained from the experimental side of the present work. Second, the vortex core is allowed to grow with age (time) in a manner derived from the solution of the Lamb-Oseen vortex, but with the inclusion of a turbulent viscosity coefficient as given by

$$r_c \propto \sqrt{\nu\delta\, t} \quad \text{where} \quad \delta = f\left(\frac{\Gamma}{\nu}\right)$$

Note that ν is the kinematic viscosity of the fluid, and δ represents the turbulent viscosity coefficient, which can be determined either empirically or by numerical experimentation which involves comparing predicted wake geometries and inflow data with experimental data. The vortex model thus obtained physically behaves in a manner very similar to that trailed from rotor blades, which have been measured by several researchers. Note that no tuning is used to manipulate the vortex model. Instead, by writing the turbulent viscosity coefficient as a function of the vortex Reynolds number, a direct solution for the turbulence coefficient is obtained, irrespective of the operating conditions or rotor geometry. The same model has been used for the twin rotor analyses as well.

Clearly, the induced velocity terms are highly non-uniform. As a result, the vorticity transport equation, which is a non-linear first order partial differential equation (PDE), cannot be solved analytically, and numerical means must be adopted. This is accomplished by discretizing the problem and transforming the governing PDE into a finite difference equation (FDE) by using finite differences to approximate the partial derivatives in the governing PDE's. In the present methodology, a five point central differencing scheme has been adopted, which allows the blade azimuthal location, ψ and the vortex age, ζ to be decoupled. Moreover, the scheme thus developed is at least second order accurate. For equal discretization resolutions in the ψ and ζ directions, discretization errors tend to zero. The only errors incurred in the scheme therefore are due to the non-linear induced velocity terms.

To numerically integrate the equations, a relaxation approach has been adopted. This is done through the introduction of an 'n' index. Although traditionally, explicit type methods have been used, in the present work some implicitness has been introduced into the scheme by using the most recently available information to update collocation point position vectors at each iteration. In other words, some current iteration information is also used at each iteration step. The resulting equation can be written in the following pseudo-implicit form

$$r^n_{j,k} = r^n_{j-1,k-1} + \left(r^n_{j,k-1} - r^n_{j-1,k}\right)\left(\frac{\Delta\psi - \Delta\zeta}{\Delta\psi + \Delta\zeta}\right) + \frac{2}{\Omega}\left(\frac{\Delta\psi\Delta\zeta}{\Delta\psi + \Delta\zeta}\right)\bar{V}^{n-1}_{j-\frac{1}{2},k-\frac{1}{2}}$$

Note that the introduction of implicitness results in very quick propagation of information through the computational domain as compared to a purely explicit method. Furthermore, because the velocity terms on the right are determined from the previous (n-1)th iteration, the scheme is not purely implicit, and therefore does not require computationally intensive matrix inversions at each iteration. Moreover, it should also be pointed out that for constant source terms and equal ψ and ζ discretizations ($\Delta\psi = \Delta\zeta$), the present scheme becomes infinitely accurate and provides the exact solution to the rigid wake problem. Enhanced numerical stability

between iterations is obtained by implementing the scheme as a two step predictor-corrector sequence.

Sample wake geometry predictions for a single isolated rotor in hover and low speed forward flight are presented in isometric view below. In hover, the wake contracts radially inwards and convects vertically below the rotor disk. With increasing advance ratio, the wake skews back and at an advance ratio of 0.1 the wake begins to roll-up along the lateral edges, downstream of the rotor. Note that there are no unusual perturbations in the wake structure, indicating that the geometries have indeed properly converged. These are particularly challenging flight conditions where other free-wake methodologies have often failed to provide meaningful results.

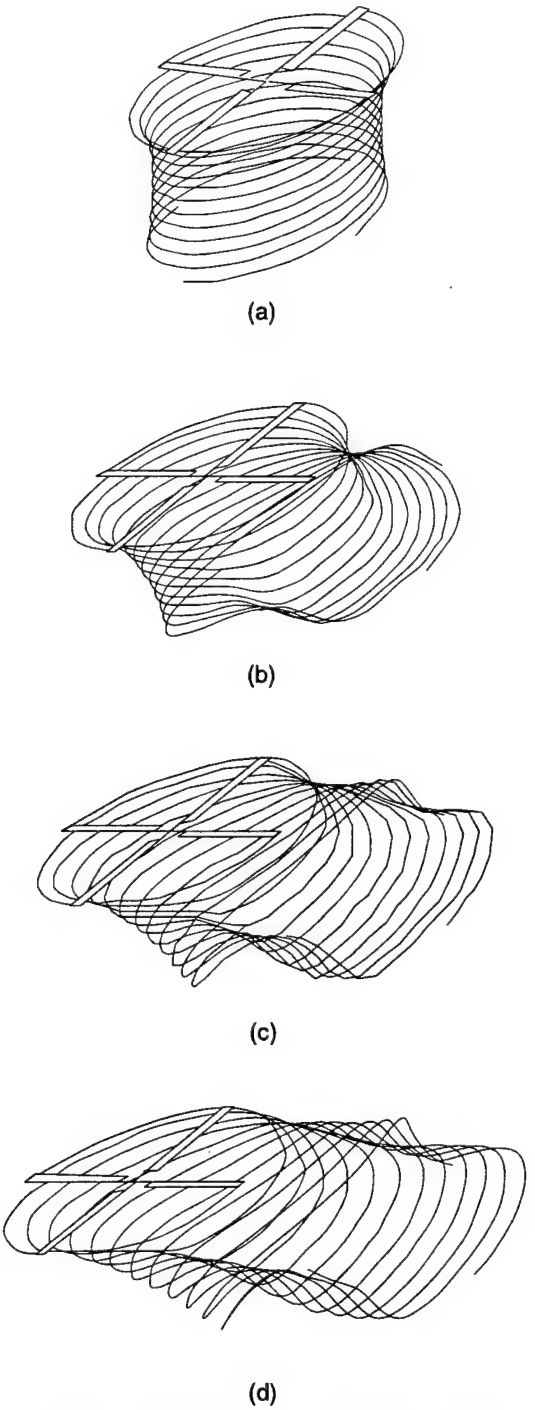

Fig. 3: Isometric views of predicted wake geometries, single isolated rotor, (a) Hover, (b) $\mu = 0.05$, (c) $\mu = 0.075$, (d) $\mu = 0.1$

The scheme has been used to predict the wake geometries over a fairly large range of advance ratios ranging up to 0.4, and numerical convergence has also been strictly monitored as a measure of the L_2 norm of the change in wake geometry between iterations. Because an iterative scheme is being used in the present analysis,

the wake is considered to have converged once it shows no appreciable change in wake geometries between successive iterations. This was found to be the case for an RMS value of the order of 10^{-4}. Typical convergence trends are shown in the figure below, from which it is clear that with the exception of hover, absolute convergence is reached within 15 iterations. In hover, the wake filaments tend to interact more severely in the absence of a superimposed free-stream, and wake exhibits some oscillatory behavior as it relaxes, nevertheless, absolute convergence is obtained in about 31 iterations in this flight condition.

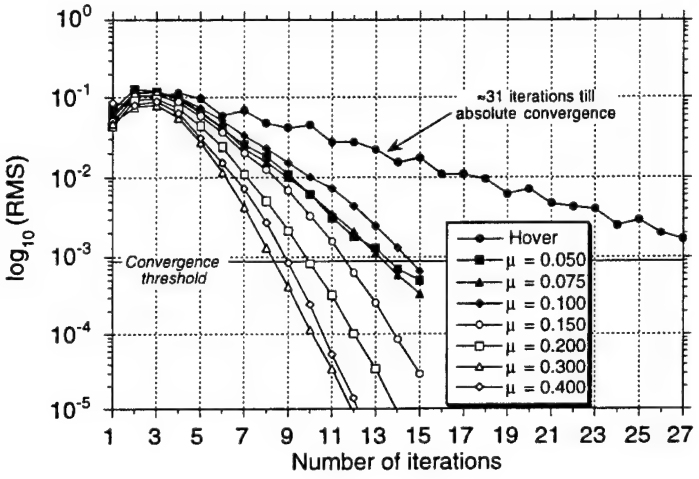

Fig. 4: Typical convergence trends for different advance ratios, single isolated rotor

A series of free-wake predictions for twin rotor systems are shown below. These are more challenging conditions compared with a single isolated rotor because the mutual interactions between vortices from two rotor wakes must now be accounted for. While the side-by-side or tilt rotor configuration is fairly simple and resembles the wake structure from two isolate rotors, there are some small mutually induced interactions between the two wakes. Also note that the wakes are symmetric as would be expected for this symmetric rotor configuration. A more challenging application is to tandem rotors where one rotor is above and behind the other with some degree of overlap. Note that here the interactions between the wakes from the two rotors are quite severe, especially in the overlapping regions. It can be seen that the aft region of the front rotors wake is vertically compressed, where as the fore region of the rear rotors wake is stretched. For the coaxial case, where the rotors overlap entirely, the mutually induced wake distortions are the most severe. Here the wake from the upper rotor is entrained entirely by the lower rotor and is axially stretched, where as the wake from the lower rotor is axially compressed. Note that both rotor wakes retain their tubular structure even at the higher advance ratios.

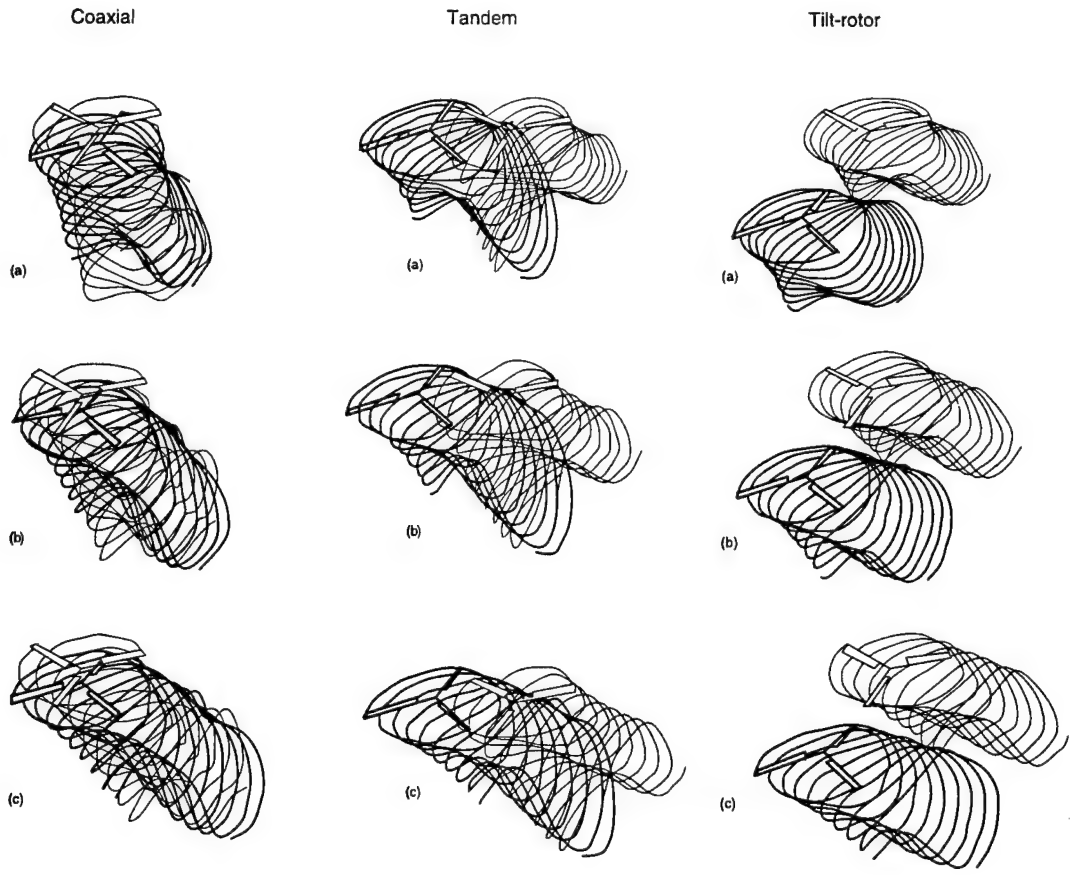

Fig. 5: Predicted twin-rotor wake geometries, (a) $\mu = 0.05$, (b) $\mu = 0.075$, (c) $\mu = 0.1$

The convergence histories for the three configurations are shown below. Here too, convergence is absolute and monotonic for the wakes from both rotors. Although typically, the coaxial rotor requires a few more iterations until absolute convergence as compared to the tilt-rotor and tandem configurations, the overall convergence trends are very good. Once again, note that these are particularly challenging rotor configurations and flight conditions, and it is clear that the present method is well suited to such applications.

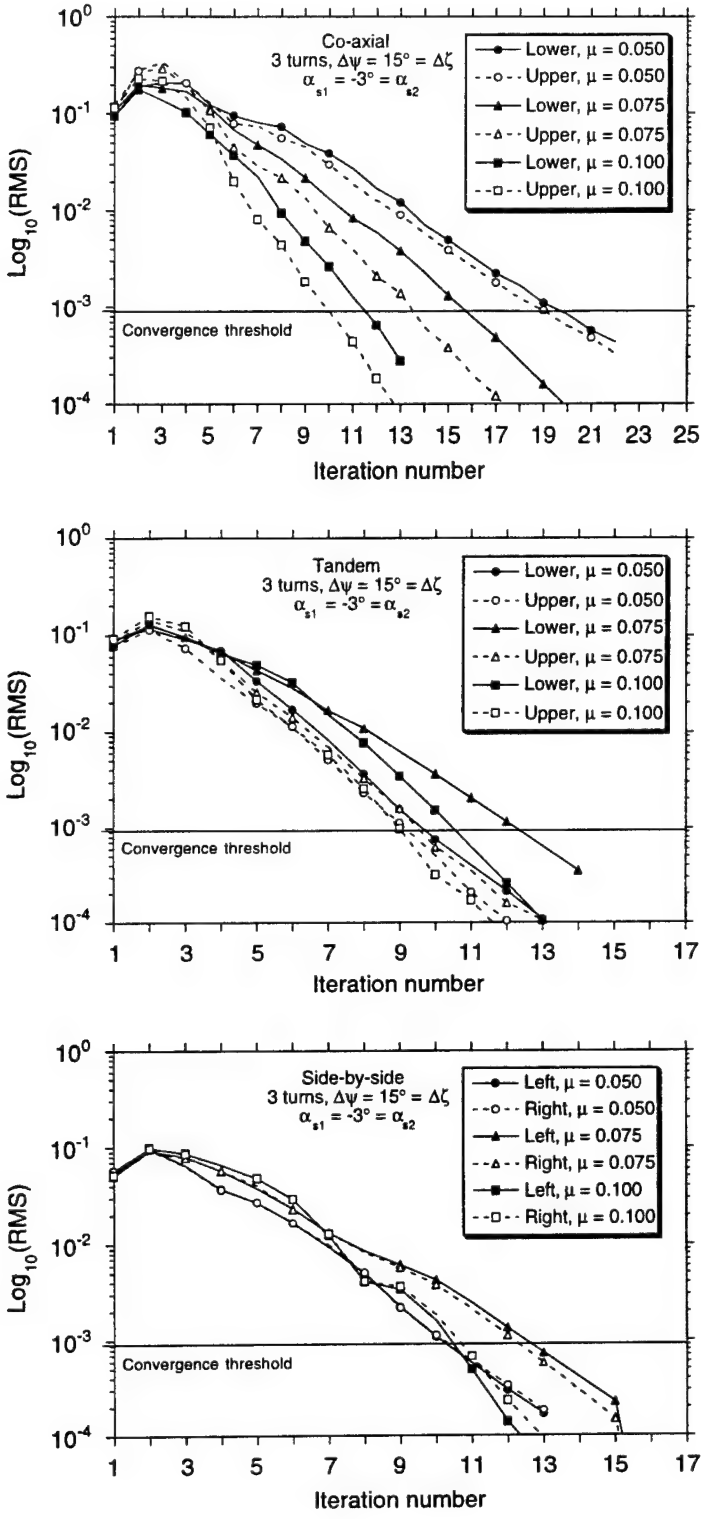

Fig. 6: Twin rotor configuration convergence trends

Numerical aspects of this new scheme have been analyzed in detail, including convergence, stability and accuracy of the methodology. Comparisons with more conventional explicit-type free-wake algorithms have been made to demonstrate the enhanced convergence trends of the new method. The method has been shown to approach a grid independent solution for increasing discretization resolutions, and converges to a unique solution. The present technique has been successfully applied to a number of different flight conditions, including variations in advance ratio, rotor shaft tilts (including descending flight), rotor thrust levels and variations in number of blades. The methodology has also been successfully applied to twin rotor configurations, namely tandem, tilt and coaxial rotor systems.

Efforts have been made to validate the wake geometry and induced velocity predictions by comparing computed results with measured data. Much of these data have been measured at Maryland in a parallel effort. Overall, the comparisons are in good agreement, and the new scheme is able to capture the physical trends of the wake structure and induced velocity field very well, thereby lending considerable confidence to the methodology.

Throughout the development of the present technique, efforts have been made to overcome limitations of previously developed free-wake methods. These have included numerical issues, such as computational efficiency, convergence trends and numerical instabilities. From the physical standpoint as well, most previous schemes have been specialized in application to particular flight conditions (hover only or high-speed flight only). The low-speed (transition) flight regime has been particularly challenging for most previous methods. Efforts have therefore also been made to develop a free-wake scheme which is universally applicable throughout the rotor flight envelope.

Another aspect that has often been overlooked in previous analyses is the physical meaningfulness of the predicted results. Because the computed rotor induced velocity field is very sensitive to the predicted structure of the rotor wake, it is imperative to ensure that the computed wake structure is physically realistic. This can only be done by comparing predictions with experimental data. This is an aspect that has often been lacking in previous work. Often, wake geometry predictions have exhibited chaotic behavior with no repeatability, which bear little resemblance to flow visualization observations of rotor wakes.

Where comparisons have been made in the past, these have been based primarily on blade loads, where artificial tuning parameters such as vortex core radii have been used to adjust agreement between predicted and measured loads. Unfortunately, this limits the use of such free-wake schemes as predictive tools. Another major goal of the present methodology, therefore, was to minimize empiricism and eliminate such tuning parameters from the analysis. To this end, a physically realistic vortex model has been developed that is independent of tuning factors, and incorporated into the free-wake scheme.

Several papers have been prepared on this work including:

Bagai, A., Leishman, J. G., " Rotor Free-Wake Modeling using a Relaxation Technique – Including Comparisons with Experimental Data," Presented at the 50th Annual National Forum of the American Helicopter Society, May 1994.

Bagai, A., Leishman, J.G., "Rotor Free-Wake Modeling using a Relaxation Technique - Including Comparisons with Experimental Data," Journal of the American Helicopter Society, Vol. 40, No. 3, July 1995, pp. 29-41.

Bagai, A., Leishman, J. G., "Rotor Free-Wake Modeling using a Pseudo-Implicit Relaxation Algorithm," Presented at the AIAA 12th Applied Aerodynamics Conference, June 1994. – Accepted for Publication in the AIAA Journal of Aircraft.

Bagai, A., Leishman, J.G., "A New Rotor Free-Wake Model using a Predictor-Corrector Methodology," Journal of Aircraft,, Vol. 32 , No. 6, Nov.-Dec. 1995, pp. 1276-1285.

Leishman, J. G., Bagai, A., "Free-Wake Analysis of Twin Rotor Systems," Presented at the 20th European Rotorcraft Forum, October, 1994.

Bagai, A., Leishman, J. G., "Free-Wake Analysis of Tandem, Tilt-Rotor and Coaxial Rotor Configurations," Presented at the 51st Annual National Forum of the American Helicopter Society, May 1995.

Bagai, A. , Leishman, J. G., " "Free-Wake Analysis of Tandem, Tilt-Rotor and Coaxial Rotor Configurations," Journal of the American Helicopter Society, Vol. 41, No. 3, July 1995, pp. 196-207.

Bagai, A., "Contributions to the Mathematical Modeling of Rotor Flow-Fields using a Pseudo-Implicit Free-Wake Analysis," Doctoral Dissertation, University of Maryland, May 1995.

On the experimental side of this task, experiments have been performed using 3-component LDV and a single bladed rotor model to study the wake and tip vortex evolution. The advantage of using a single blade is that this allows only a single helical vortex filament to be trailed into the wake, removing the possibility of mutual interactions from the results. The generation of a single vortex also helps to preserve the periodic nature of the flow, which is essential when using LDV. The rotor has a 406 mm radius, and 43 mm chord, with a NACA 2415 airfoil section. This model has been used previously for the purposes of examining rotor wakes by means of shadowgraph and schlieren flow visualization methods. Tip Mach numbers of up to 0.8 are possible with this rotor, although for the present tests the tip Mach number was approximately half of full-scale helicopter rotors.

A 5W argon-ion laser was used for the experiments. Three laser lines at 476.5 (violet), 488.0 (blue) and 514.5 nm (green) were obtained from a TSI ColorBurst beam splitter unit. Each color was divided into two beams, one of each shifted in frequency by 40 MHz with the use of a Bragg cell. The six laser beams were then coupled into 10m length single mode glass fibers, which are sent to the transmitting optics. The transmitting optics had a focal length of up to 2200mm, although for the present tests 750mm focal length lenses were used. The probes were arranged on a three-axis traverse adjacent to the rotor. This traverse was controlled remotely, with a typical grid being 50 to 75 or more points in a plane. The system was arranged to obtain the three components of velocity, which were subsequently transformed into the rotor axis system. Data acquisition was performed using a digital burst processor (TSI IFA-750). A rotating machinery resolver (RMR) was used with a 1/rev. from the rotor to define azimuthal bins of 0.9 degrees for the measured data. Velocity data were obtained together with the azimuthal time tag. Based on the assumption of periodic flow (justified from flow visualization), conditional sampling was used to obtain velocity field measurements with respect to the blade azimuth angle. Data acquisition could be windowed to confine the measurements to part of a rotor revolution. The flow was seeded using atomized olive oil, which gave a mean seed size of 0.8 microns and was small enough to faithfully follow the flow in regions of high rotational velocity.

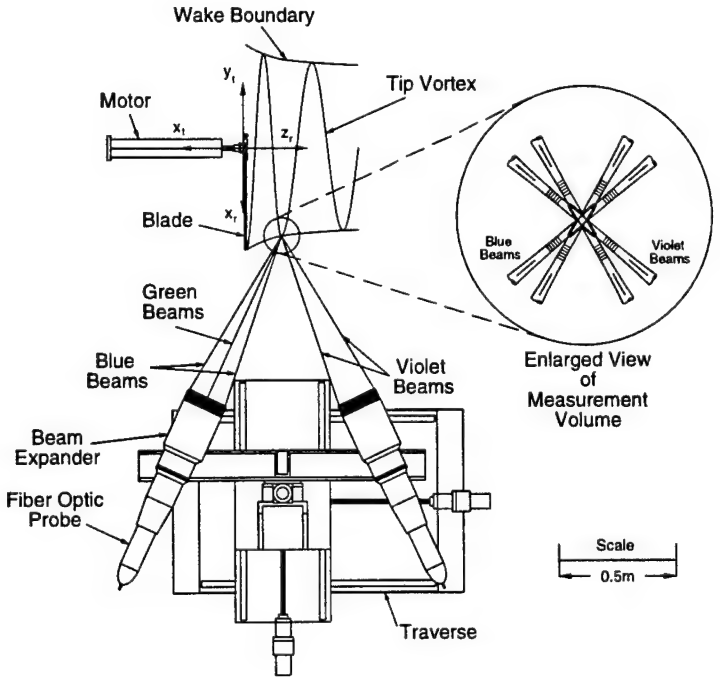

Fig. 7

A suite of computer programs was written to extract a snapshot of the wake velocity field over a particular grid. A typical set of LDV measurements obtained in the rotor wake is shown below. This is a tip vortex velocity profile obtained for a wake age of about 85 degrees. The profile is typical of that expected with a core region of solid body rotation, a peak peripheral velocity and a hyperbolic decay far away from the vortex axis. From the measurements, the initial core radius has been determined to be approximate one-eighth of the blade tip chord. Note also in these measurements, the high spatial resolution and the relatively high number of points obtained near and inside the viscous core. More recent measurements have achieved as many as ten spatial points inside the core. In general, this is difficult because the high rotational velocities tend to make the entertainment of seed particles more difficult, and data rates tend to be low. Many more results have been obtained, including blade circulations, tip vortex circulations, vortex axial velocity deficiency, and quantitative information on the viscous decay of the tip vortices with age.

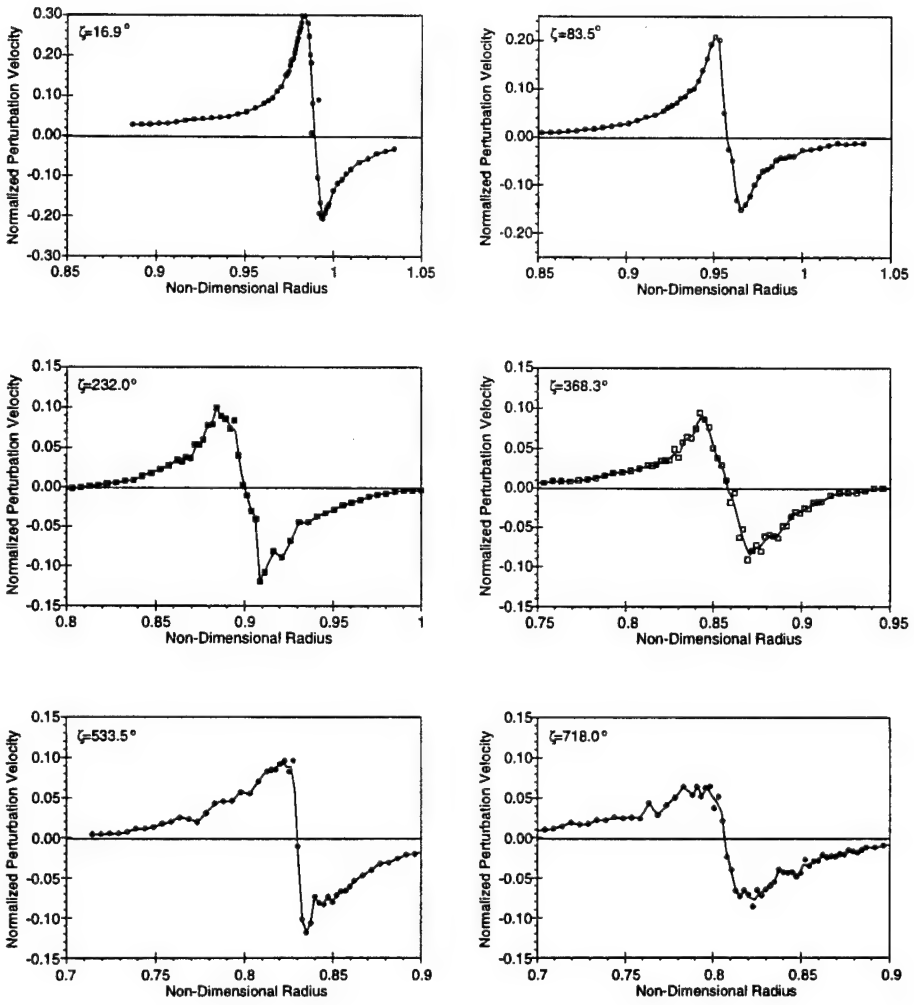

Fig. 8: Measurements of the tangential (swirl) velocity component inside the tip vortex at various wake ages.

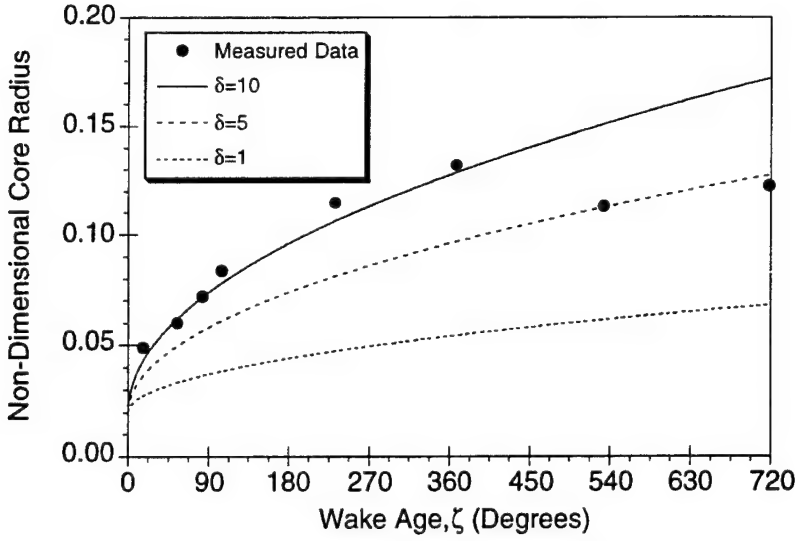

Fig. 9: Graph showing growth in vortex core with wake age as a result of viscous diffusion.

Several papers on this work have been prepared, including:

Leishman, J.G., Baker, A., Coyne, A., Measurements of Rotor Tip Vortices Using Three-Component Laser Doppler Velocimetry, Proceedings of the *2nd International Aeromechanics Specialists' Conference*, Bridgeport, CT, Oct. 11-13, 1995.

Leishman, J.G., Baker, A., Coyne, A., Measurements of Rotor Tip Vortices Using Three-Component Laser Doppler Velocimetry, Journal of the American Helicopter Society, Vol. 41, No. 4, pp. 342-353.

Han, Y., Leishman, J.G., Coyne, A.J., "On the Turbulent Structure of a Tip Vortex Generated by a Rotor," Presented at the 52nd Annual Forum of the American Helicopter Society, Washington DC, June 4-6, 1996.

Leishman, J.G., "On Seed particle Dynamics in Tip Vortex Flows," *Journal of Aircraft*, Vol. 33, No. 4, July-Aug. 1996, pp. 823-825.

Baker, A. M., "Three-Component Laser Doppler Velocimeter Measurements of a Tip Vortex Generated by a One-Bladed Rotor," MS Thesis, Dept. of Aerospace Engineering, University of Maryland, Dec. 1995.

1.3 Modeling of Unsteady Aerodynamics

Work on an improved and computationally efficient time-domain model for three-dimensional unsteady aerodynamics has continued. The method uses linear unsteady theory for the effects of the noncirculatory loads, the shed wake vorticity, and the trailed wake. Generalized approximations to the indicial lift response due to angle of attack and pitch rate derived previously are included for two-dimensional subsonic flow. Starting from an assumed functional representation, these approximations have been accomplished by means of a nongradient optimization algorithm in which the coefficients of the approximation are free-parameters. However, the optimization is subject to prescribed constraints in terms of the known initial and asymptotic behavior of the indicial response, and by requiring the response duplicate the known exact (analytic) solutions at earlier values of time. The approach has been applied to extract the intermediate forms of the indicial lift response, generalized in terms of Mach number and pitch axis location, from a variety of experimental measurements of the unsteady lift in the frequency domain. CFD data have also been used for this task with the help of Dr. Baeder. Corresponding indicial functions for the trailed wake have been derived on the basis of classical vortex theory. These exact solutions are used to obtain indicial response functions in appropriate functional form to enable numerical superposition procedures to be performed.

Some work has centered around improving the coupling process of the shed and trailed wake algorithms in a numerical scheme that provides a suitable basis for calculating the three-dimensional unsteady lift on wings undergoing arbitrary motion in a subsonic flow. Earlier work had used an iterative scheme for this coupling, however, this has proved somewhat time consuming and numerical convergence errors have been encountered. The present approach is based on an influence coefficient approach, where the trailed wake is set-up as a single matrix, but with the circulation terms for the vortex trailers appearing on the right hand side. After the matrix is inverted, the wing bound circulation can be determined uniquely. The numerical scheme has been set-up such that the time dependent effects of trailed wake vorticity is computed as a one step recursive relation (as in the case of the shed wake), where all the time-dependent terms also appear on the right hand side of the equations. The indicial theory of this unsteady finite wing problem has also been combined with a semi-empirical model for dynamic stall. Initial comparisons have been made with experimental measurements made on oscillating finite wings in both attached flow and under dynamic stall conditions.

Work on modeling the unsteady aerodynamics of airfoils with trailing edge flaps has been completed, and has been integrated into the 3-D model. Based on the work conducted previously for the lift, a model has been obtained to calculate the unsteady aerodynamic moments in subsonic flow, namely the airfoil pitching moment about the quarter chord and the moment on the flap about the hinge. The model has been developed in the spirit of classical unsteady airfoil theory, but also

includes subsonic compressibility effects. Complete indicial functions for the pitching moment and hinge moment have been obtained, using the known exact solutions for the chordwise pressure distribution in conjunction with the "Reverse Flow Theorems." Also, the unsteady, inviscid pressure drag on a flapped airfoil has been obtained.

Using the indicial functions, complete response to any arbitrary input motion of the flap has been obtained in a convenient numerical forms useful for many rotorcraft analyses. Both finite-state and recursive formulations have been obtained. The results computed have been validated against experimental data, both in the frequency domain and in the time domain. The comparisons were quite satisfactory, and clearly indicated the use of a theory which models compressibility effects (as opposed to classical incompressible theory).

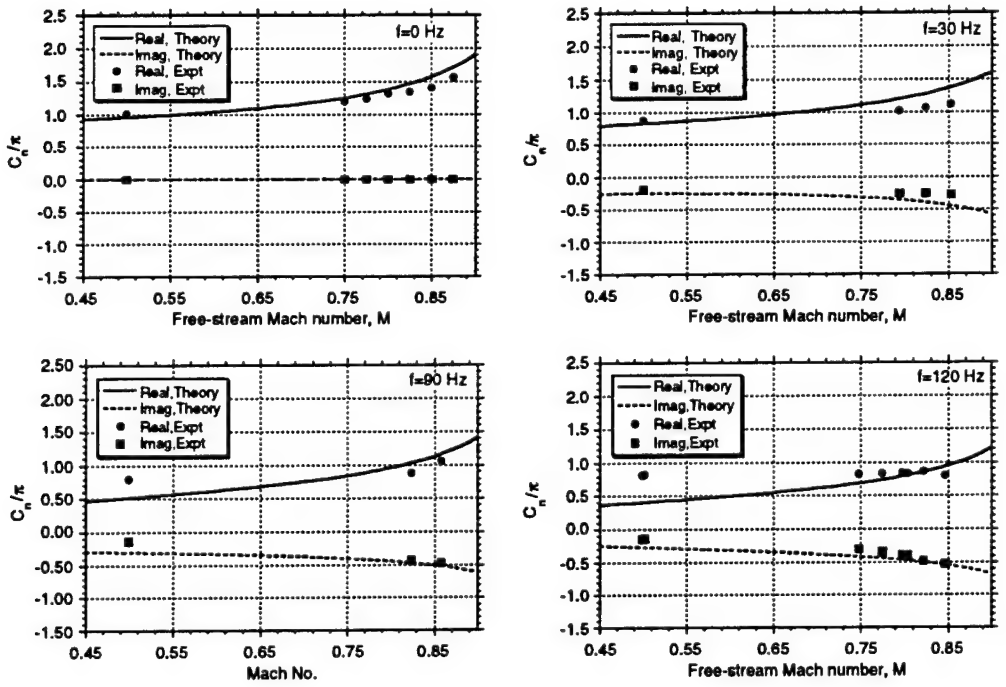

Fig. 10: Sample predictions of unsteady lift resulting from oscillatory flap motion and comparison with experimental data

Indicial approximations have also been derived for the lift on an airfoil penetrating a stationary sharp-edge gust in two-dimensional subsonic flow. Using an assumed exponential form, the approximations have been generalized in terms of Mach number alone by means of an optimization algorithm where certain coefficients of the approximations are free-parameters. The optimization is subject to prescribed constraints in terms of the initial and asymptotic behavior of the gust response, and by requiring the response closely match the known exact solutions given by subsonic linear theory at earlier values of time. An alternative approximation is obtained by using results from a direct numerical simulation of the gust problem using computational fluid dynamics (CFD). For an airfoil-vortex interaction problem, comparisons were made with experimental data and CFD results. Finally, the indicial method was integrated into a three-dimensional rotor simulation, and the near and far-field acoustics were computed using the Ffowcs Williams-Hawkins equation. Good agreement was found with simultaneously measured airloads and acoustics data (see figures).

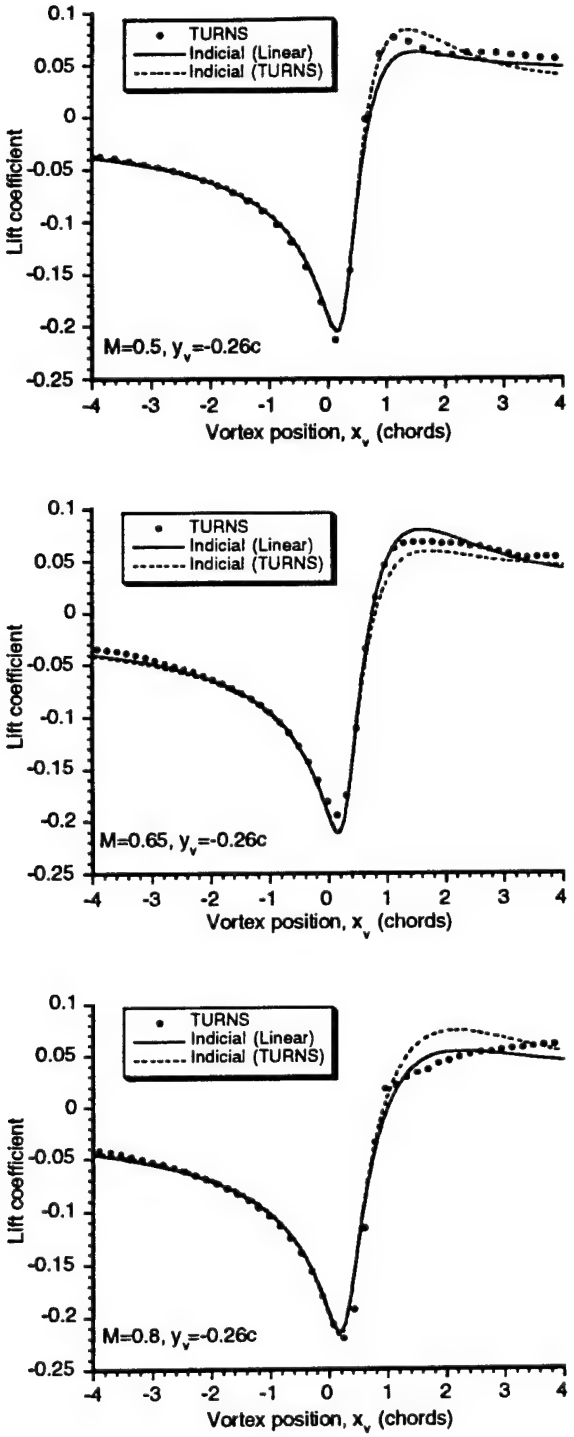

Fig. 11: Predictions of the unsteady lift during a 2-D blade vortex using the indicial method and comparison with CFD (Euler) results.

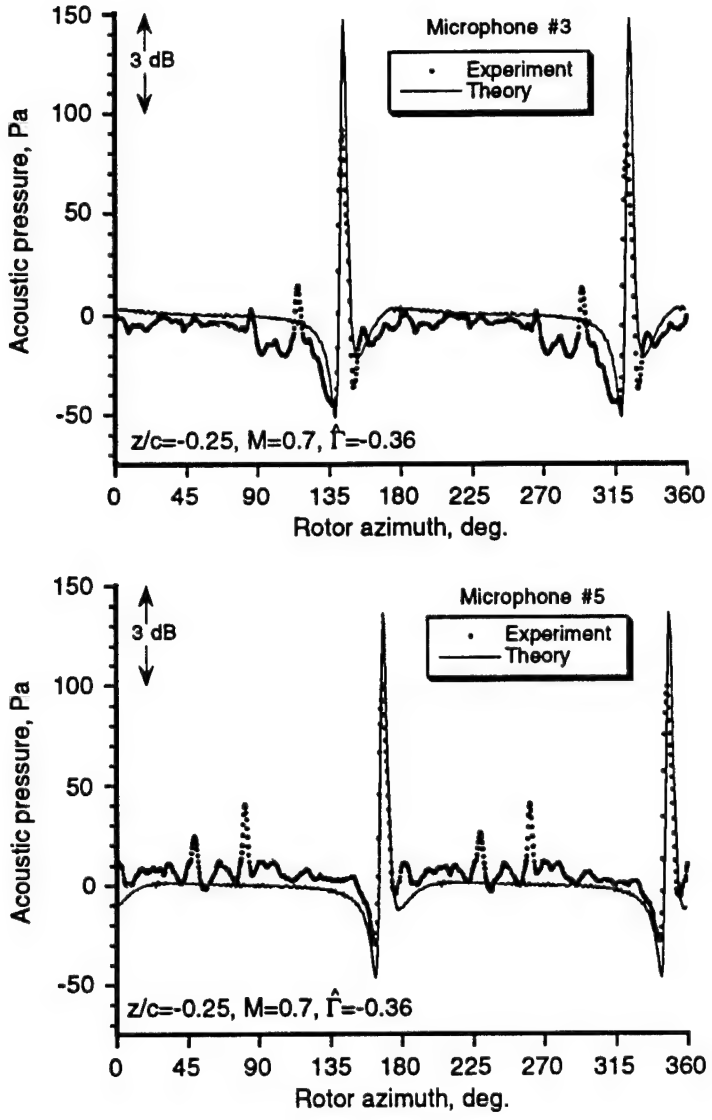

Fig. 12: Sample predictions of sound pressure using the indicial method for an idealized 3-D BVI problem and comparison with experimental data.

A preliminary study has been conducted to investigate the reduction of BVI noise using a "smart" trailing edge flap. Initial results showed that complete elimination of BVI noise is possible, in principle, using active control of trailing edge flaps. However, with the current technology in actuators, the flap deflection

rates required may not be possible. Nevertheless, an active control method has been obtained, whereby BVI noise, if not eliminated can be minimized.

Several papers have been prepared on this work, including:

Leishman, J.G., "Subsonic Unsteady Aerodynamics Caused by Gusts Using the Indicial Method," Journal of Aircraft, Vol. 33, No. 5, Sept.-Oct. 1996, pp. 869-879.

Hariharan, N, and Leishman, J. G., "Unsteady Aerodynamics of a Flapped Airfoil in Subsonic Flow By Indicial Concepts," Journal of Aircraft, Vol. 33, No. 5, Sept.-Oct. 1996, pp. 855-868.

Leishman, J.G., "Aeroacoustics of 2-D and 3-D Blade Vortex Interaction Using the Indicial Method," Presented at the 52nd Annual Forum of the American Helicopter Society, Washington DC, June 4-6, 1996.

Leishman, J.G., "Aeroacoustics Blade Vortex Interaction Using the Indicial Method," Presented at the 22nd European Rotorcraft Forum, Brighton, U.K., 17-19 Sept. 1996.

Hariharan, N. "Unsteady Aerodynamics of a Flapped Airfoil in Subsonic Flow Using Indicial Concepts," M.S. Thesis, Dept. of Aerospace Engineering, University of Maryland, 1995.

DYNAMICS

Dynamics

Inderjit Chopra

Task 2

2.1 DYNAMIC ANALYSIS OF COMPOSITE ROTOR BLADES

Anita L. Tracy

With the application of composite materials, many advanced rotor systems are becoming feasible today. These advanced rotor systems include hingeless and bearingless rotors. A bearingless configuration is a specialized case of a hingeless rotor, in which the pitch bearing as well as the flap and lag hinges is eliminated. Advanced rotor configurations offer mechanical design simplicity (fewer parts), more control power, and better maintainability. Due to blade stress and weight considerations, these rotors are typically designed as soft in-plane rotors, thus making them susceptible to aeromechanical instabilities such as air and ground resonance. To improve the stability of the system, external lag dampers are routinely used. The objective of this research is to examine the potential of using structural couplings due to composites to improve the aeromechanical stability of a bearingless rotor, eliminating the need for external lag dampers. A typical bearingless configuration is shown in Figure 1. The main blade is attached to the hub by means of a torsionally soft flexbeam which allows flap and lag bending as well as elastic twist. This flexbeam is surrounded by a torsionally stiff torque tube that is attached to the main blade and flexbeam at the outboard end and a pitch link at the inboard end. Blade pitch control is achieved by using the pitch link to rotate the torque tube which in turn rotates the main blade and in the process twists the flexbeam.

Successful investigation of the dynamic behavior for a tailored composite bearingless rotor requires a systematic approach. The first phase requires a physical understanding of the structural behavior of composite beams. Particular emphasis is placed on the non-classical behavior such as anisotropic elasticity, transverse shearing, cross-sectional warping, and constrained warping. The present work builds upon the work of Hong and Chopra(1985). The model considers the main blade and torque tube to be modeled as a number of thin-walled closed section composite beams. The flexbeam is modeled as a thin-walled open section beam. The modeling of the thin-walled structural members is based upon the modified Vlasov theory developed by Chandra and Chopra (1990-1993). Laminated beam theory is used to determine the static elastic properties of the tailored composite blade. Constrained warping effects are incorporated as a variation of the torsion stiffness along the length of the flexbeam. Transverse shearing effects are implicitly captured by statically reducing the sectional structural characteristics. These reduced properties are used as input to a non-linear finite element rotor aeroelastic analysis

for the dynamic behavior. The second phase is the implementation of the new beam analysis into the comprehensive rotor analysis (UMARC). A new beam finite element structural analysis has been developed for a coupled composite blade which incorporates the effects of transverse shear and constrained warping implicitly. Once the implementation of the new structural element has been accomplished, in-depth studies can be made of the effects of elastic tailoring on the dynamics of advanced bearingless rotor systems.

The first area of work was to further investigate the structural modeling of the composite beams. For anisotropic materials the out-of-plane warping of the cross-section becomes more pronounced. For greater accuracy, the previously used linear warping distribution is now increased to a cubic distribution. The constrained warping model of the flexbeam has been upgraded to capture the restraint at both ends of the flexbeam. These improved structural models are used as input into the finite element analysis to calculate blade response and rotor-body aeroelastic stability.

A second area of work has been the investigation of a composite flexbeam designed for use with a model hingeless rotor. Both H-beam and rectangular section flexbeams were designed to investigate the effects of chordwise bending-torsion coupling. The flexbeam were designed to approximate the dynamic characteristics of conventional soft inplane hingeless rotors. Static tests on the preliminary design were performed to verify the actual stiffness properties of the flexbeam. The next step was to use the final design flexbeam with the model hingeless rotor and run dynamic tests on the hover stand to validate the overall dynamic analysis. Figures 2 and 3 present typical results for lag damping as a function of collective pitch. Figure 2 shows the percent lag damping for the negative chordwise bending-torsion coupled configuration (lag back/pitch down), while Figure 3 shows the percent lag damping for the positive chordwise bending-torsion coupled configuration (lag back/pitch up). The dashed line in both figures represents theoretical predictions with the coupling term set to zero but all other stiffness properties held fixed. For the negative coupling case, an increase in lag mode damping is seen for increasing positive collective pitch angles relative to the uncoupled configuration both theoretically and experimentally. Good correlation is seen between the theoretical predictions and experimental data for positive pitch angles. As negative collective pitch increases, a disparity between theoretical and experimental values becomes larger. Experimentally, the influence of negative chordwise bending-torsion coupling diminishes for negative collective pitch angles. For the positive chordwise bending-torsion coupling configuration, the opposite trends to the negative coupling configuration are seen. The lag mode damping is increased for negative collective pitch angles and exhibits excellent correlation between experimental values and theoretical predictions. The influence of positive chordwise bending-torsion coupling diminishes for positive collective pitch angles.

Publications:

Tracy, A. and Chopra, I., "Formulation and Evaluation of an Analytical Model for Composite Box-Beams Including Thermal Effects," *32nd AIAA/ASME/ASCE/AHS/ASC Structures, Structural Dynamics and Materials Conference*, Baltimore, MD< April 1991.

Tracy, A.L. and Chopra, I., "Aeromechanical Stability of a bearingless Composite Rotor in Forward Flight," *34th AIAA/ASME/ASCE/AHS/ASC Structures, Structural Dynamics and Materials Conference*, La Jolla, California, April 1993.

Tracy, A.L., and Chopra, I., "Aeroelastic Analysis of a Composite Bearingless Rotor in Forward Flight with Improved Warping Modeling," *American Helicopter Society Aeromechanics Specialists Conference*, San Francisco, California, January 1994. Also, *Journal of American Helicopter Society*, Vol. 40, No. 3, July 1995, pp. 80-91.

Tracy, A. and Chopra, I., "Aeromechanical Stability Analysis and Testing of a Composite Bearingless Rotor," *37th AIAA/ASME/ASCE/AHS/ASC Structures, Structural Dynamics and Materials Conference and Adaptive Structures Forum*, Salt Lake City, Utah, April 1996.

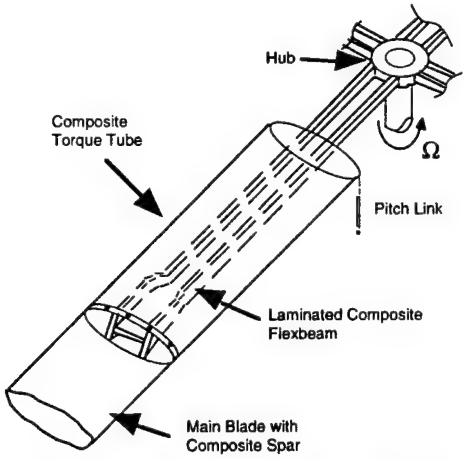

Figure 1: Typical bearingless rotor configuration

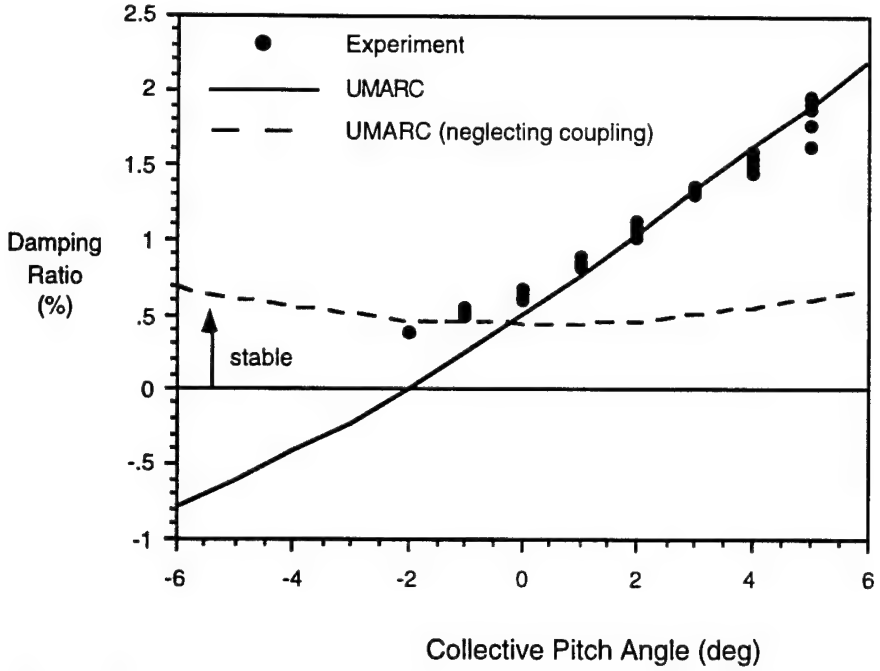

Figure 2: Lag damping as a function of blade pitch angle for negative chordwise bending-torsion coupled configuration (Ω=600RPM).

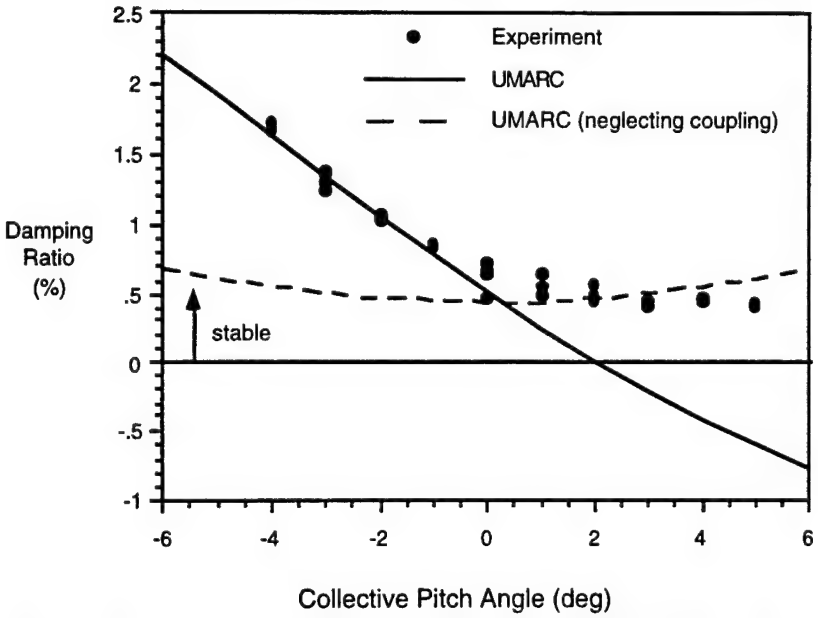

Figure 3: Lag damping as a function of blade pitch angle for positive chordwise bending-torsion coupled configuration (Ω=600RPM).

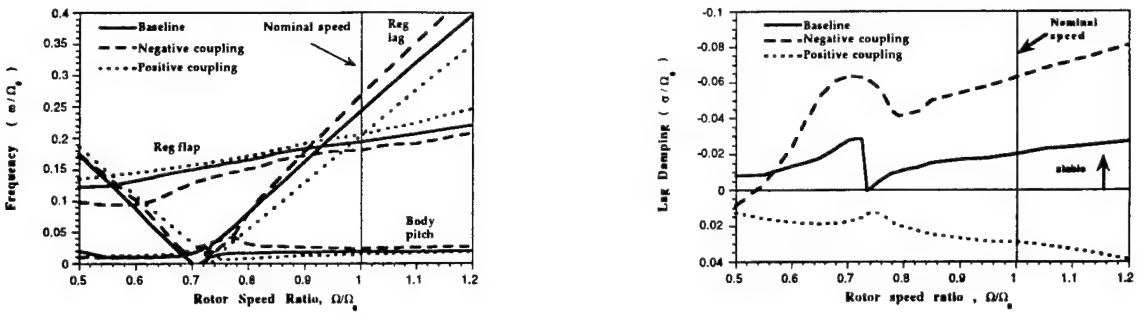

Figure 4: Variation of baseline and chordwise bending-torsion coupled frequencies and decay rates with rotor rotational speed in hover ($C_T / \sigma = .08$)

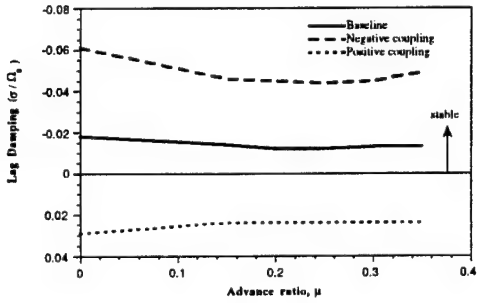

Figure 5: Variation of baseline and chordwise bending-torsion coupled damping ratios with advance ratio ($C_T / \sigma = .08$)

2.2.1 Helicopter Vibration Reduction with Trailing Edge Flaps

Judah Milgram

This investigation examines the possiblities for vibration reduction using rotor-blade mounted trailing edge flaps. The use of trailing edge flaps for 1/rev cyclic control dates back to 1920 with the development of the Pescara helicopter (U.S. Paent 1,449,129). Subsequently, servo flaps for 1/rev control found their way into several production aircraft. In 1958, servo flaps were suggested as a means for implementation of multicyclic control (Payne, *Aircraft Engineering*, Aug., 1958). The first detailed analysis of a servo flap system for multicyclic control was performed at Kaman Aircraft by Lemnios and others during the 1970's (NASA CR-151959). Recently, using a more detailed analysis, Millott and Friedmann (SDM 1992, 93, 94) showed that significant reductions in vibration could be achieved using an actively controlled servo flap. The leading edge of such servo flaps is located aft of the blade trailing edge. The resulting hinge gap is unsealed, resulting in reduced flap effectiveness. In addition, some of the linkage and/or hinge support structure is exposed to the free stream.

The present study considers plain trailing edge flaps in which the hinge line is located in the blade itself (as with, for example, the aileron of a fixed wing aircraft). These flaps provide less aerodynamic pitching moment than servo flaps. Despite this, they offer the advantage of an internally sealed hinge gap and elimination of externally exposed linkage and/or hinge support. In addition, they lend themselves to combination with internally mounted "smart" actuation with piezo bimorph beams (see, European Rotorcraft Forum, 1993).

A comprehensive analysis was developed based on the University of Maryland Advanced Rotor Code (UMARC). The unsteady aerodynamic model has been extended to include terms arising due to flap motion. The flap motions are determined using a multicyclic flap control algorithm. An extensive validation study was performed using wind tunnel data for a 12 foot diameter model rotor with trailing edge flaps. Correlation between predicted and measured blade natural frequencies was generally fair. Results for hover thrust and power agreed well with the experimental data. Some discrepancy was observed near the low thrust conditions. In forward flight, fair correlation was observed for the power required and trim controls. For the rotor with no trailing edge flap motion, overall correlation of blade loads was fair, although significant discrepancies were observed in individual cases. Typical results are in Fig. 1. The figure compares measured and predicted 4/rev flatwise blade bending moments as a function of advance ratio with a 5/rev trailing edge flap input of $\pm$ 4 deg. The blade bending is predicted fairly well by the UMARC models, although the correlation degrades at the higher advance ratio. The CAMRAD/JA correlation is poor, particularly at the higher advance ratios.

A parametric study was conducted for a four-bladed Sikorsky S-76 main rotor. The combination of trailing edge flap and multicyclic controller is predicted to provide significant reductions in fixed system 4/rev hub loads. The flap motions could be optimized to reduce either hub shears or hub moments through variation of a single scalar weighting parameter in the control algorithm. The effects of parametric variations of design parameters such as flap length and chord, and spanwise location could largely be offset by compensating adjustments to the flap motions as determined by the multicyclic algorithm, provided the flap motions did not become too large. The results suggest that a flap with the smallest possible chord and largest possible deflections is preferred.

Representative results are shown in Figures 2 and 3. In Figure 2 the flap chord ratio (flap depth) is varied for a flap centered at .74R. Two flap sizes are shown, .10R and .14R. For each of the flap sizes, varying the flap depth has little effect on the vibration reduction. This is a result of the multicylic controller increasing the input to compensate for the reduced flap size. At very low values of flap chord ratio, the controller reaches a preset limit, and the vibration begins to increase. Figure 3 presents the time history of the flap deflections for a typical operating condition. Two cases are shown. In one case the flap aerodynamic efficiency factors are set to yield zero moments due to the flap, so that the flap's effect is limited to the generation of lift inputs. In the other case the parameters are reversed, so that the flap produces only profile moments. The vibration reduction in either case was predicted to be approximately the same. An examination of the time histories in Fig. 3 shows that the flap can function either as a "lift" flap or a "moment" flap because the multicyclic control adapts automatically to provide inputs that are appropriate to the aerodynamic characteristics of the flap.

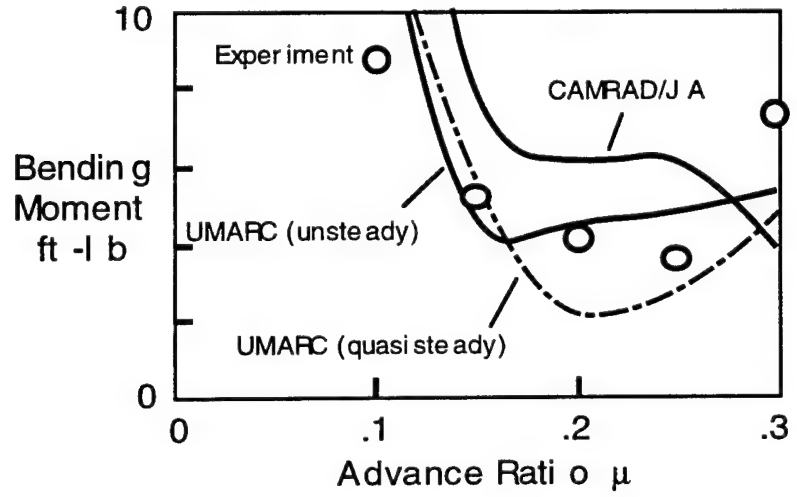

Fig. 1: Harmonics of AFR blade flatwise bending at 0.33R with 5/rev flap input at +/- 4 deg, μ=0.35, and $C_T/\sigma = 0.65$.

Publications:

Milgram, J. and Chopra, I., "Helicopter Vibration reduction with Trailing Edge Flaps," *36th AIAA/ASME/ASCE/AHS/ASC Structures, sructural Dynamics and Materials Conference and Adaptive Structures forum*, New Orleans, LA, April 1995.

Milgram, J. and Chopra, I. "Active Control of Helicopter Vibratory Loads Using Trailing Edge Flaps," American Helicopter Society 2nd International Aeromechanics Specialists' Conference, Bridgeport, CT, Oct. 1995.

Milgram, J. and Chopra, I., "A Comprehensive Rotorcraft Aeroelastic Analysis with Trailing-Edge Flaps: Validation with Experimental Data, *52nd Annual Forum of the American Helicopter Society*, Washington DC, June 1996.

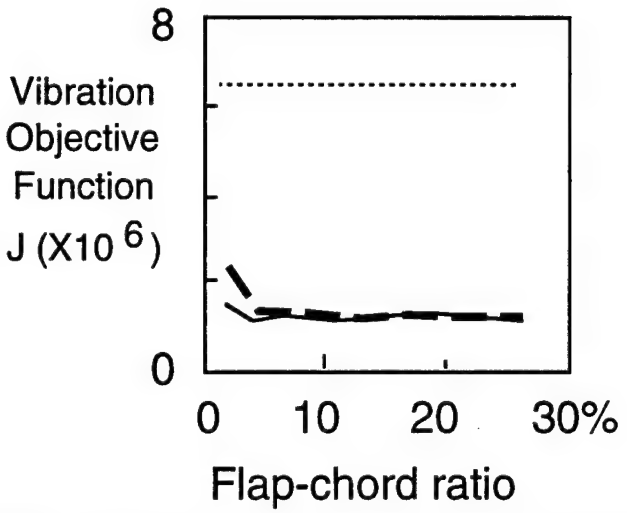

Fig. 2: Effect of flap-chord ratio (hinge location) on trailing edge flap system performance for two flap lengths, with flap centered at .74R, μ=0.35, and C_T/σ = 0.80.

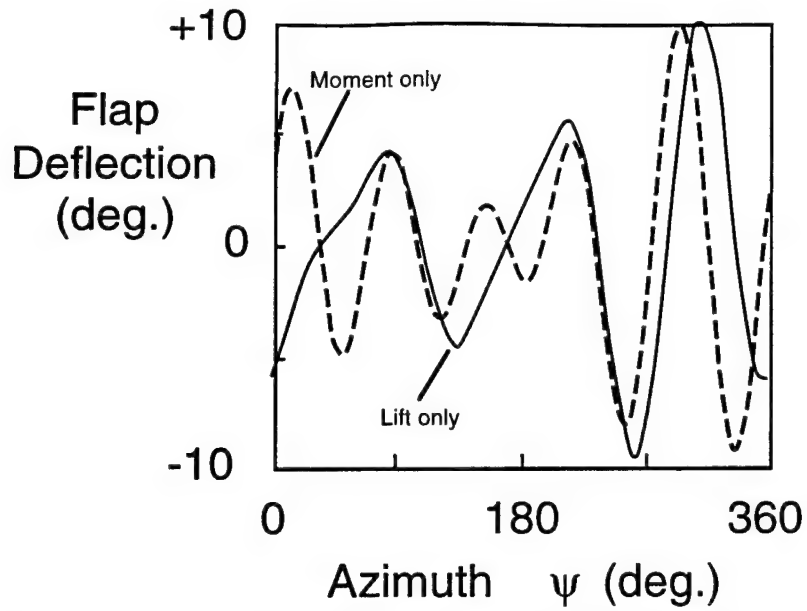

Fig. 3: Comparison of trailing edge flap motions with aerodynamic efficiency parameters set to produce either moment inputs or lift inputs for 10% flap-chord ratio flap extending from .67R to .81R, μ=0.35, and C_T/σ = 0.80.

2.2.2 TILTROTOR COMPREHENSIVE AEROELASTIC ANALYSIS

Venkat Srinivas

Tiltrotor aircraft have a unique ability to combine VTOL capability with efficient long-range cruise performance. They are similar to helicopters in VTOL capability and can fly from and to restricted urban areas and ship decks, while combining the higher cruise speed advantages of conventional turbo-prop transport airplanes. Figure 1 shows a tiltrotor in the airplane mode of operation. Conventional rotary-wing aeroelasticity problems such as pitch-flap, flap-lag and aeromechanical instabilities and fixed-wing instabilities such as wing divergence and flutter as well as unique tiltrotor instabilities such as whirl flutter could occur in tiltrotors. Whirl flutter is caused by large in-plane rotor forces acting to destabilize the wing. Present tiltrotor configurations incorporate the use of a gimballed rotor system. The gimbal mechanism plays an important role in transferring the rotor forces to the pylon; hence has a considerable influence on the stability of the system. The rotor blades, gimbal, pylon and wing have to be modeled in detail to predict the occurrence of such instabilities accurately.

Modification of the above analyses for advanced configurations with composite-coupled blades, advanced geometry blades, kinematic couplings and bearingless rotors adds further complexity to an already complex problem. Advanced geometry rotor blades utilizing blade distributed twist, sweep, anhedral and planform taper along the blade span modify the vibratory forces on the rotor,

delay drag divergence and minimize induced power losses. The use of advanced geometry blade design concepts in tiltrotor configurations could have a considerable impact on rotor performance, vibratory hub loads and noise levels. Advanced geometry modifications also affect the aeroelastic stability characteristics of the rotor. Blade kinematic couplings such as pitch-flap and pitch-lag couplings modify the rotor response and also alter the aeroelastic stability of the rotor system. Composite materials provide the potential for tailoring the blade structural properties by introducing distributed couplings like pitch-flap, pitch-lag and extension-torsion coupling. These structural couplings have a powerful influence on rotor dynamics similar to those of kinematic couplings.

Present Comprehensive Tiltrotor Analysis

An aeroelastic analysis for tiltrotors with advanced geometry composite-coupled rotor blades was formulated. Advanced geometry blades are modeled with arbitrary sweep, anhedral, pretwist and planform taper variation with span. The rotor blade is composed of an arbitrary number of Euler-Bernoulli type straight beam segments each with different sweep, anhedral, pretwist and planform taper. The only constraint imposed on the formulation is that the elastic axes of different beam segments used in the model are connected as piecewise continuous straight lines. Blade section warping and shear deformation effects and composite-couplings along the blade span are modeled. Each blade segment is modeled using one or more finite elements and inter-segment compatibility relations are satisfied using nonlinear transformations. Gimballed rotor systems, typically considered for tiltrotors, as well as hingeless, articulated and bearingless rotors can be modeled in this formulation. The rotor can be modeled in the powered or windmilling configuration. The rotor pylon is assumed to be rigid. Both the tiltrotor wing and fuselage are assumed to be elastic and are modeled using beam finite elements; wing sweep, anhedral, pretwist and planform taper are also modeled. Quasi-steady or unsteady aerodynamics are used in the rotor model. Sophisticated wake models like the prescribed wake and free wake models as well as simple uniform inflow and linear inflow models are included to compute the local inflow velocities over the rotor disk. An aerodynamic rotor/fuselage interference is modeled as well. Blade loads are calculated using a force summation method. A coupled trim analysis yields the solution to the blade response and vehicle equilibrium equations. Aeroelastic stability is calculated using a linearized eigenanalysis of the rotor-wing system. This analysis has been implemented in the comprehensive aeroelastic rotor code UMARC.

A parametric study of the effects of blade tip sweep, anhedral and planform taper on whirl flutter stability was carried out. Figure 2 shows the various blade tip configurations analyzed; all tip modifications were given only to the outboard 15% of the blade. The baseline configuration represents the XV-15 rotor with no blade sweep, droop or taper. Figure 3 shows the effect of blade tip sweep on wing beam, chord and torsion mode damping at the XV-15 cruise velocity of 240 knots. It can be seen that sweep back has, in general, a beneficial effect and sweep forward has a

detrimental effect on wing damping. Figure 4 shows a similar plot for the blade tip anhedral case. Blade tip droop of about 5° increases the stability and tip anhedral (up) of 5° makes the configuration unstable. Significant conclusions from the parametric study pertaining to flutter speed predictions were:

Baseline flutter speed	275 knots
Backward tip sweep 30°	370 knots
Forward tip sweep 30°	Unstable for all speeds
Tip droop 5°	350 knots
Tip anhedral (up) 5°	140 knots
Planform tapered tip (3:1)	260 knots

Figure 5 shows the correlation of predicted wing beam mode damping with full scale test data for the XV-15 configuration. Stability predictions from an analysis by Johnson are also included in the figure. The plot shows that the present analysis correlates well with the test data and with the other comprehensive analysis.

Publications:

Srinivas, V., Chopra, I. and Nixon, M., "Assessment of Aeroelastic Analyses of Advanced Tiltrotor Aircraft," *36th AIAA/ASME/ASCE/AHS/ASC Structures, Structural Dynamics and Materials Conference and Adaptive Structures Forum,* New Orleans, LA, April 1995, Accepted for publication in *Journal of American Helicopter Society,* 1996.

Srinivas, V. and Chopra, I., "An Assessment of Aeroelastic Analyses for Tiltrotor Aircraft," *37th AIAA/ASME/ASCE/AHS/ASC Structures, Structural Dynamics and Materials Conference and Adaptive Structures Forum,* Salt Lake City, Utah, April 1996.

Srinivas, V. and Chopra, I., "Validation of a Comprehensive Aeroelastic for a Tiltrotor Aircraft," *52nd Annual Forum of the American Helicopter Society,* washington, DC, June 1996, Accepted for publication in the *Journal of the American Helicopter Society,* 1996.

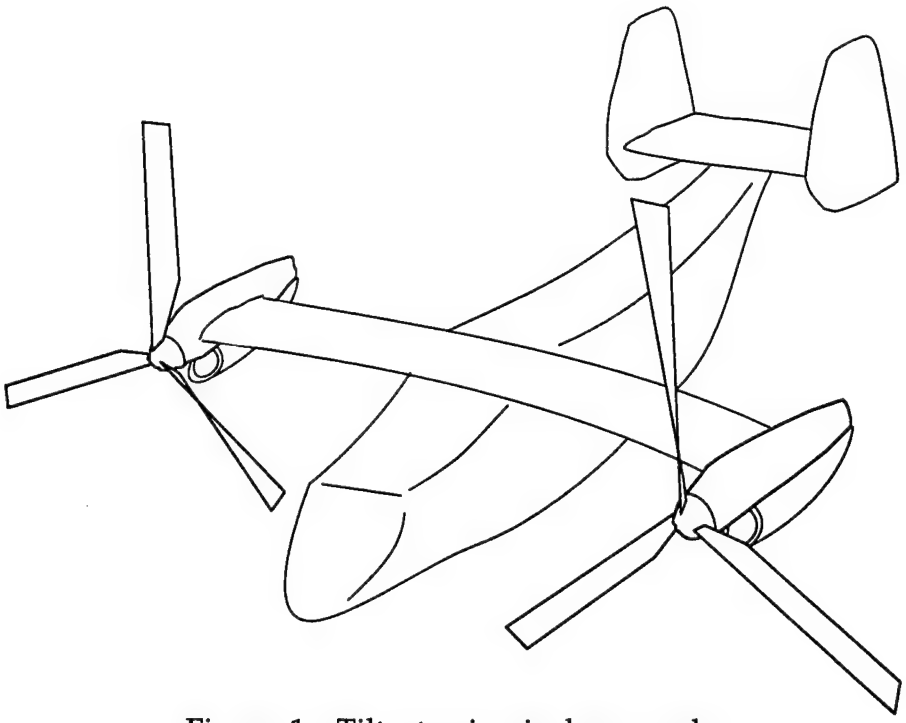

Figure 1: Tiltrotor in airplane mode.

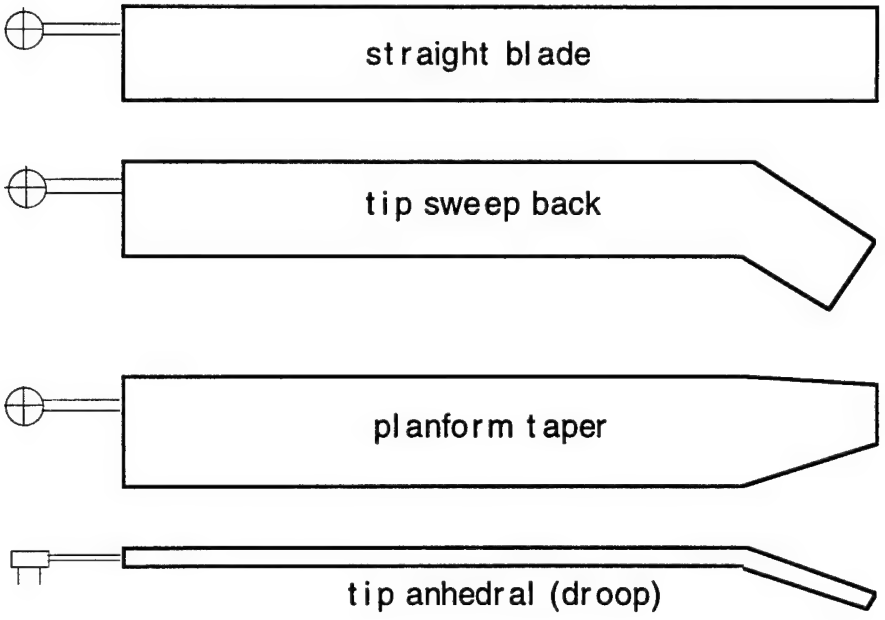

Figure 2: Advanced tip configurations studied
(outboard 15% of blade tip is swept, drooped or tapered).

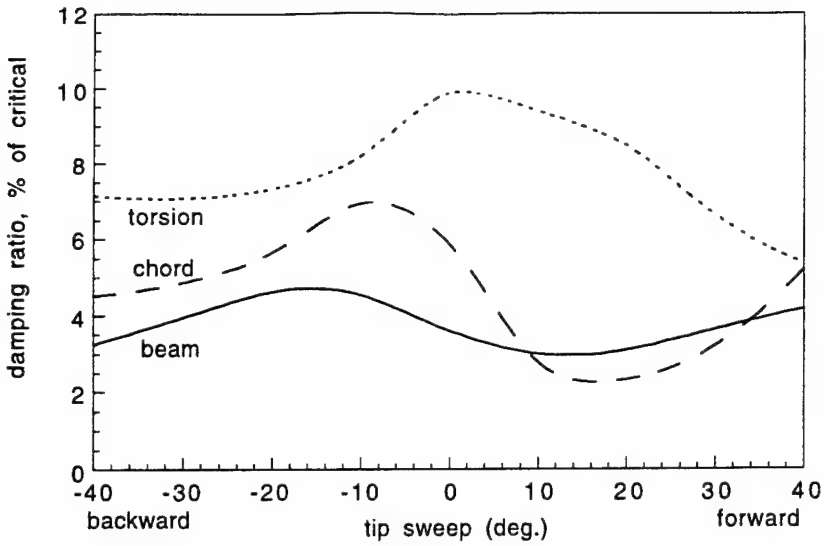

Figure 3: Effect of blade tip sweep on wing mode damping (at 240 knots).

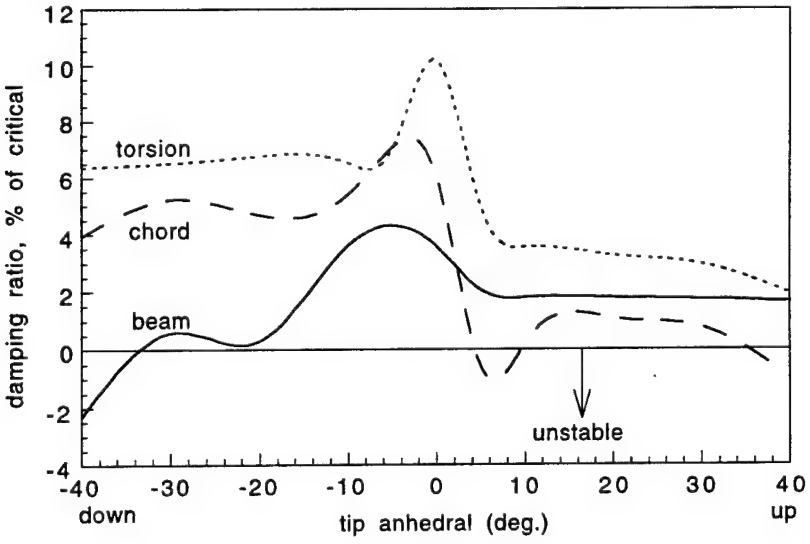

Figure 4: Effect of blade tip anhedral on wing mode damping (at 240 knots).

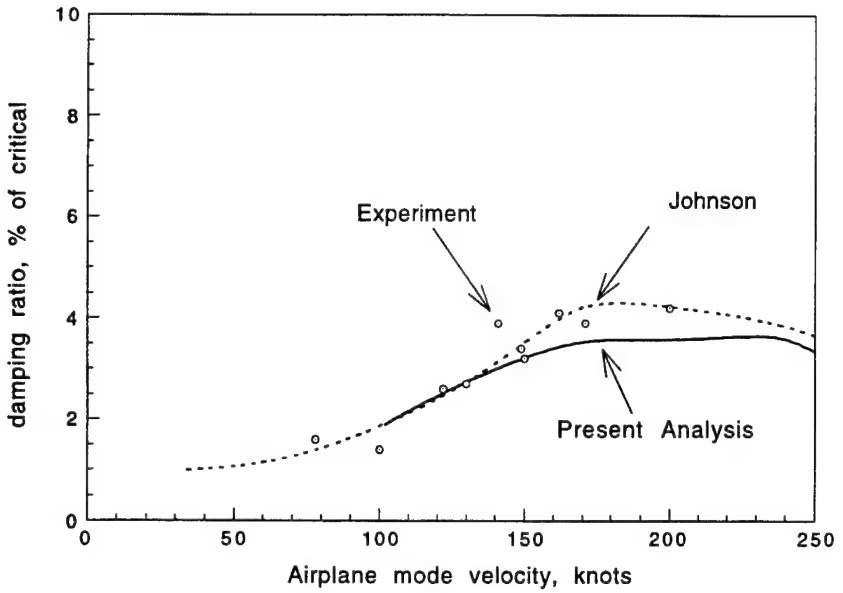

Figure 5: Comparison of predicted wing beam mode damping with full-scale test data and other analysis.

2.3 Aeroelastic Optimization

Ranjan Ganguli

Helicopters are susceptible to high vibrations and high blade dynamic stresses due to harmonic loading on the rotor caused by an unsteady aerodynamic environment and highly flexible rotating blades. For example, for a rotor with N blades, the N/rev forces and moments are transmitted by the rotor to the fuselage as a primary source of vibration. A direct approach for reducing helicopter vibration is to design the rotor so as to minimize the vibratory hub loads. The rotor blade is also subjected to dynamic stresses at several harmonics caused by the vibratory bending and torsional moments acting along the blade span. These dynamic stresses cause structural fatigue, leading to a reduction in blade life. The critical dynamic stresses generally occur at the spanwise location where the bending moment is highest; for hingeless rotors this occurs at the blade root and for articulated rotors around the blade mid-section. Therefore, a direct approach for increasing the life of a blade is to design the rotor with low vibratory bending and torsional moments at the critical spanwise locations.

Most studies on aeroelastic optimization of helicopter rotors have been conducted using straight metal blades. Typically, the objective is to minimize vibratory loads acting on the helicopter in forward flight while keeping the blade aeroelastically

stable. Design variables in these studies are often limited to spanwise stiffness distribution and mass distribution. In recent years, selected attempts have been made to use design variables such as blade sweep, anhedral and planform taper as well as ply angles of composite blades to minimize vibratory hub loads using optimization methods.

Advanced geometry rotor blades involve variable sweep, anhedral, pretwist and planform taper along the blade length. Such blades are receiving increasing attention from rotor designers seeking to reduce compressibility drag rise, stall effects and acoustic noise. The application of composite materials has made fabrication of such complex geometry rotors feasible. Composite materials offer other advantages over metals such as superior fatigue characteristics, higher stiffness-weight ratio, and flexibility in tailoring structural characteristics, which can be exploited by the rotorcraft industry. Recent research has shown vibratory hub loads can be reduced by tailoring the blade geometry, as well as by the use of composite tailoring. The objective of this paper is to apply the optimization method to minimize vibration and blade dynamic stresses for helicopters by tailoring both blade spanwise geometry and composite couplings.

Using an analytical approach, sensitivity analysis and aeroelastic optimization procedures are developed for advanced geometry and composite rotors. Aeroelastic and sensitivity analyses of the rotor based on a finite element method in space and time are linked with automated optimization algorithms to perform optimization of a low-vibration soft inplane hingeless rotor.

For the advanced geometry rotor, design variables include nonstructural mass and its placement, blade bending stiffness (flap, lag and torsion) and blade geometry (sweep, droop and planform taper) at five spanwise stations. The objective function constitutes minimization of all six vibratory hub loads subject to constraints on frequency placement, autorotational inertia and aeroelastic stability of the blade in forward flight. Optimization results show a reduction in the /rev hub loads of 25-60 percent.

In another part of the study, aeroelastic optimization is performed for a composite rotor with the blade spar modeled as a single-cell as well as a two-cell box-beam. The design variables are the ply angles of the cross-section of the blade spar. Optimization is performed for several layups and configurations and it is concluded that elastic stiffnesses reduce the objective function by about 20-40 percent; composite couplings yield a further reduction in the objective function of about 10-15 percent.

Using vibratory hub loads alone in the objective function can cause an increase in the blade root bending moments leading to higher dynamic stresses. This issue is addressed by performing a multi-objective optimization on the composite rotor by using a combination of vibratory hub loads and vibratory bending moments in the objective function. Optimum designs for the multi-objective optimization show a

reduction in the objective function of about 30 percent from the starting design; 20 percent of this reduction is due to elastic stiffness and 10 percent due to composite coupling (flap bending-torsion coupling). As compared to the starting design, the optimum solution results in a 15-60 percent reduction of the 4/rev hub loads (Figures 1 and 2) as well as a reduction in the peak-to-peak flap and lag bending moments of 11 and 14 percent respectively, compared to the starting design. Starting with an initially infeasible design with a 3 percent requirement on lag mode damping, the optimum solution with composite chordwise bending-torsion coupling results in an increase in the lag mode damping of 130-200 percent, compared to the starting design (Fig. 3).

Publications:

Ganguli, R. and Chopra, I., "Aeroelastic Optimization of an Advanced Geometry Helicopter Rotor" *33rd AIAA/ASME/ASCE/AHS/ASC Structures, Structural Dynamics and Materials Conference*, Dallas, Texas, April 1992, *Journal of the American Helicopter Society*, Vol. 41, No. 1, Jan. 1996, pp. 18-28.

Ganguli, R. and Chopra, I., "Aeroelastic Optimization of a Helicopter Rotor with Composite Tailoring," *48th Annual Forum of the American Helicopter Society*, St. Louis, Missouri, May 1993, also *Journal of Aircraft*, Vol. 32, No. 6, Nov.-Dec. 1995, pp. 1326-1334.

Ganguli, R. and Chopra, I., "Aeroelastic Optimization of a Helicopter Rotor to Reduce Vibration and Dynamic Stresses," *35th AIAA/ASME/ASCE/AHS/ASC Structures, Structural Dynamics and Materials Conference*, Hilton Head, SC, April 1994, also *Journal of Aircraft*, Vol. 12, No. 4, July-August, 1996, pp. 808-815.

Ganguli, R. and Chopra, . "Aeroelastic Optimization of a Helicopter Rotor with Two-Cell Composite Blades," *20th European Rotorcraft Forum*, Amsterdam, Netherlands, October, 1994, also, *AIAA Journal*, Vol. 34, No. 4, April 1996, pp. 835-841.

Ganguli, R. and Chopra, I., "Aeroelastic Tailoring of Composite Couplings and Blade Geometry of a Helicopter Rotor Using Optimization Methods, *51st Annual Forum of the American Helicopter Society*, Fort Worth, Texas, May 1995, also, *Journal of American helicopter Society*, Vol. 42, No. 3, July 1997, pp. 218-228.

Ganguli, R., Chopa, I. and Weller, W., "Validation of Calculated Vibratory Rotor Hub Loads with Experimental Data," *53rd Annual Forum of the American Helicopter Society*, Virginia Beach, VA, April 1996.

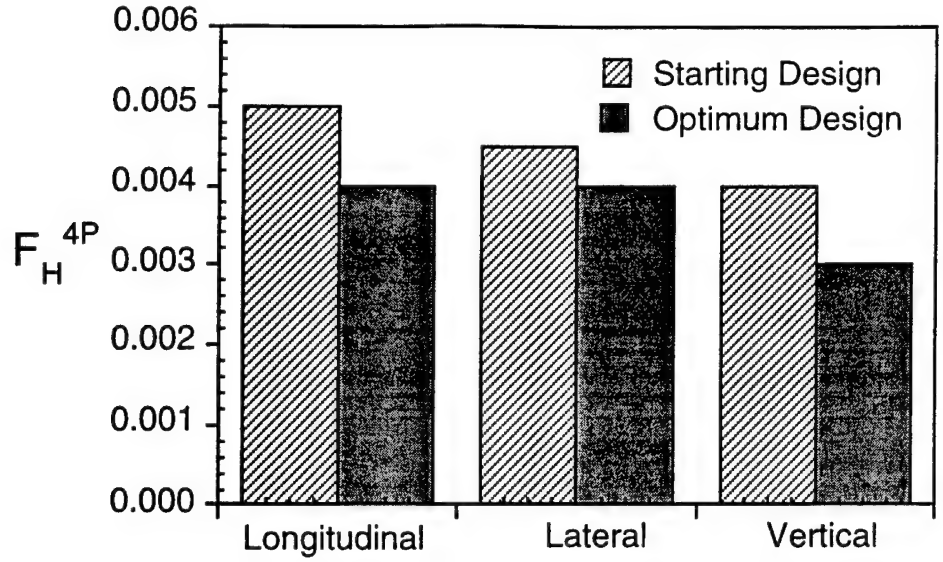

Fig. 1. Vibratory hub forces corresponding to the initial and optimum designs, normalized by steady thrust (μ=0.3, C_T/σ=0.07)

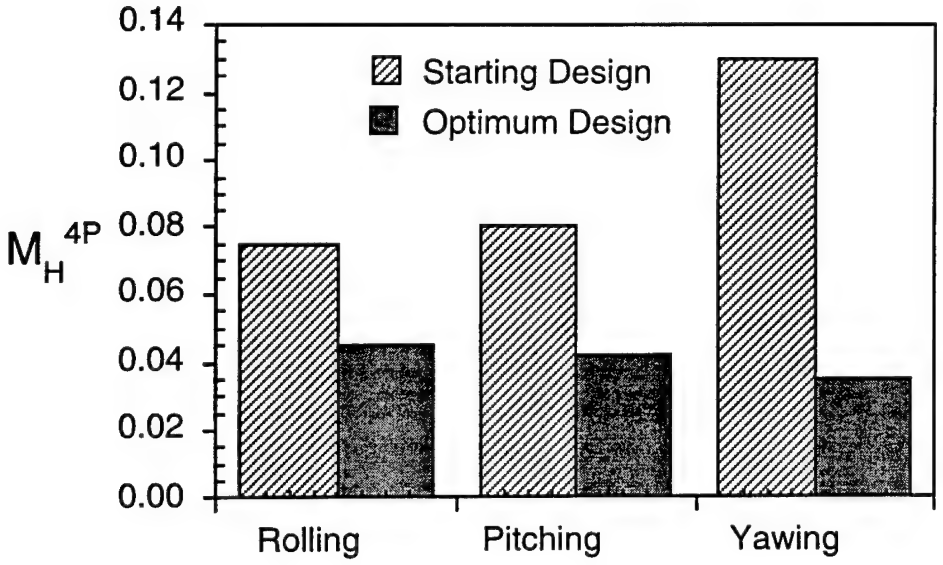

Fig. 2. Vibratory hub moments corresponding to the initial and optimum designs, normalized by steady torque (μ=0.3, C_T/σ=0.07)

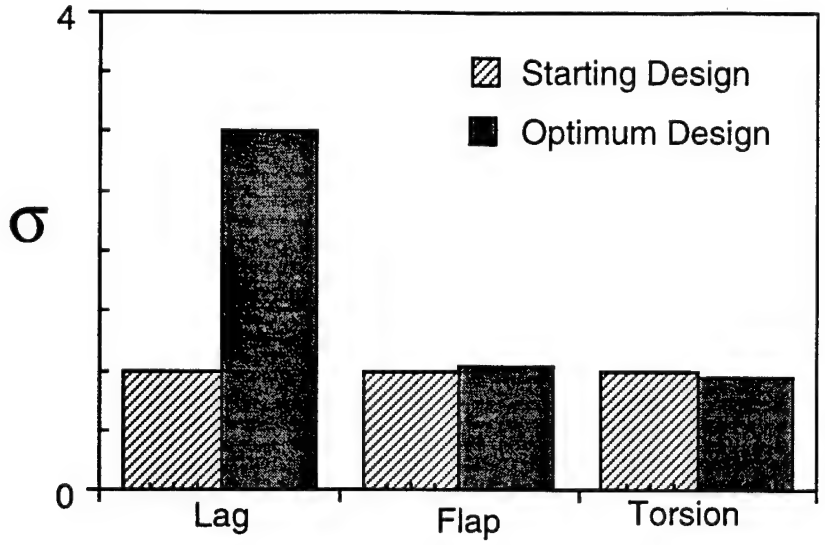

Fig. 3. Damping of first lag, flap and torsion modes for the initia and optimum designs, normalized by starting design values (μ=0.3, C_T/σ=0.07)

2.4 Frequency Domain System Identificaton of Helicopter Rotor Dynamics Incorporating Models with Time Periodic Coefficients

Sunghwang Hwang
Norman M. Wereley

Introduction and Prior Work

This research was motivated by individual blade control [Ham87] using active pitch link [Kre77, Jac93, Tis94] and actively controlled flaps [Spa90, Milg95] for helicopter vibration reduction. Accurate blade dynamic model is a key to predict response, estimate stability, and design control systems. Identification techniques provide an avenue of getting such a dynamic model from wind tunnel test or flight test data. Therefore, lots of research focused on the development of identification techniques. The equation error and output error methods [Lee91] are typical techniques developed in the time domain, CIFER (Comprehensive Identification from FrEquency Response) code [Tis92] is a representative tool developed using the spectral theory in the frequency domain. In applicatons of these techniques, most concerns have been given to identify the rigid body fuselage model [Kal89], or approximated constant coefficient blade dynamic model [Tis94] for rotor blade equatons of motion. However, the incorporation of blade dynamics into the six degree of freedom rigid body fuselage model introduces periodic terms in forward flight [Joh80]. These periodic terms generate the signal power at sideband frequencies as well as at the input frequency to an input of only one frequency. The

spectral theory for linear time invariant systems cannot account for the sideband powers for identification procedures. Therefore, non-parametric and parametric identification techniques, which can account for the sideband effects of periodic terms, were developed and applied to the coupled flap-lag-inflow dynamic model of rotor blade in forward flight using computer simulated data.

Frequency Domain System Identification

A test signal used is an exponentially modulated periodic [Wer91] signal defined as

$$u(t) = \sum_{n=-\infty}^{\infty} u_n e^{jn\Omega t} \tag{1}$$

A modulated complex Fourier series expansion was introduced to eliminate the smearing effect due to the complex Foureir series expansion of an exponentially modulated periodic signal

$$u_n = \frac{1}{T}\int_0^T \left[u(t)e^{-j\omega_f t}\right] e^{-jn\Omega t} dt \tag{2}$$

Then, based on the signal block diagram in Fig 1., the spectral theory for linear time periodic systems was developed so that the resultant expressions can account for the sideband effects due to the periodic terms. Relationships for getting the frequency response, or harmonic transfer functon, and coherence functions were obtained as follows, depending on the presence of noise processes.

Case 1: Perfect measurement at input and output

When there are no noise processes at input and output, the identified harmonic transfer function can be obtained by

$$g_{nm}(j\omega_n) = S^n_{u_m y}(j\omega_n) S^m_{uu}(j\omega_m)^{-1} \tag{3}$$

where m and n represent the input and output frequency strips, and $\omega_n = \omega_f + n\Omega$. The coherence function is given by

$$\gamma^2_{uy}(j\omega_n) = \left|S_{uy}(j\omega_n)\right|^2 \left\{S_{uu}(j\omega) S_{yy}(j\omega)\right\}^{-1} \tag{4}$$

and the value is equal to one, because of no noise.

Case 4: Noise processes present at input and output

Given input noise intensiy, $S^m_{\eta\eta}(j\omega_m)$, the harmonic transfer function can be computed by

$$g_{nm}(j\omega_n) = S^n_{v_m z}(j\omega_n)\left\{S^m_{vv}(j\omega_m) - S^m_{\eta\eta}(j\omega_m)\right\}^{-1} \tag{5}$$

where v is the measured input corrupted by the input noise, and z the measured output corrupted by the output noise. The coherence function is given by

$$\left\{\gamma^n_{x_m z}(j\omega_n)\right\}^2 = \left[\left\{1 + S^m_{\eta\eta}(j\omega_m)/S^m_{uu}(j\omega_m)\right\}\left\{1 + S^n_{vv}(j\omega_n)/S^n_{yy}(j\omega_n)\right\}\right]^{-1} \tag{6}$$

Parameter Identification

Assuming that the system structure is known and has distinct poles, parameters are identified to match the identified harmonic transfer function by minimizing a quadratic objective function as follows.

$$J(\tilde{\theta}) = \frac{1}{N_f}\sum_{k=1}^{N_f} \frac{\mathrm{tr}\left[\varepsilon(j\omega_k,\tilde{\theta})^{*T} W\, \varepsilon(j\omega_k,\tilde{\theta})\right]}{\mathrm{tr}\left[G_M(j\omega_k,\theta)^{*T} W\, G_M(j\omega_k,\theta)\right]} \tag{7}$$

where $\varepsilon(j\omega_k,\tilde{\theta})$ is defined as an error between an estimated harmonic transfer function using identified parameters, $G(j\omega_k,\tilde{\theta})$, and identified harmonic transfer function by the spectral theory, $G_M(j\omega_k,\theta)$.

Identification of coupled flap-lag-inflow dynamic model of a rotor blade in forward flight

A coupled flap-lag-inflow dynamic model in forward flight was identified using the above technqiue. The dynamic equations used are the flap-lag equations of motion from Johnson {Joh80] and dynamic inflow model from Pitt and Peters [Pit81]. Fig. 2 shows the spectral density distribution, which shows the symmetrical property between the spectral density functions to an input of mth frequency strip and those to an input of -mth frequency strip. From this, clearly we can see the sieband powers due to the periodic terms. Fig3. shows the harmonic transfer function identified by the above technique. Results are in good agreement with analytical results. Fig. 4 shows the errors of identified parameters in the presence of input and output noise processes as the signal to noise ratio varies from 50 to 6.3, compared with the results of perfect case. It can be said that the identified results are insensitive to the noise intensity.

Reference

[Ham87] N. D. Ham, B. L. Behal and R. M., McKillip, Jr., "Helicopter Individual Blade Control Research at MIT 1977-1985." *Vertica*, vol 11, no. 1/2, 1987.

[Kre77] M. Kretz, "Relaxation of Rotor Limitations by Feedback Control." *Proceedings of the 33th Annual Forum of the American Helicopter Society*, 1977, Washington, D.C.

[Jac93] S. A. Jacklin, J. A. Leyland, and A. Blaas, "Full-Scale Wind Tunnel Investigation of a Helicopter Individual Blade Control System." *Proceedings of the 34th AIAA Structures, Structural Dynamics, and Materials Conference*, 1993, LaJolla, CA.

[Tis94]M. B. Tischler , J. T. Driscoll, M. G. Cauffman, and C. J. Freedman, "Study of Bearingless Main Rotor Dynamics from Frequency Response Wind Tunnel Test Data." *Proceedings of the American Helicopter Society Aeromechanics Specialists Conference*, 1994, San Francisco, CA.

[Spa90] R. L. Spangler and S. R. Hall, "Piezoelectric Actuators for Helicopter Rotor Control." *Proceedings of the 31st AIAA Structures, Structural Dynamics, and Materials Conference*, 1990, Long Beach, CA.

[Milg95] J. Milgram and I. Chopra, "Helicopter Vibration Reduction with Trailing Edge Flaps.*Proceedings of the 36th AIAA Structures, Structural Dynamics, and Materials Conference*, 1995, New Orleans, LA.

[Lee91] J. H. de Leeuw, "Identification Techniques : Model Structure and Time Domain Methods." *AGARD LS-178 : Rotorcraft System Identification*, NATO, Oct. 1991.

[Tis92] M. B. Tischler and M. G. Cauffman, "Frequency Response Method for Rotorcraft System Identification: Flight Applications to BO-105 Coupled Rotor/Fuselage Dynamics." *J. American Helicopter Society*, vol 37, no. 3, 1992.

[Joh80] W. Johnson, *Helicopter Theory*, 1980, Princeton University Press, Princeton, NJ.

[Wer91]N. M. Wereley and S. R. Hall, "Linear Time Periodic Systems: Transfer Function, Poles, Transmission Zeros and Directional Properties." *IEEE Transactions on Automatic Control* vol. 37, no. 7, 1992.

[Pit81] D. M. Pitt and D. A. Peters, "Theoretical Prediction of Dynamic-Inflow Derivatives." *Vertica*, vol. 5, no. 1, 1981.

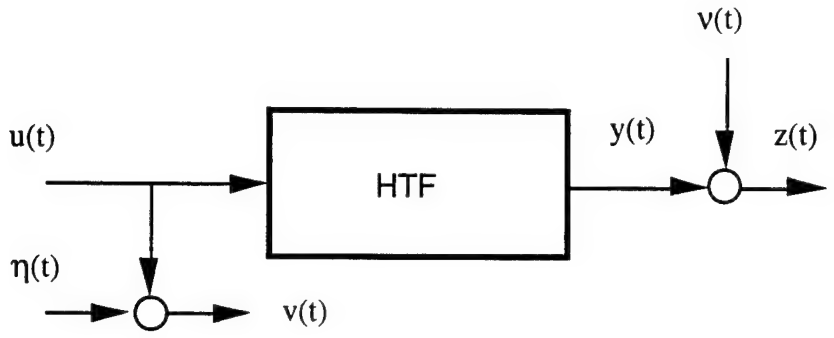

Fig. 1 Canonical signal block diagram for linear time periodic systems

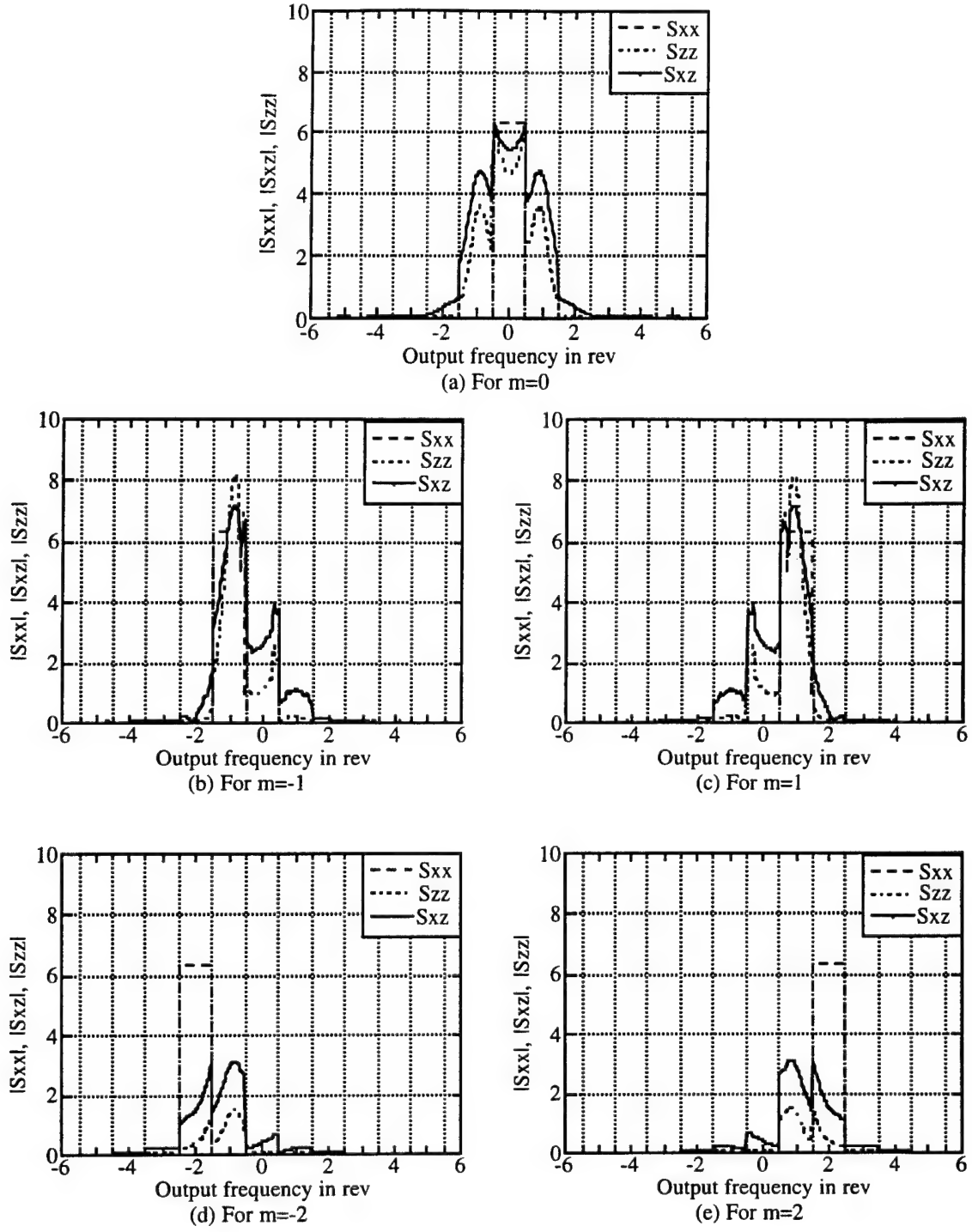

Fig 2. Spectral density distributions of flap response versus input frequency strips, m=-2 through m=2

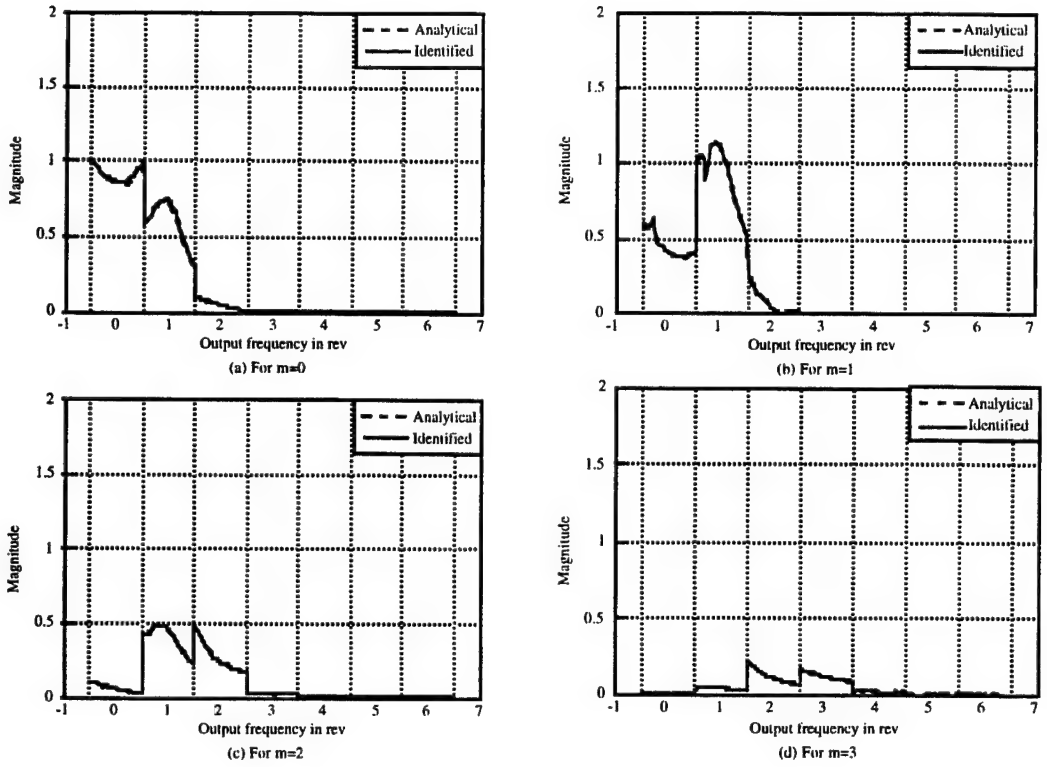

Fig 3. Comparison of identified and analytical harmonic transfer functions of flap response

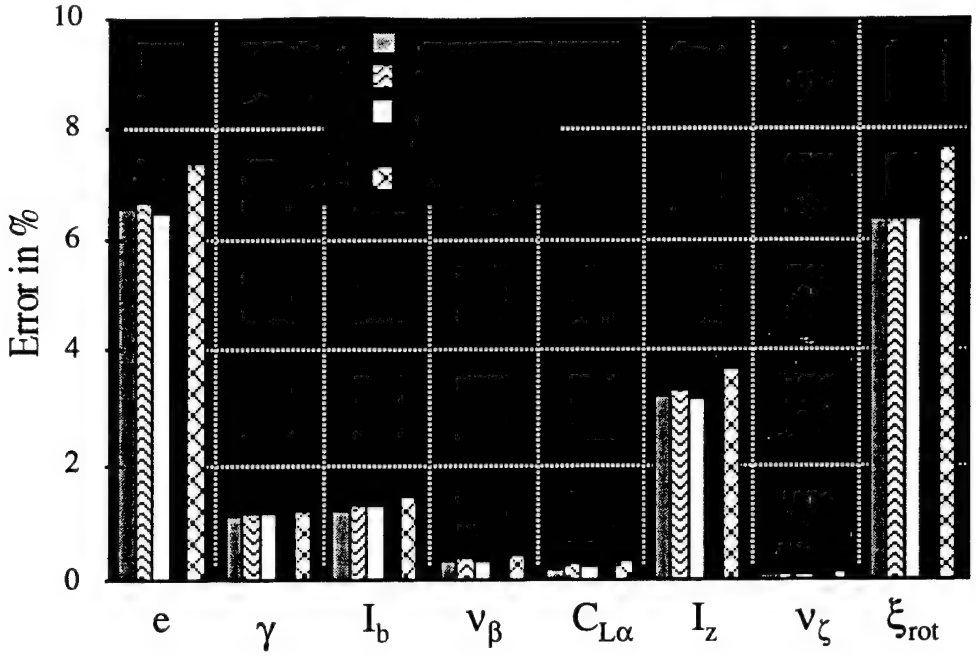

(a) $\mu = 0.0\,5$

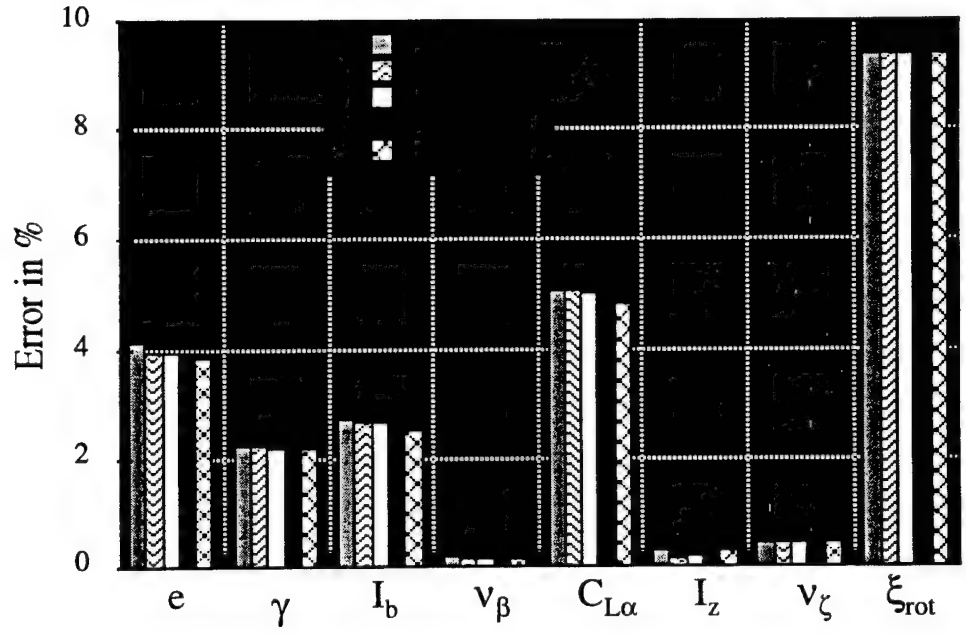

(b) $\mu = 0.30$

Fig. 4. Identified parameter errors in the presence of boh input and output noise processes

FLIGHT DYNAMICS

Task 3. Flight Dynamics and Control

Roberto Celi

Introduction

This section presents the accomplishments of three subtasks in the general area of helicopter flight dynamics and control. The subtasks addressed basic issues of mathematical modeling, system identification, and multi-disciplinary plant-control system optimization, that are key building blocks for the successful design of high-performance military helicopters. The activities in each subtask are described in the next subsections.

3.1 Simulation Modeling and Sensitivity Analysis

3.1.1 Simulation modeling for bearingless rotor helicopters

The objectives of this work were: to formulate a mathematical model of the flight dynamics of bearingless rotor helicopters, and to use the model to study the effect of design parameters and flight conditions on various stability and control characteristics.

A flight dynamic simulation model, previously developed at Maryland, and suitable for articulated rotor helicopters, was extended to allow for the modeling of hingeless and bearingless rotor configurations. The mathematical model is based on a nonlinear, blade element-type formulation A brief outline of the main features of the model is provided here. Each main rotor blade is modeled as a flexible beam with flap, lead-lag, torsion, and axial degrees of freedom. The structural model is based on the Rosen-Friedmann formulation, substantially similar to the traditional Hodges-Dowell formulation. However, a new implementation of the theory was devised: the various mathematical expressions that make up the model are now combined numerically during the solution process, rather than expanded symbolically during the formulation process. As a result, most of the approximations, based on the use of ordering schemes, required to perform symbolic manipulations in the original versions of the model are no longer required. It is these approximations that limit the original theory to "moderately large" elastic deflections. Therefore, removing these approximations effectively extends the validity of the theory to much larger elastic deflections. As a consequence, the same model can be applied to both the main portion of the blade and to the flexbeam, which may undergo large torsional deflections. The hub model is composed of a flexbeam and a torque tube, and includes a dual load path.

The aerodynamic model is based on a two-dimensional strip theory, with tip corrections. The aerodynamic coefficients of the blade airfoils are calculated using the state space version of Leishman's unsteady aerodynamic theory for attached flow, which includes the effects of compressibility. The dynamics of the main rotor

wake is described by the He-Peters finite state wake model. Both the inertia and the aerodynamic model fully take into account the effects of an arbitrary rigid body motion of the hub (within the range of validity of Euler angle representations); they are formulated numerically in much the same way as the structural model, and therefore it is easy to account

The fuselage is modeled as a rigid body. The overall, 6-degree of freedom rigid body motion of the aircraft is described by nonlinear Euler equations. The aerodynamic characteristics of the fuselage and of the tail surfaces are formulated in the form of look-up tables. The tail rotor is modeled as a thrust generating disk; a one-state dynamic inflow model is included.

The equations of motion of the main rotor blades are written as partial differential equations; they are converted to ordinary differential equations (ODE) using a finite element discretization. The same finite element is used for the main portion of the rotor blade, the torque tube, and the flexbeam. The combined rotor-fuselage equations initially contain acceleration-dependent terms on both sides of the equal sign. The acceleration dependent terms on the right-hand-side are identified and moved to the left-hand-side, so that the equations can be rewritten in a form compatible with typical ODE solvers. These transformations are all performed numerically and require a very limited amount of symbolic manipulations. The number of degrees of freedom of the finite element model of the blade is reduced using a modal coordinate transformation based on coupled bending torsion-axial modes.

The solution algorithms include the following:
Free flight trim. The equations of motion of the main rotor blades and those for the finite state wake are transformed into a system of nonlinear algebraic equations using a classical Galerkin method (similar to a Fourier series method). The resulting equations are coupled with the equations that enforce force and moment equilibrium for the complete aircraft and other kinematic conditions that have to be satisfied in trim. The combined system of nonlinear algebraic equations is solved simultaneously if a quasi-steady model is used for the calculation of aerodynamic coefficients of the airfoils. If the unsteady model is used, the trim values of the additional states are calculated using a new inner-loop/outer loop scheme, developed as part of this subtask. According to this scheme, the aerodynamic states are trimmed for fixed values of the other rotor-fuselage states; the resulting values are then held fixed and updated values of the rotor-fuselage trim variables are calculated; the new values of these states are then used to recalculate trim values of the aerodynamic states and the procedure is repeated iteratively until convergence. The basic flight condition is a steady, coordinated, helical turn; trim in steady, straight, horizontal flight is treated as a special case of turn.

Extraction of a linearized model. A system of linearized equations of motion is obtained by perturbing the full system of nonlinear ODE about a trimmed equilibrium position. The perturbations are performed numerically, and the state and control matrices are calculated using finite difference approximations. Because the blade equations of motion are formulated and solved in a rotating system, a multiblade coordinate transformation is performed on the main rotor portions of the linearized matrix. After this transformation, the linearized system refers entirely to a nonrotating coordinate system. Finally, the state and control matrices are averaged over one rotor revolution, to obtain a time-invariant system of equations.

The linearized system provides information on the coupled rotor-fuselage stability of the aircraft, and on its frequency response to pilot inputs.

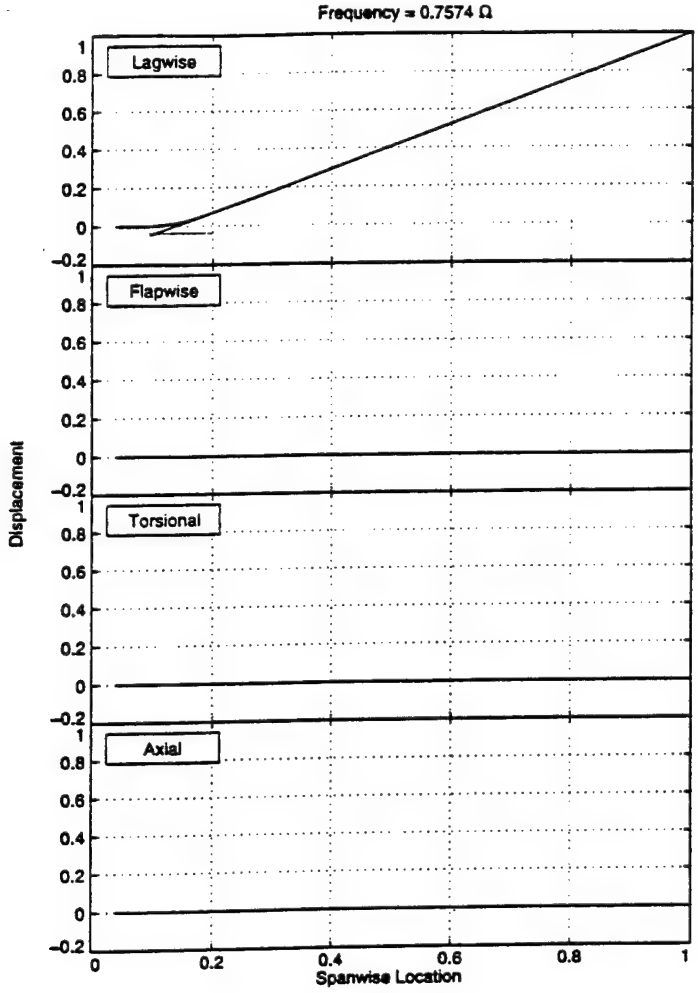

First mode shape (rigid lag) for bearingless rotor

Because no flight test data for a bearingless rotor helicopter are widely available, it was not possible to validate the code fully. (The articulated rotor version of the code had been previously validated using UH-60 data provided by NASA/Army Ames, and a validation of the hingeless rotor version is in progress using BO-105 data provided by ONERA.) A partial validation was performed by comparing its results with those of the comprehensive aeromechanic code UMARC, which can only model nonmaneuvering flight conditions, but which includes a bearingless rotor model. An example of the correlation is shown in the figure below.

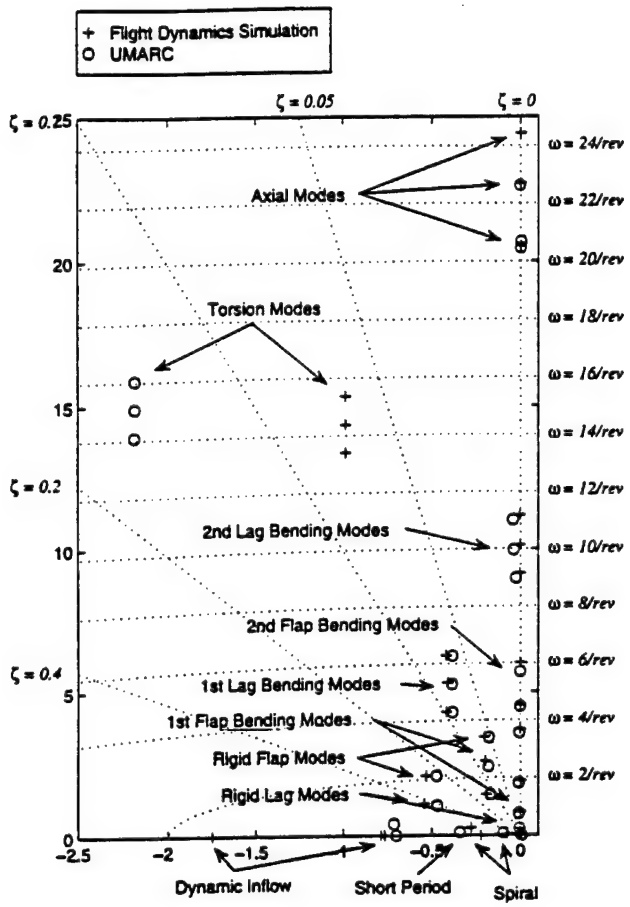

Comparison of poles for helicopter at μ=0.15.

Free flight response to pilot inputs. The response of the aircraft to prescribed pilot inputs is obtain by a direct numerical integration of the nonlinear differential equations of motion. The integration is carried out using a general purpose variable-step variable-order ODE solver.

A small selection of representative results will be provided in this document. The figure above shows the first mode shape for the configuration of this study. The frequency of this mode is 0.76/rev. This is essentially an uncoupled, rigid body lag mode, with the elastic deformation mostly limited to the flexbeam region. The torque tube is largely undeformed, as clearly visible from the figure.

The figure shows the poles for a forward flight condition at an advance ratio of μ=0.15. The agreement between the two codes is good, especially since the two codes are based on very different formulation and solution methodologies. The discrepancy between the torsion poles is due to an error present in UMARC at the time the comparison was performed, and that caused the aerodynamic damping in pitch to be counted twice.

The next figure shows the on-axis frequency response in roll for a straight forward flight condition with μ=0.3. The figure contains curves showing the effect of the number of blade modes used in the modal coordinate transformation. The positions of the poles and zeros of the linearized system in each case are also indicated in the figure. The results show the importance of including at least one torsional mode---torsion is present only in the results with 8 modes.

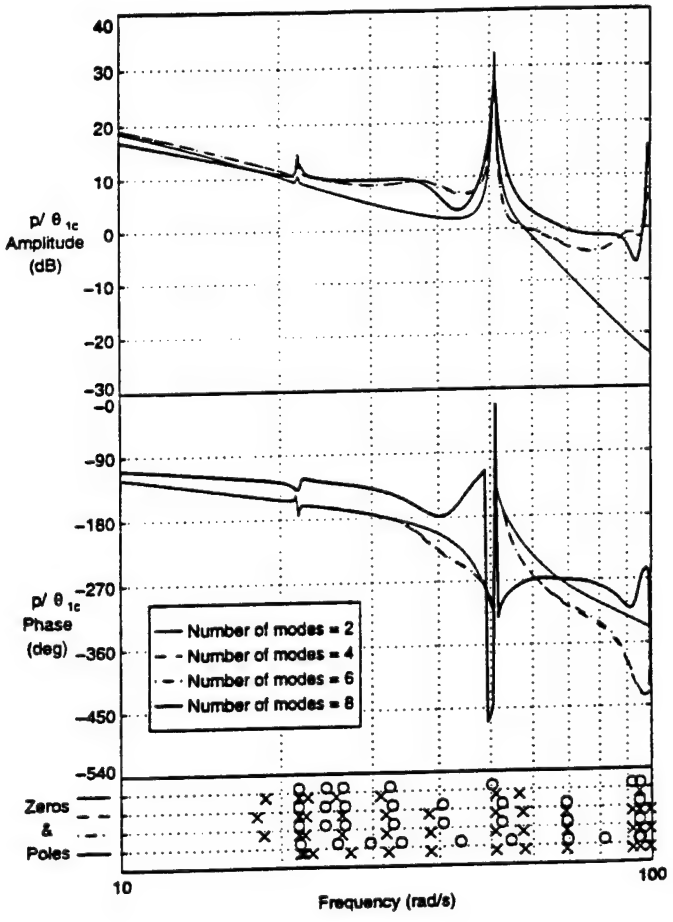

Effect of number of blade modes on the roll rate frequency response to lateral cyclic; advance ratio μ=0.3.

The figure below shows the effect of varying the effective hinge offset on the roll rate frequency response in hover. Increasing the offset from about 10% to about 15% of the rotor radius increases the crossover frequency by almost 2 rad/sec. The phase bandwidth, as defined by the ADS-33 handling qualities specifications, increase by about 1 rad/sec. The changes in gain bandwidth are smaller, and the system remains phase-limited.

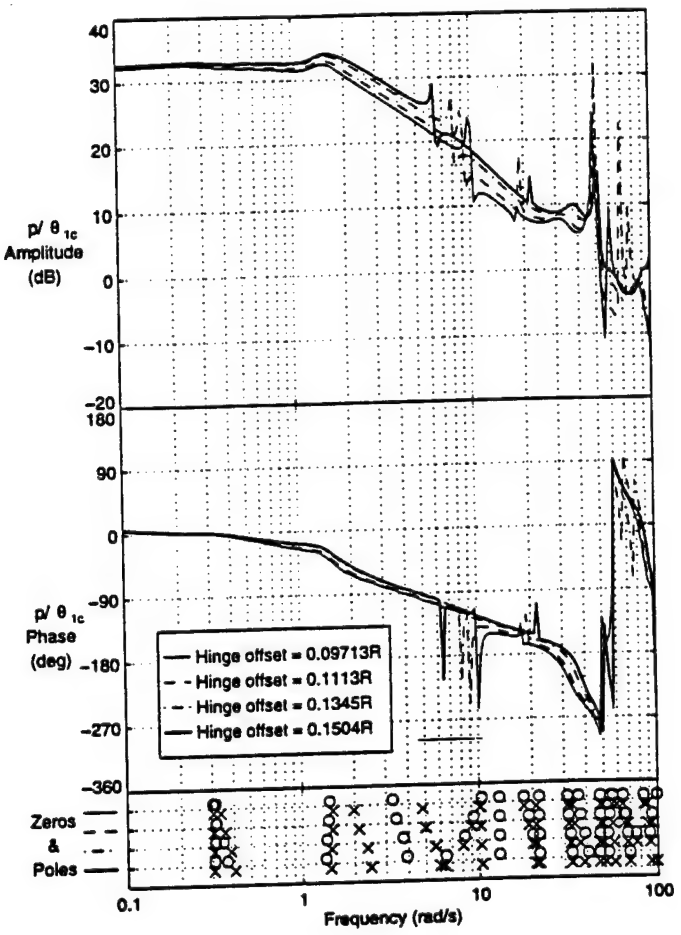

Effect of effective hinge offset on the roll rate frequency response to lateral cyclic; advance ratio μ=0.3.

The next figure again shows the roll rate frequency response. The advance ratio is now μ=0.15 and the various curves show the effect of varying the turn rate. It is interesting to note the behavior in the vicinity of the crossing by the phase curve of the -90° line. In general, all the curves show the expected first-order like trend. However, as the turn rate increases, the relative position of one pole and two zeros changes noticeably. This causes changes in the shape of the phase curve near the -90° crossing. What was a notch-like, substantial phase decrease in straight flight, becomes a small increase and then a rather large peak as the turn rate is increased. The crossing frequency increases from about 4 rad/sec to about 7 rad/sec, and it is

highly dependent on the details of the features of the phase plot. The phase bandwidth is the same at all turn rates except for the highest, for which it decreases dramatically. The gain bandwidth appears to increase substantially with turn rate, but this is due more to the presence of sharp, localized peaks and valleys in the Bode plots than to changes in the fundamental dynamic behavior of the helicopter. The changes at lower frequencies are due to an increasing instability as the turn rate increases. The modes that become unstable are a collective lag mode and a coupled heave/regressive lag mode. The increase in frequency of the former pole can be seen clearly in the lower portion of the figure.

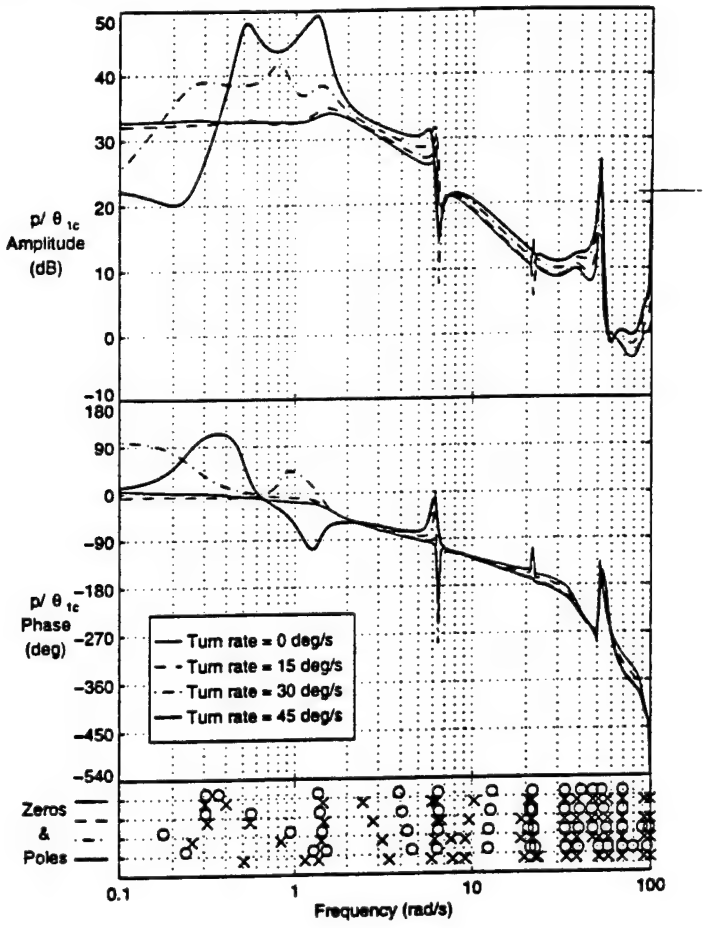

Effect of turn rate on the roll rate frequency response to lateral cyclic; advance ratio μ=0.15.

3.1.2 Formulation of a design-oriented analysis.

Currently, it is often impractical to use optimization methods in aeromechanic and flight dynamic design if the design includes the rotor. An important barrier is the computational cost of calculating the gradients of objective function and constraints

which include the rotor; these gradients are required by the most powerful optimization algorithms currently available. Therefore, the objective of this research was to develop efficient mathematical methods to calculate gradients of behavior quantities with respect to design parameters. "Efficient" means that the total computational cost of calculating a gradient must be substantially less than the two analyses required when finite difference approximations are used. "Behavior quantities" for this study are: (i) the components of the blade root loads (that is the loads in the rotating system), (ii) the components of the hub loads (nonrotating system), and (iii) the characteristic exponents, which determine the stability of the system with periodic coefficients according to Floquet theory. "Design variables" for this study are the blade mass, stiffness, and chordwise position of the cross-sectional center of mass.

The approach is based, first on obtaining an expression of the derivatives using chain-rule differentiation, and then on recognizing that some of the terms in the chain-rule expression are already available as part of the analysis and don't have to be recalculated for the gradients. With the partial exception of the gradients of the characteristic exponents, the quantities that are already available are also those that require the largest computational effort. Thus, the additional cost of calculating the gradient of blade and hub loads with respect to one design variable is of about 5-10% of the cost of one analysis. This is to be compared with an additional cost of 100% (that is another complete analysis) when finite difference approximations are used.

The figure below shows a comparison of the gradient of the root torsion moment with respect to the blade distributed mass, calculated using the semi-analytical method of this study and conventional finite difference approximations. The results refer to a hingeless rotor configuration in straight and level forward flight. Note that the gradient is a time dependent quantity. The dashed lines in the figure are the various component of the semi-analytical derivative. The excellent agreement between the semi-analytical and the finite difference gradients, apparent from the figure, is typical of all the results obtained in the study.

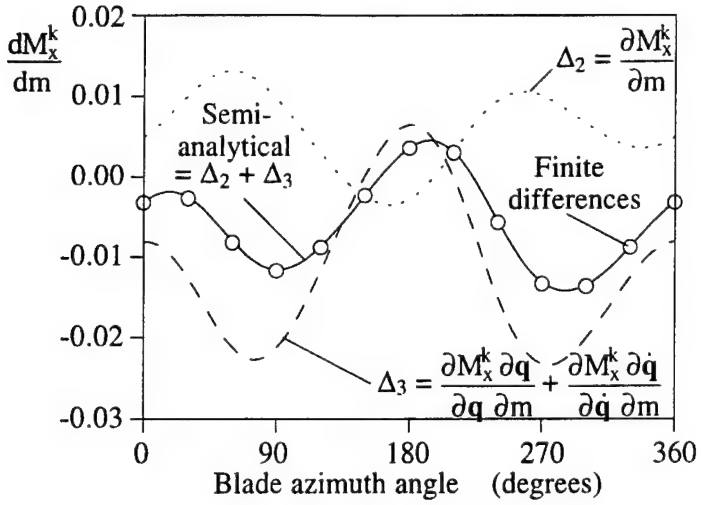

Comparison of finite difference and semi-analytical gradients of root torsion moment with respect to distributed mass

The sensitivity analysis was extended to provide the gradients of the characteristic exponents (which, according to Floquet theory, indicate the linearized aeroelastic stability level of the rotor). The task of calculating these gradients is substantially more complex and computationally intensive than that of calculating gradients of hub and root loads. A change in design parameter affects the characteristic exponents in two different ways. The first, or "linear", is by through the direct changes in the dynamic characteristics of the rotor. The second, or "nonlinear", is due to the changes in trim conditions and in the steady-state periodic equilibrium position about which the equations are linearized. The latter contribution was identified and studied in this research for the first time.

The figures below illustrate a potential pitfall of the use of finite difference based gradients, first identified in the present research. In typical computer implementations, the characteristic exponents are output sorted by real parts. The finite difference sensitivities are then built using the real parts of the characteristic exponents in the same position of the output for the perturbed configuration and for the baseline configuration. The results of this process are shown in the figure below for a perturbation of the distributed mass of the blade. The agreement is excellent for four of the ten characteristic exponents shown in the figure, but only fair for the remaining six. When sorted by real parts, these six exponents are clustered close together. More troublesome, the finite difference and the semi-analytical predictions have the opposite sign for two of the exponents. This means that if these gradients were used in an optimization procedure, the optimizer might be driven into the wrong direction. The reason for this problem is that, when sorted by real parts, some exponents switch positions between the baseline and the

perturbed configurations. In other words, using the k-th item of the baseline and of the perturbed output list of exponents, does not guarantee that one is using the baseline and the perturbed value of the k-th characteristic exponent.

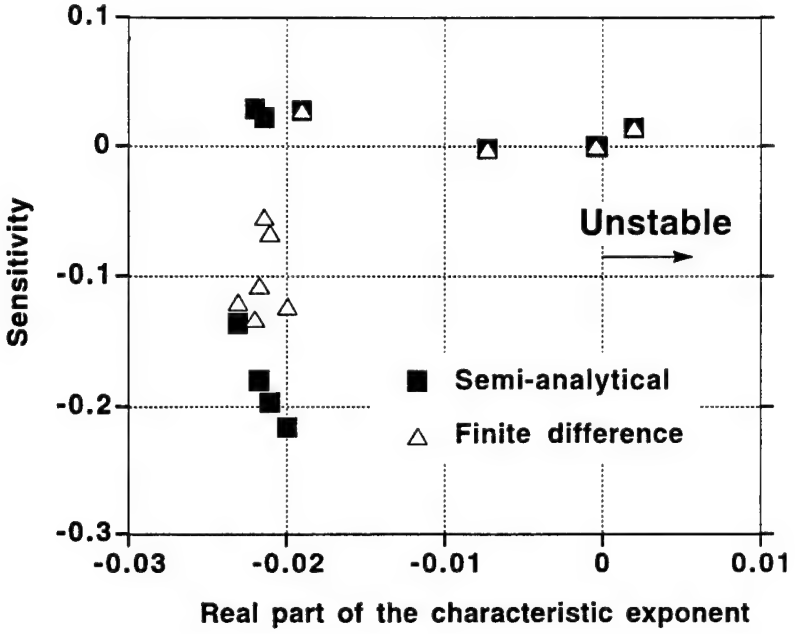

Comparison of semi-analytical and finite difference gradients of the real parts of selected characteristic exponents with respect to rotor blade mass.

Several sorting criteria were explored in this study, but none generated a consistent list of characteristic exponents between the baseline and the perturbed configurations. The criteria included: (i) real part or (ii) imaginary part of the characteristic exponent, (iii) real part or (iv) imaginary part or (v) absolute value of the corresponding characteristic multiplier. The semi-analytical method developed as part of this research does not have this problem because it intrinsically contains eigenvector information, and therefore the correct gradient is always obtained.

Several papers on this work have been prepared:

Spence, A., and Celi, R., "Efficient Sensitivity Analysis for Rotary-Wing Aeromechanical Problems," Proceedings of the AIAA/ASME/ASCE/AHS 34th Structures, Structural Dynamics and Materials Conference, La Jolla, California, April 1993, pp. 3012-3022.

Turnour, S. R., and Celi, R., "Effects of Blade Flexibility on Helicopter Stability and Frequency Response," Proceedings of the Nineteenth European Rotorcraft Forum, Cernobbio, Italy, September 1993.

Celi, R., and Kim, F.D., "Stability and Frequency Response Simulation of an Articulated Rotor Helicopter in Turning Flight," Proceedings of the Nineteenth European Rotorcraft Forum, Cernobbio, Italy, September 1993.

Spence, A., and Celi, R., "Effect of Rotor Design Parameters on Aeromechanic Stability and Flight Dynamics," Proceedings of the NASA/AHS Aeromechanics Specialists Conference, San Francisco, California, January 1994.

Shih, I.-C., Spence, A. M., and Celi, R., "Semi-Analytical Sensitivity of Floquet Characteristic Exponents with Application to Rotary-Wing Aeroelasticity." Proceedings of the 35th AIAA/ASME/ASCE/AHS/ASC Structures, Structural Dynamics and Materials Conference, Hilton Head, S.C., April 1994.

Celi, R., "Aeroelasticity of Helicopters in Maneuvering Flight." Symposium on Aeroelasticity and Fluids/Structure Interaction Problems, International Mechanical Engineering Congress and Exposition, Chicago, IL, November 1994, AD-Vol. 44, pp. 69-98.

Spence, A. M., and Celi, R., "Efficient Sensitivity Analysis for Rotary-Wing Aeromechanical Problems," *AIAA Journal.*, Vol. 32, No. 12, December 1994, pp. 2337-2344.

Spence, A. M., and Celi, R., "Coupled Rotor-Fuselage Dynamics and Aeroelasticity in Turning Flight," *Journal of the American Helicopter Society*, Vol. 40, No. 1, January 1995, pp. 47-58.

Turnour, S. R., and Celi, R., "Modeling of Flexible Rotor Blades for Helicopter Flight Dynamics Applications," *Journal of the American Helicopter Society*, Vol. 41, No. 1, January 1996, pp. 52-66; correction published in Vol. 41, No. 3, pp. 191-193.

plus the dissertations:

Spence, A. M., "A Design-Oriented Aeromechanical Analysis for Hingeless Rotor Helicopters in Straight and Turning Flight," Ph.D. Dissertation, Department of Aerospace Engineering, University of Maryland, College Park, 1994.

Turnour, S. R., "Flight Dynamics Simulation Modeling for Hingeless and Bearingless Rotor Helicopters," Ph.D. Dissertation, Department of Aerospace Engineering, University of Maryland, College Park, 1996.

3.2 Frequency Domain Identification for Coupled Rotor-Fuselage Dynamics

The objective of this research was to develop a series of mathematical tools that would help simplify planning, execution, and interpretation of a state-space, frequency domain based system identification procedure. The construction of these tools start from the recognition that the identification is an unconstrained optimization problem. Therefore, a variety of tools of optimization theory can be usefully applied to the identification. The identification was carried out using simulated flight test data. The research showed that it is possible to identify directly individual elements of the state and control matrices of a state-space model of the helicopter. The sensitivity to noise and inaccuracies of the initial guesses were quantified for some representative examples. The resistance to noise was found to be generally good. The identification is rather insensitive to inaccuracies in the initial guesses, but it is still important to start from the best possible estimates.

A frequency response sensitivity function, which describes the sensitivity of the frequency response of a linear system to changes in elements of the state and control matrices, was defined in this study. Variants of this function were found to be useful in determining which types of inputs and outputs, and over which frequency bands, are the best for the identification of given elements of the state and control matrices. These functions provided quantitative results consistent with engineering judgment, and therefore can help automate some critical phases of the system identification. The figure below shows an example of the use of one of these functions, namely the "cumulative frequency response sensitivity function". The figure shows its value for the speed stability derivative X_u as a function of frequency for the four main pilot control inputs. The fact that the highest values of the function are those for a longitudinal cyclic input, and below 1 rad/sec, indicates that the derivative is best identified from the results of a low frequency longitudinal cyclic sweep.

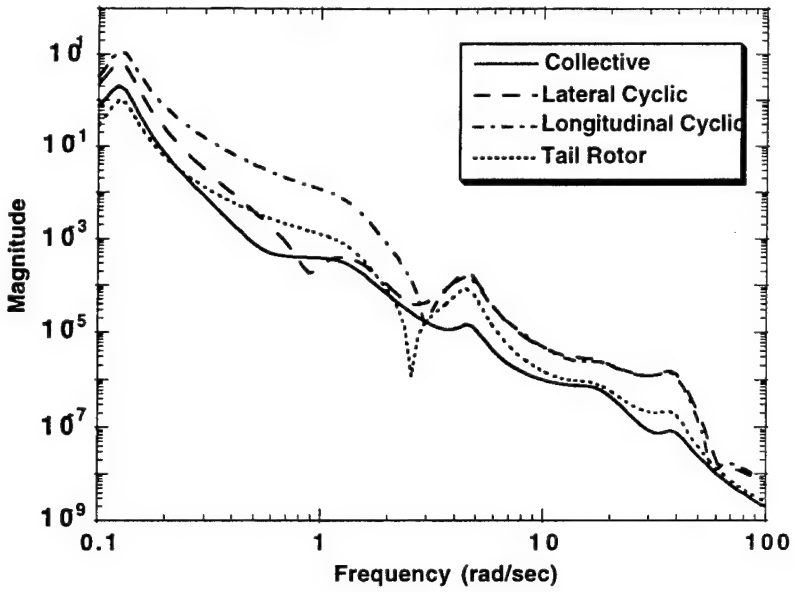

Frequency response sensitivity functions for the speed stability derivative X_u for the four main pilot control inputs.

A technique was developed to determine which elements of the state-space model are important over given frequency bands, and to identify the elements in each frequency band independently. The accuracy of this "frequency-banded" identification was found to be comparable or better than that obtained from a simultaneous identification of all the unknown elements, and the computational cost is lower. The table below shows some representative results.

	CPU Time	Average Pole Error		
Method	(Minutes)	Rotor	Fuselage	Total
Baseline	160	1.58%	6.56%	3.24%
Frequency-Banded	94	1.17%	5.89%	2.75%

The table shows the required CPU time and the error in both types of identification. The accuracy of the prediction of the poles of the identified system was chosen as an overall measure of the accuracy of the entire identification. The CPU time shown for the frequency-banded identification was the sum of the times required for the two portions in which the identification had been divided, namely a high frequency identification and a low frequency identification. The rotor and fuselage pole error data represent the average of the relative errors for all the poles in the respective portion of the model.

A method was also developed to calculate the sensitivity of the eigenvalues of the aeromechanic response of the helicopter to changes in elements of the state matrix of the system. Using this method it was possible to determine which elements of the state matrix most affected the accuracy of a given pole, and therefore the identification could be focused on precisely those elements.

Several papers on this work have been prepared:

Jones, C. T., and Celi, R., "Determination of Rotor Damping From Simulated Data Using Frequency Domain System Identification." Proceedings of the 36th AIAA/ASME/ ASCE/AHS/ASC Structures, Structural Dynamics and Materials Conference, New Orleans, LA, April 1995.

Jones, C. T., and Celi, R., "Frequency Response Sensitivity Functions for Helicopter System Identification," Proceedings of the AHS Northeast Region International Technical Conference, Stratford, CT, October 1995, pp. 4.70-4.87.

Jones, C. T., and Celi, R., "Frequency Response Sensitivity Functions for Helicopter System Identification," *Journal of the American Helicopter Society.*, Vol. 42, No. 3, July 1997, pp. 244-253.

plus the dissertation

Jones, C.T., "Contributions to Helicopter Frequency Domain System Identification," Ph. D. Dissertation, Department of Aerospace Engineering, University of Maryland, College Park, 1997.

3.3 Multidisciplinary optimization of airframe and flight control system

The objectives of this study were: to develop mathematical tools to integrate the optimization of a helicopter rotor and flight control system subject to simultaneous aeroelastic and handling qualities constraints; to study the basic mathematical features of the optimization problem; and to study its practical implications on helicopter design.

The objective functions to be minimized were the cumulative violation of the constraints, if it was not possible to obtain a feasible design, or the swashplate control effort if a feasible design was possible. The set of design variables consisted of three rotor variables (stiffness of lag and flap springs and flap-lag elastic coupling factor) plus five flight control system variables per flight condition (feedback gains and poles in prefilter block). The constraint set was composed of constraints on the aeroelastic stability of the rotor, plus a variety of constraints associated with the ADS-33 handling qualities specifications. These constraints were obtained by reformulating a representative subset of ADS-33 criteria in inequality form; the subset included constraints on the shape of the frequency response plots, on pole

placement, and on the time histories of the response following a moderately large and large pilot inputs.

A basic mathematical property of the design space defined by the combined aeroelastic and handling qualities constraints is that it is not convex. For example, the constraint on the aeroelastic stability of the regressive lag mode creates a "ridge" in the design space, and the optimizer will drive the design to two very different rotor configurations depending on the initial rotor design. The figure below shows the constraint as a function of flap and lag frequencies (recall that the constraint is satisfied if its value is negative).

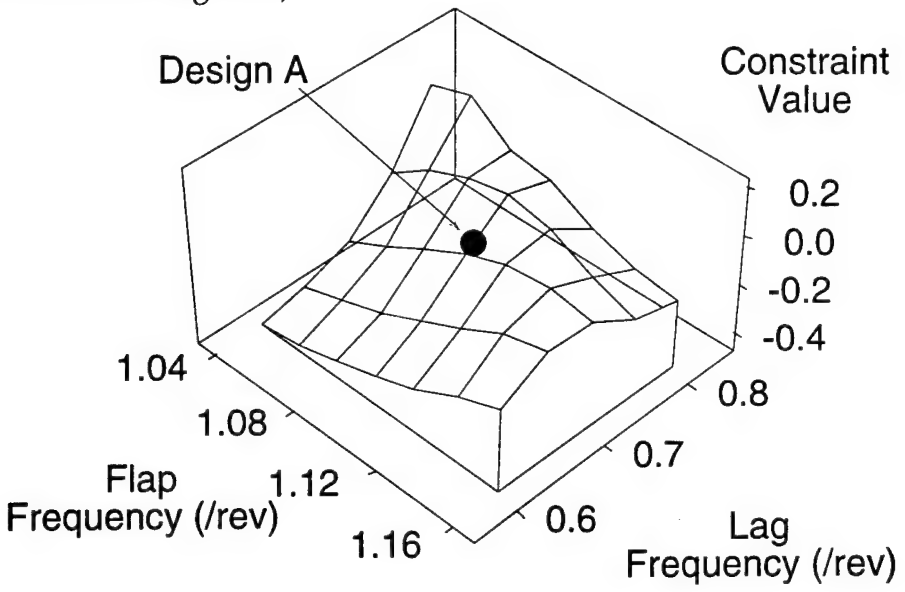

Constraint enforcing stability of the regressive lag mode.

It was not possible to satisfy the entire set of handling qualities constraints using just the three rotor design parameters, but feasible designs could be obtained using both rotor and flight control system design variables. The results also indicate that if the design is optimized for one flight condition, optimizing the rotor and the flight control system simultaneously leads to substantially better designs (i.e., designs with lower required control effort) than by optimizing the rotor first, and the flight control system next. This is clearly shown in the figure below, in which the iteration history of the objective function is plotted for the two design methodologies. In both cases the initial design is the best that could be obtained without changing the flight control system parameters. In the case denoted with "Sequential Optimization" the flight control system is optimized but the rotor design variables are frozen at their initial value. In the case denoted with "Integrated Optimization" both rotor and flight control system parameters are optimized.

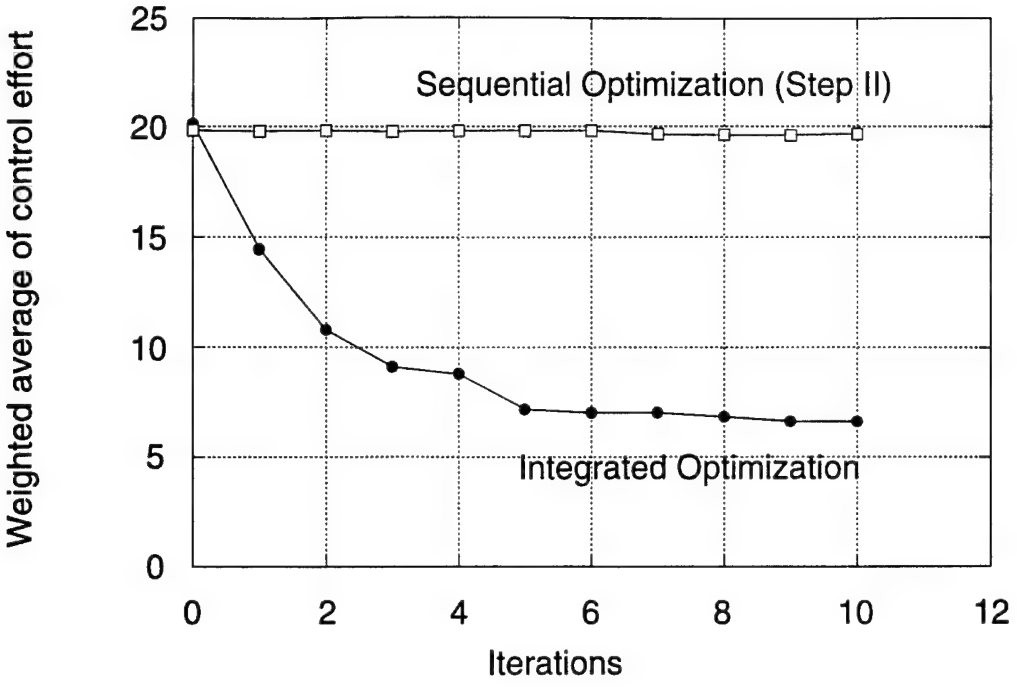

Comparison of the results of two different optimization procedures.

Two problems observed while carrying out a simultaneous rotor/flight control system optimization were the high computational requirements and the non-robustness of the optimal design. Therefore, a subsequent objective of the research was to design methods that would alleviate these problems.

The high computational requirements were due in large part to the many calculation of the helicopter response to pilot inputs required to generate the gradients of the constraints associated with the moderate amplitude (quickness) criteria of ADS-33. Because these gradients were calculated using finite difference approximations, the calculation of each gradient required the evaluation of one baseline response plus as many responses as there were design variables. This resulted in hundreds of such calculations in a typical optimization. Therefore, a new technique for an efficient calculation of these gradients was developed. This technique was based on obtaining a low order linear model of the helicopter that matched the frequency response of the full model in a frequency band between about 1 and 15 rad/sec. Then, the calculations required for the evaluation of the gradient were performed on the low order linear approximation rather than the full order nonlinear model. This technique was accurate enough to obtain good approximations to the gradients of the response (although not enough for the evaluation of the response itself), and led to a reduction of computational requirements of between one and two orders of magnitude.

The second problem encountered in the optimization, namely the lack of robustnes of the optimum (i.e., if the design was optimized at one advance ratio, the design

would become non-optimal and even infeasible at other advance ratios), was greatly alleviated by using special robustness constraints based on results of multivariable feedback control theory. This work was performed outside the period covered by the present final report, and therefore is not further described here.

Several papers on this work have been prepared:

Sahasrabudhe, V., Celi, R., and Tits, A., "Integrated Rotor-Flight Control System Optimization with Aeroelastic and Handling Qualities Constraints," Proceedings of the 51st Annual Forum of the American Helicopter Society, Ft. Worth, TX, May 1995, pp. 905-923.

Sahasrabudhe, V., and Celi, R., "Efficient Treatment of Moderate Amplitude Constraints for Handling Qualities Design Optimization," Proceedings of the 52nd Annual Forum of the American Helicopter Society, Washington, DC, June 1996, pp. 1253-1270.

Sahasrabudhe, V., Celi, R., and Tits, A., "Integrated Rotor-Flight Control System Optimization with Aeroelastic and Handling Qualities Constraints," Journal of Guidance, Control, and Dynamics. Vol. 20, No. 2, March April 1997, pp. 217-225.

Sahasrabudhe, V., and Celi, R., "Efficient Treatment of Moderate Amplitude Constraints for Handling Qualities Design Optimization," accepted for publication in the *Journal of Aircraft*.

plus the dissertation:

Sahasrabudhe, V., "Multidisciplinary Optimization of a Helicopter Rotor and Flight Control System," Ph. D. Dissertation, Department of Aerospace Engineering, University of Maryland, College Park, 1996.

COMPOSITE STRUCTURES

COMPOSITE STRUCTURES

Task 4

Anthony J. Vizzini

4.1 Structural Integrity

Structural integrity of tapered structures was investigated in two areas. The first was an extension of the analytical effort by the implementation of a shear-lag analysis to describe the method that load is transferred in the tapered region. The second was part of the enhancement program and involved sandwich to laminate tapered structure.

The region around a terminated ply was modeled as several elastic layers separated by shear regions. A shear-lag analysis was then performed allowing for the thickness of the elastic and shear layers to vary. Boundary conditions, away from the ply drop, were based on the deflections determined by a finite element model. The interlaminar stresses were compared against those generated by the finite element model for tapered laminates under pure extension, pure bending, and extension-bending coupling. The shear-lag analysis predicted the interlaminar shear at and near the ply drop for pure extension and in cases involving bending if the deflections due to bending were removed (Figures 3--5). The interlaminar shear stress and force equilibrium were used to determine the interlaminar normal stress. The trends in the interlaminar normal stress shown by the finite element model were partially captured by the shear-lag analysis (Figures 6--8). This simple analysis indicated that the mechanism for load transfer about a ply drop is primarily due to shear transfer through the resin rich areas.

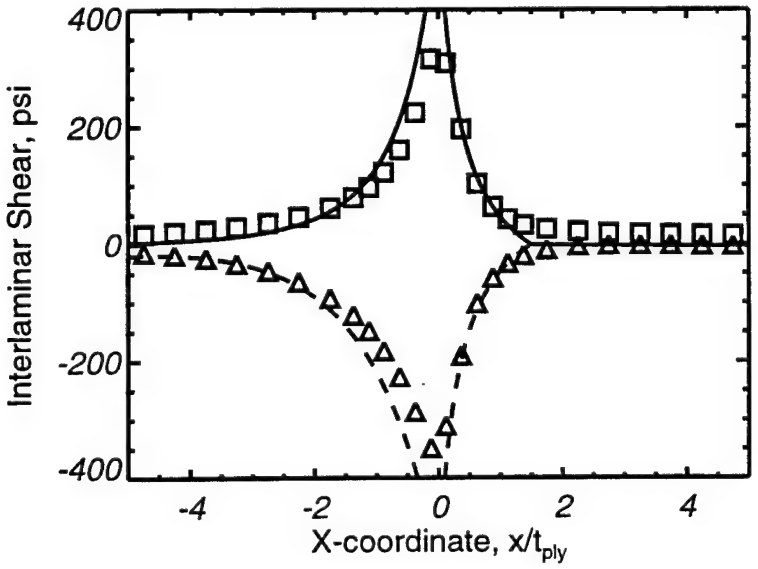

Figure 3 Interlaminar shear stress for symmetric tapered laminate under uniaxial tension

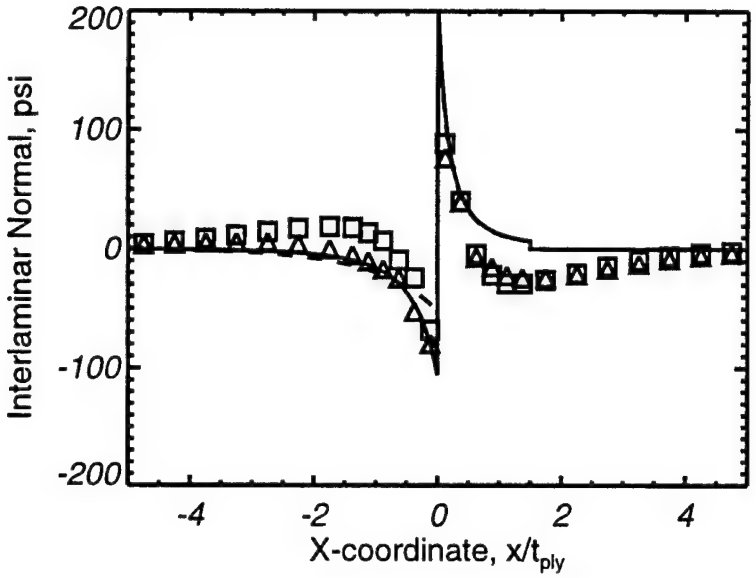

Figure 4 Interlaminar normal stress for symmetric tapered laminate under uniaxial tension

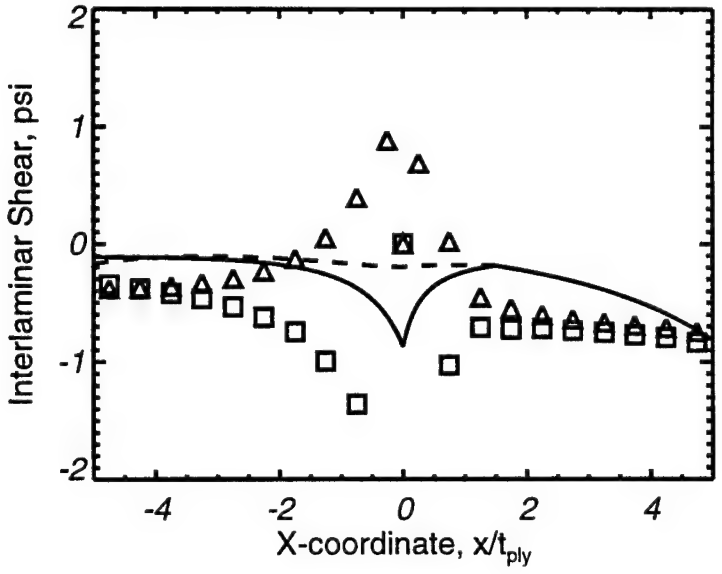

Figure 5 Interlaminar shear stress for symmetric tapered laminate under bending deflection

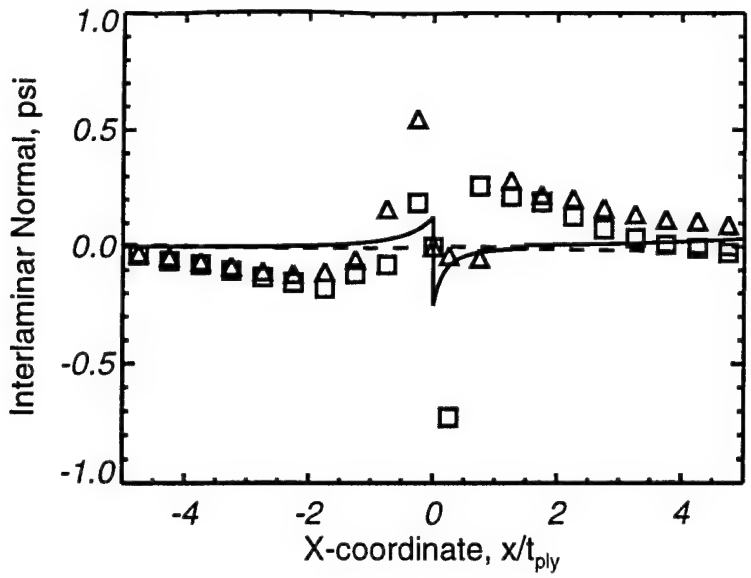

Figure 6 Interlaminar normal stress for symmetric tapered laminate under bending deflection

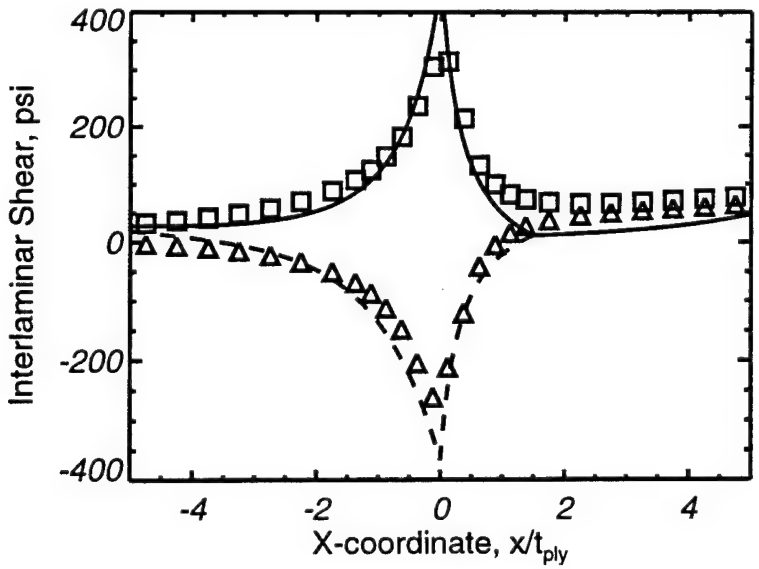

Figure 7 Interlaminar shear stress for unsymmetric tapered laminate under uniaxial tension

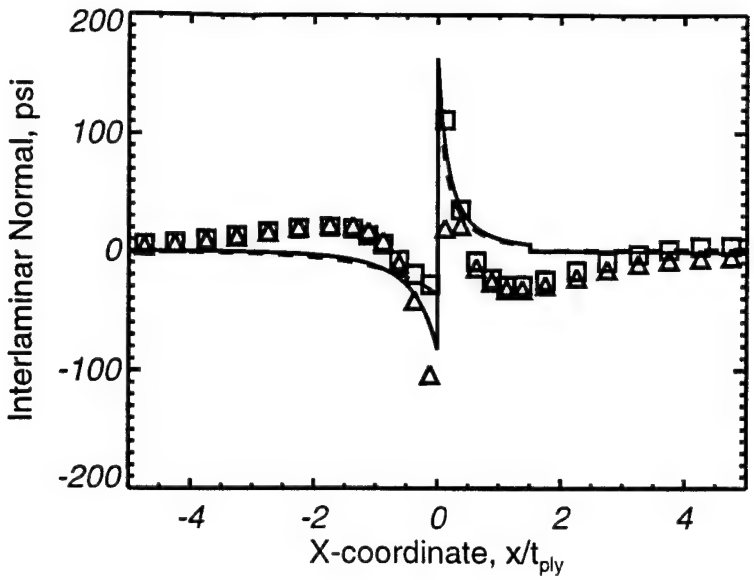

Figure 8 Interlaminar normal stress for unsymmetric tapered laminate under uniaxial tension

A total of 36 unidirectional graphite-epoxy/Rohacell foam core structures were manufactured with varying taper angles and core thicknesses. The specimens were subjected to tensile, compressive, and bending loads. Initial failure occurred at the root of the taper for specimens tested in tension and compression while specimens tested in bending were observed to fail via debonding between the core and facesheet away from the root of taper. The initial failure load for the tension specimens was found to be dependent upon the core thickness and not the taper angle, while the failure load for the compression specimens was found to be virtually independent of both the core thickness and taper angle. In addition, out-of-plane bending deformations resulted in significant load redistributions in the tapered sandwich structures.

Experimental data were correlated to a three-dimensional finite-element model with resin-rich areas located between the sandwich core and the upper and lower facesheets. The model predicted an increase in the interlaminar stresses in the resin layers at the root of the taper for all three loading scenarios. Through comparison of the experimental data and the rate of change in these interlaminar stresses for different tapered geometries, the interlaminar shear stress, xz, was found to govern initial failure for both tension and compression specimens.

4.2 Multiaxial Energy Absorption

The energy absorption of composite materials was investigated along multiple paths. The effect of side loads on Kevlar/epoxy truncated cones was determined experimentally. In addition, a flat-plate testing methodology was developed to assist

in the development of analytical tools to predict the energy absorption capability of a given structure under off-axis loads.

Tapered, truncated cones were manufactured from net-resin American Cyanamid K-49 Kevlar/epoxy preimpregnated tapes and were crushed quasistatically under uniaxial loadings. The effects of taper angle and load incidence angle on the energy absorption characteristics were determined (Figure 1). In general, Kevlar/epoxy is less sensitive to off-axis loadings than similar graphite/epoxy cones; however, it only absorbs about half as much energy per unit mass. Highly tapered Kevlar/epoxy cones (10 degrees) actually absorb more energy than nearly cylindrical cones. The energy absorption and post-crush structural integrity of the cones is related to observed failure modes.

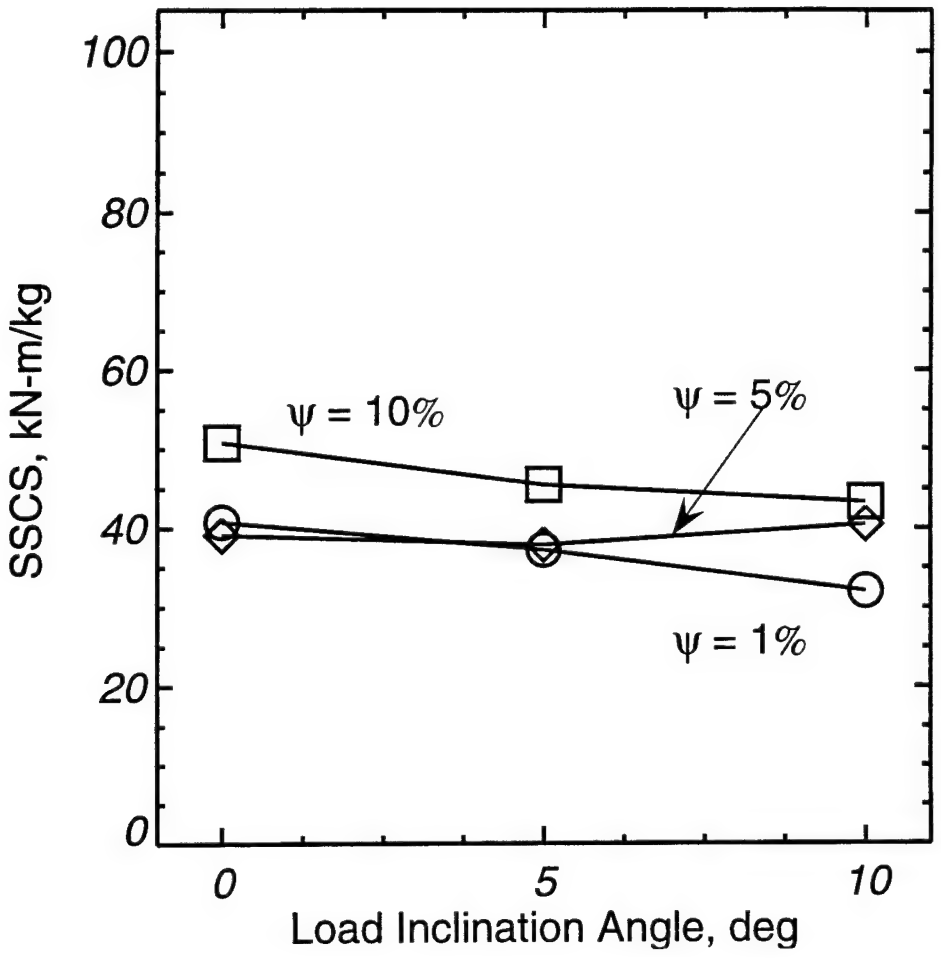

Figure 1 Energy Absorption of Kevlar/Epoxy

The characterization of the off--axis crushing of composite materials was investigated experimentally and analytically. A fixture for crushing plate specimens against an adjustable inclined plane was developed. The fixture stabilized the plates by providing simply-supported boundary conditions on the sides. Graphite/epoxy

plates were crushed and their energy absorbency measured. Consistent data were obtained that were similar to those obtained using different specimen geometries, indicating the acceptability of the testing method. Energy absorbing performance of the observed failure modes was assessed. A phenomenological finite element model was developed based upon the experimentally observed failure modes (Figure 2). The model was based upon quasistatic crack growth along ply interfaces and resulted in a one-parameter representation to predict the failure mode at a given ramp angle. No quantitative performance estimation was provided by the model. The model and the experimental results together provided a hybrid method whereby the crushing performance can be predicted for a given loading condition.

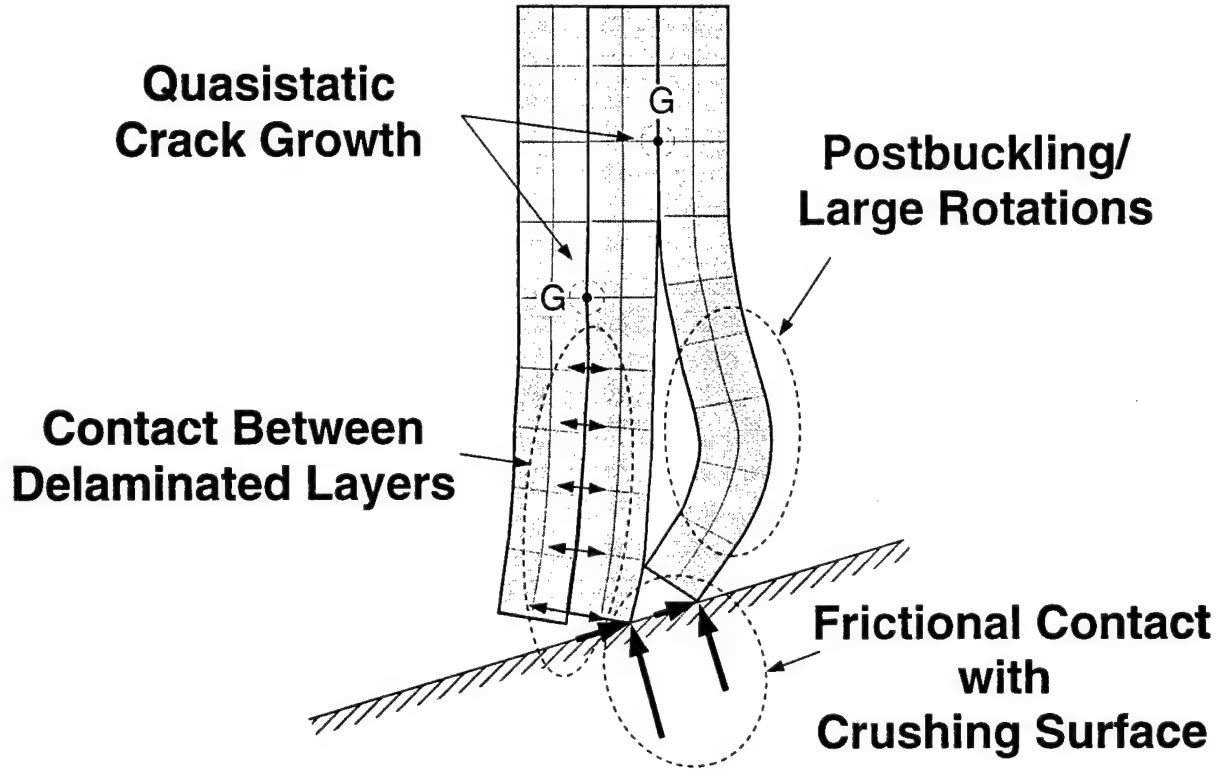

Figure 2 Schematic drawing of analytical model

4.3 Helicopter Rotor-System Health Monitoring

Ranjan Ganguli and Inderjit Chopra

The helicopter rotor operates in a highly dynamic and unsteady aerodynamic environment leading to severe vibratory and fatigue loads on many critical components within the enginer, transmission, drive-shaft and rotor-system. Repeated exposure to this severe loading condition can induce damage in critical structural components, which, if unchecked, could lead to failure. To address this problem, damage sensitive parts are frequently inspected and often, prematurely

replaced. This leads to higher operating and maintenance costs. In addition, excessive downtime of helicopters for inspection and maintenance may reduce availability and even jeopardize the mission. The need for a sizable reduction in the operating costs and for enhancement of flight reliability has directed attention to the development of rotorcraft health monitoring systems. In this task, a mathematical model of the rotor system is used to examine the system response of the helicopter due to selected rotor blade damages.

A helicopter rotor-system damage detection methodology is formulated for an articulated rotor in hover, and in forward flight. Damages modeled are moisture absorption, loss of trim mass, misadjusted pitch-link, damaged pitch-control system and inoperative lag damper. These damages are represented by changes in mass, stiffness, damping and aerodynamic properties of the rotor blade. A rotor aeroelastic analysis based on finite element discretization in space and time, and capable of modeling dissimilar blades, is used to simulate the undamaged and the damaged rotor. Changes in rotor system faults are identified for the selected faults and tables of rotor system diagnostics are compiled.

For a N-bladed undamaged rotor, the N/rev forces and moments are transmitted by the rotor to the fuselage. For a damaged rotor, all harmonics of rotor forces and moments are transmitted to the fuselage. For example, Fig. 1 shows the vertical hub shear for the undamaged rotor and a rotor with a damaged lag damper. Rotor faults detectable from blade tip response include moisture absorption, misadjusted pitch-link, damaged trailing edge flap and damaged pitch-control system. Rotor faults detectable from vibratory hub forces include moisture absorption, loss of trim mass, damaged pitch-control system and damaged lag damper. Finally, rotor faults detectable from vibratory hub moments include misadjusted pitch-link, damaged trailing-edge flap and damaged pitch-control system.

The simulated fault data obtained from the mathematical model of the damaged rotor system is used to develop a neural network based approach for rotor system health monitoring. Both single and multiple faults on the damaged rotor blade are considered. A feedforward neural network with backpropagation learning is trained using both "ideal" and "noisy" data. Testing of the trained neural network shows that it can detect and identify damage in the rotor system from simulated blade response and vibratory hub loads data. A neural network trained on "noisy" data shows better damage detection capability than a network trained on "ideal" data alone, especially when the test data are polluted with noise (Fig. 2).

When the blade tip response, hub forces and hub moments are used together to train the network, damage can be detected without relying significantly on higher harmonic data. For the damages investigated it was found that monitoring the steady lag and flap response, 1/rev flap response, 1/rev longitudinal and lateral forces, 1/rev and 3/rev vertical forces, 4/rev rolling moment and 1/rev pitching moment data was sufficient for detection and identification.

The variation of system parameters with respect to the selected damage level is linear for moisture absorption, mildly nonlinear for damaged lag damper, and highly nonlinear for the damaged pitch-control system. The nonlinear and complicated behavior of the system parameters with respect to damage level for the damaged pitch-control system may be due to strong interactions between the elastic twist and the unsteady and nonuniform aerodynamic flowfield around the rotor disk in forward flight.

Publications:

Ganguli, R., Chopra, I. and Haas, D., "Formulation of a Rotor Head Damage Detection Methodology," *36th AIAA/ASME/ASCE/AHS/ASC Structures, Structural Dynamics and Materials Conference and Adaptive Structures Forum,*, New Orleans, LA, April 1995. Also, *Journal of American Helicopter Society*, Vol. 41, No. 4, October 1996, pp. 302-312.

Ganguli, R., Chopra, I. and Haas, D., "Helicopter Rotor-System Damage Detection," American Helicopter Society 2nd International Aeromechanics Specialists' Conference, Bridgeport, CT, Oct. 1995.

Ganguli, R., Chopra, I. and Haas, D., "Simulation and Detection of Rotor-System Faults Using Neural Networks," *37th AIAA/ASME/ASCE/AHS/ASC Structures, Structural Dynamics and Materials Conference and Adaptive Structures Forum*, Salt Lake City, Utah, April 1996, also *Journal of the American Helicopter Society*, Vol. 42, No. 2, April 1997, pp. 161-171.

Ganguli, R., Chopra, I. and Haas, D.J., "A Physics Based Model for Rotor System Health Monitoring," Proceedings of the 22nd *European Rotorcraft Forum* and 13th European Helicopter Association Symposium, Brighton, UK, September 1996.

Ganguli, R., Chopra, I. and Haas, D.J., "Helicopter Rotor System Health Monitoring Using Numerical Simulation and Neural Networks," *53rd Annual Forum of the American Helicopter Society*, Virginia beach, VA, April 1996.

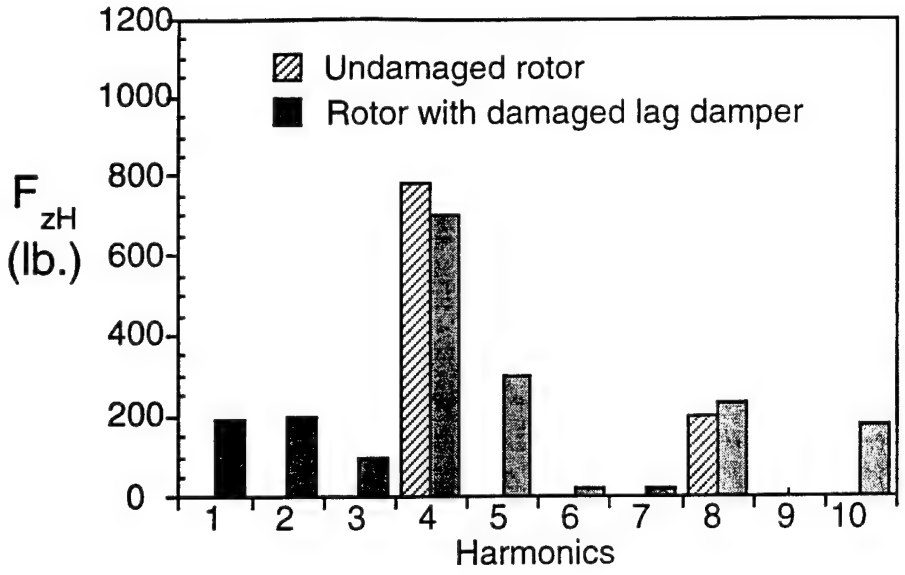

Fig. 1. Vibratory vertical hub shear for the damaged and undamaged rotor (μ=0.3, C_T/σ=0.073)

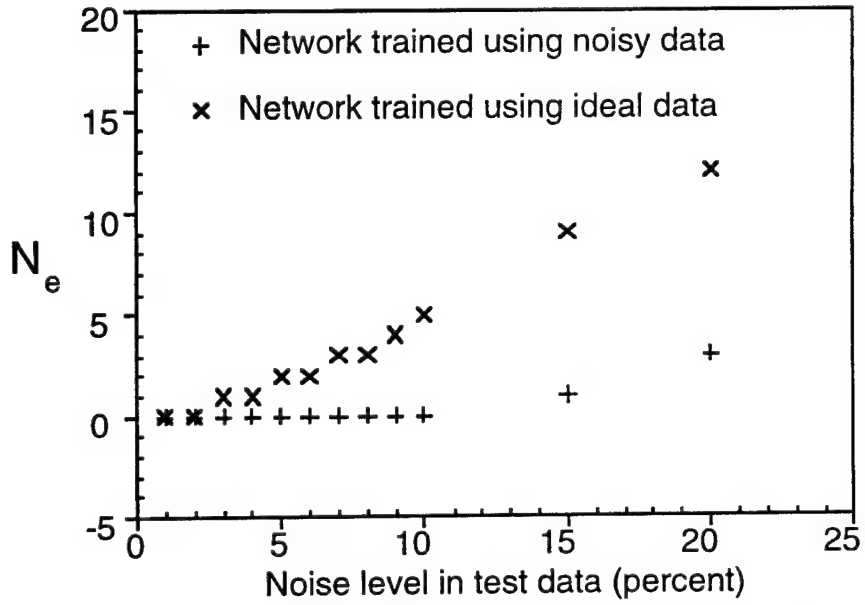

Fig. 1. Number of errors in pattern classification with increasing noise level for neural network trained on ideal data and noisy data (all test data simultaneously presented to the trained network)

4.4 Elastomeric Damping

Farhan Gandhi and Inderjit Chopra

Elastomeric lag dampers are becoming an increasingly common feature on advanced rotor systems such as bearingless main rotors. Since the behavior of these dampers is nonlinearly dependent on the amplitude and frequency of motion, as well as temperature, they have traditionally been difficult to model analytically. In this research, a representation for elastomeric dampers as a combination of linear and nonlinear springs and dashpots was developed, and the spring and dashpot parameters were determined by comparison with experimental damper data. The damper behavior was then described by a *nonlinear differential equation* in the *time domain*. Such a representation is very powerful and versatile and can be easily used in multi-frequency excitation conditions, at various equilibrium preloads, and for large amplitude oscillations. The damper model was integrated into rigid blade representations of articulated and hingeless rotors, and its effect on hover aeromechanical stability and forward flight aeroelastic stability was examined.

Subsequent efforts included: (*i*) refined damper modeling - to represent *reduced damping at small dynamic amplitudes* and the associated occurrence of *limit cycle oscillations* (*ii*) integration of the refined damper model into the new bearingless main rotor model in the comprehensive analysis, UMARC, and (*iii*) examination of the effects of the nonlinear elastomeric damper on the dynamics and aeroelasticity of bearingless main rotor helicopters.

Refined Damper Modeling

It has been recently observed that the complex modulus component G" (a measure of the damping in the system) of the elastomeric damper shows a sharp decrease at small dynamic amplitudes. The original spring-dashpot model was augmented with additional nonlinear springs S3 and S4 (Figure 1) to represent this phenomena. The nonlinear force/displacement behavior of springs S3 and S4 is chosen such that the augmented model only causes a decrease in G" at small dynamic amplitudes and has no effect on G' and G" elsewhere. Figures 2a and 2b show the variation of G' and G" with dynamic amplitude for the old and refined models, respectively. The reduced damping at small dynamic amplitudes, in conjunction with negative aeromechanical damping, can result in limit cycle oscillations shown in Figures 3a and 3b.

Integration into Bearingless Main Rotor Analysis

Since the damper nonlinear constitutive equation contains *derivative of damper force*, an explicit expression for damper force in terms of damper motion is not available. The damper constitutive differential equation is solved simultaneously

with the rotor-fuselage equations, with damper force as an *independent state*. Since the elastomeric damper is attached between the flexbeam and torque tube of the bearingless main rotor (Figure 4), the damper motion is expressed in terms of the nodal geometric displacements and velocities at the flexbeam and torque tube points of attachment. These are further expressed in terms of modal coordinates, since the rotor equations are expressed in terms of a few modes to reduce computational expense. In the evaluation of the rotor and damper periodic response using temporal finite elements, the modal coordinates *as well as the independent damper state* are calculated at a number of azimuthal locations. Stability of the system is evaluated by carrying out a Floquet analysis of the perturbation rotor-fuselage-damper equations about the equilibrium condition.

Effects on Bearingless Rotor Dynamics and Aeroelasticity

Two Dampers, A and B, of increasing strength but similar nonlinear characteristics were considered. Figure 5 shows the blade periodic tip lag response at an advance ratio of 0.15. It is seen that the lag response *increases* with increasing damper strength. This can be attributed to the increased lag frequency (due to damper stiffness) being closer to the forcing frequency (1/rev). As the amplitude of periodic damper motion increases with increasing forward flight speed, the decrease in G" (Figures 2), generally, causes the lag mode stability to reduce (Figure 6). For the weaker damper, A, a slight increase in lag mode stability may be seen at higher advance ratios due to the increase in aerodynamic damping. Other observations made included the variation of second lag frequency with advance ratio, due to the nonlinear characterization of the damper, and the effect of the damper impedance on the lag mode shapes.

Publications:

Gandhi, F. and Chopra, I., "An Analytical Model for a Nonlinear Elastomeric Lag Damper and its Effect on Aeromechanical Stability in Hover," *American Helicopter Society Aeromechanics Specialists Conference*, san Francisco, California January 1994. Also, *Journal of the American Helicopter Society*, Vol. 39, No. 4, 1994, pp. 59-69.

Gandhi, F. and Chopra, I., "A Nonlinear Viscoelastic Damper Model: Constitutive Equation and Solution Scheme" *1994 North American Conference on Smart Structures and Materials*, Orlando, Florida, Feb. 1994. *Smart Materials & Structures*, Vol. 5, No. 5, October 1996, pp. 516-528.

Gandhi, F. and Chopra, I., "Elastomeric Lag Damper Effects on Flap-Lag Stability in Forward Flight" *35th AIAA/ASME/ASCE/AHS/ASC Structures, Structural Dynamics and Materials Conference*, Hilton Head, SC, April 1994.

Gandhi, F. and Chopra, I., "Analysis of Bearingless Main Rotor Dynamics with the Inclusion of an Improved Time Domain Nonlinear Elastomeric Damper Model,"

51st Annual Forum of the American Helicopter Society, Fort Worth, Texas, May 1995, Also, *Journal of American Helicopter Society*, Vol. 41, No. 3, July 1996, pp. 267-277.

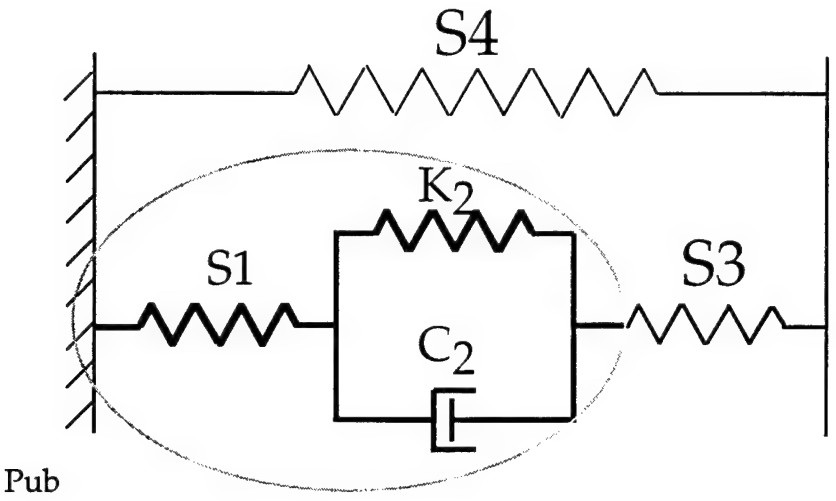

Figure 1: Refined spring-dashpot model for elastomeric damper with additional nonlinear springs S3 and S4

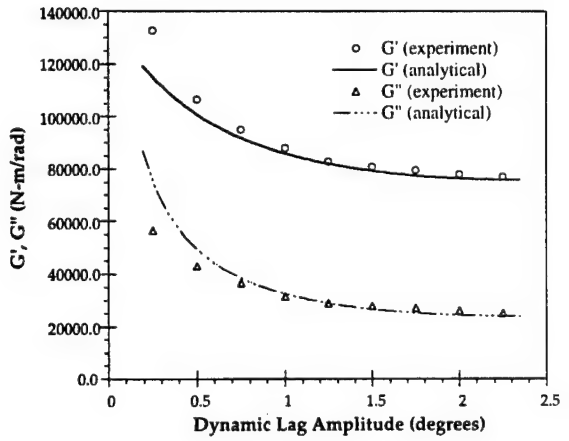

Figure 2a: Variation of Complex Moduli G′ and G″ with dynamic lag amplitude (old model)

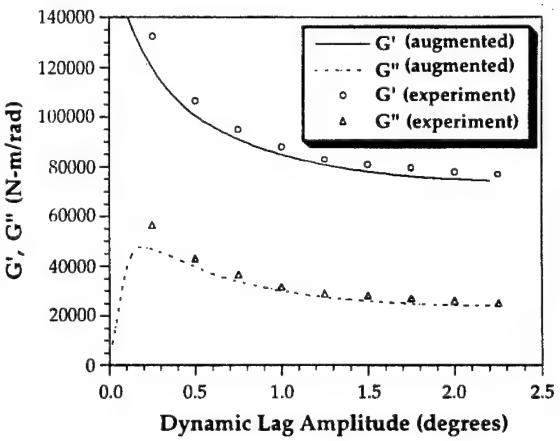

Figure 2b: Variation of G′ and G″ with dynamic lag amplitude (augmented model)

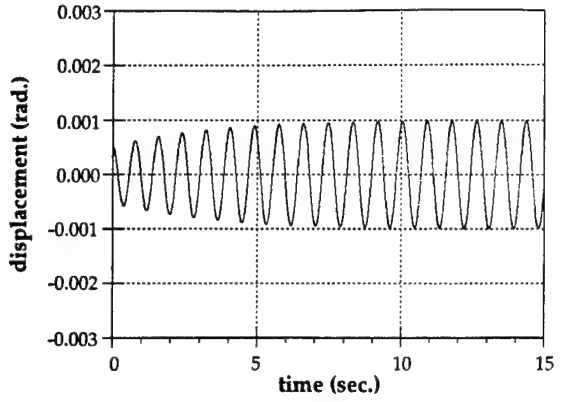

Figure 3a: Limit cycle oscillations for small initial perturbation

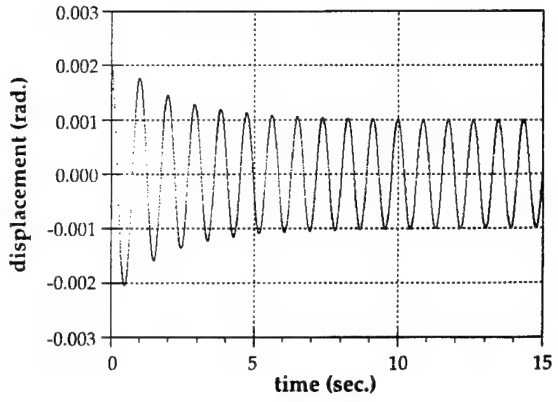

Figure 3b: Limit cycle oscillations for large initial perturbation

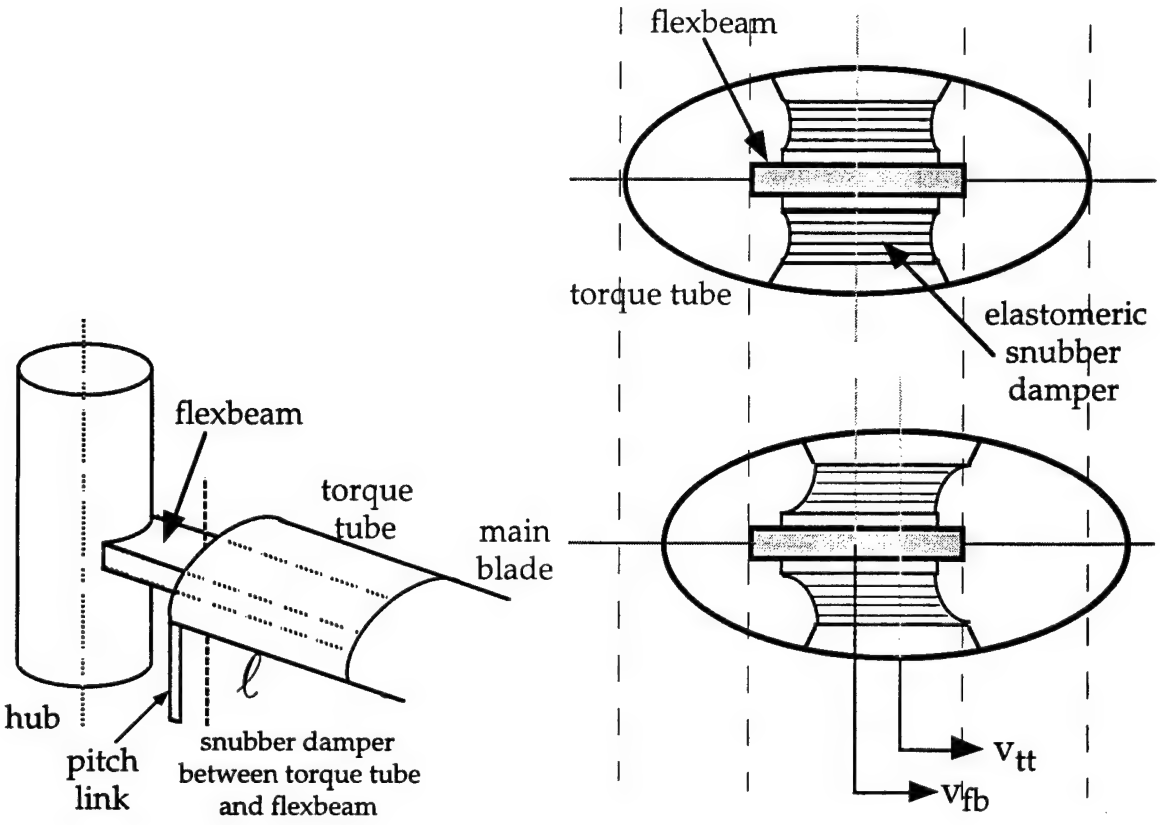

Figure 4: Elastomeric snubber damper at bearingless rotor hub. Attached between inboard end of torque tube and flexbeam - shears during relative lag motion

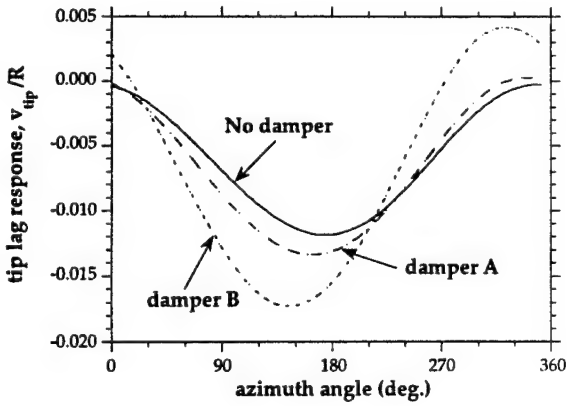

Figure 5: Periodic tip lag response at mode advance ratio 0.15

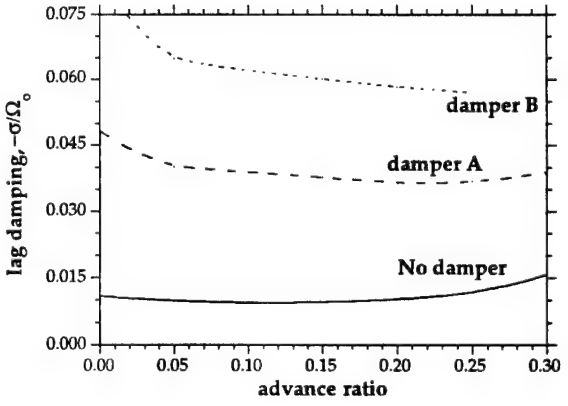

Figure 6: Bearingless rotor shaft-fixed lag tability with inclusion of elastomeric dampers

4.5 Repair of Composite Structures

The bonded repair of minimum-gage sandwich structures was investigated both experimentally and analytically. Graphite/epoxy sandwich specimens with three-ply facesheets were compression tested to investigate the percentage of strength recovery and failure mode of repairs with various numbers of plies in the patch. The test matrix included virgin (undamaged) specimens for use as a baseline, damaged specimens without a patch, and damaged specimens with one-, two- and three-ply patch repairs (Figure 9). The test results indicated that the patched specimens failed initially inside the repaired area followed closely by catastrophic failure either in the patched region or in the net section.

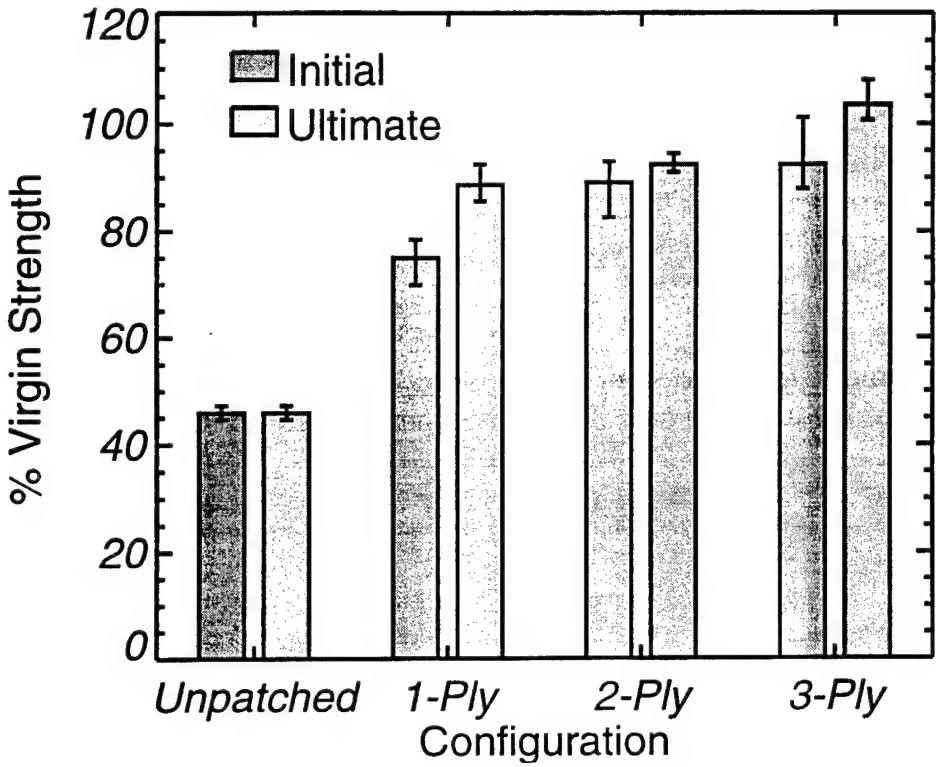

Figure 9 Strength recovery for each configuration.

The analytical investigation consisted of developing a three-dimensional finite element model to determine the stress and strain states in the patch, adhesive layer, and facesheets (Figure 10). The repair was modeled on a ply by ply basis and includes resin-rich areas between the plies of the patch and adhesive pockets at the ply drop locations. Strain gage readings from the experimental data served to validate the model. After validation, the model was used to examine the fundamental load transfer mechanisms in the patch and to identify the critical stress component and failure mode of the repaired specimens. By correlating the critical stress at failure from the model with the experimental results, a phenomenological

failure model was developed that predicts the onset of damage and the failure mode.

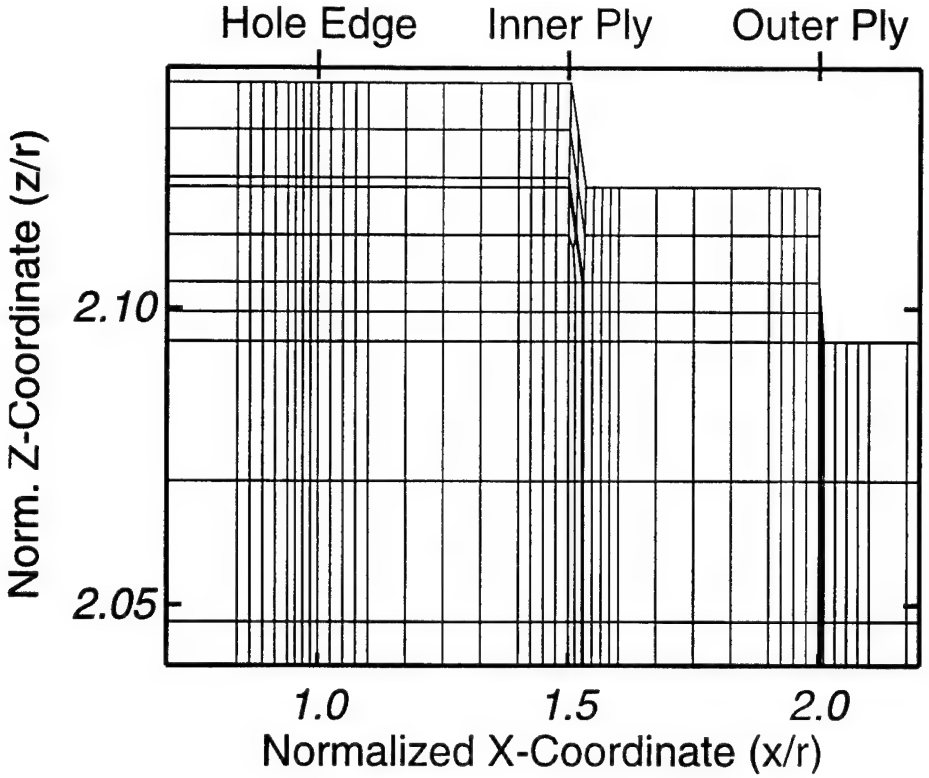

Figure 10 Finite element grid in the x-z plane for the 2-ply patch model.

Task 4.6: Active Damping Control Using ER Fluids

Norman M. Wereley, ***Assistant Professor***
Gopalakrishna M. Kamath, ***Graduate Research Assistant***
Melanie Hurt, ***Graduate Research Assistant***

A numerical study of electrorheological (ER) dampers is presented. Two models, the Newtonian and the Bingham plastic models are used to characterize the ER fluid behaviour. Damping performance of two damper configurations, the Moving Electrode and the Fixed Electrode configurations, is studied. The effects of electrode gap sizes, the field strength and the ER fluid model used are quantified. The study provides a basis for design of ER-fluid based dampers.

A comprehensive study involving different ER fluid models and damper configurations is currently lacking in the literature. The study presented here provides a basis wherein the design of ER-fluid based dampers is possible. Two electrode configurations are considered. These configurations are representative and can be easily extended to other configurations. Fluid inertia effects are not significant for low frequency applications and hence are ignored in this study. The relevant

equations are presented for the Bingham plastic model and Newtonian model. The latter is presented for its simplicity and can be used to obtain fairly accurate results for low fields.

The two damper configurations studied in this paper are shown in Fig. 2. Fig. 2(a) shows the Moving Electrode configuration. This is essentially a piston type of damper with the piston being one of the two electrodes. The other electrode is the outer casing of the damper. Thus the properties of the fluid between the piston and the casing can be controlled by suitable application of an electric field. The sources of damping in this configuration are the viscous drag of the piston and the pressure drop along the length of the electrodes. Fig. 2(b) shows the Fixed Electrode configuration. In this case, both the electrodes are fixed and the piston drives the fluid between the electrodes. The damping source here is solely due to the pressure drop along the electrodes. This configuration has the advantage of having the two electrodes separated fron the damper setup using a by-pass valve. This helps in isolating the high voltage hardware from the main damper.

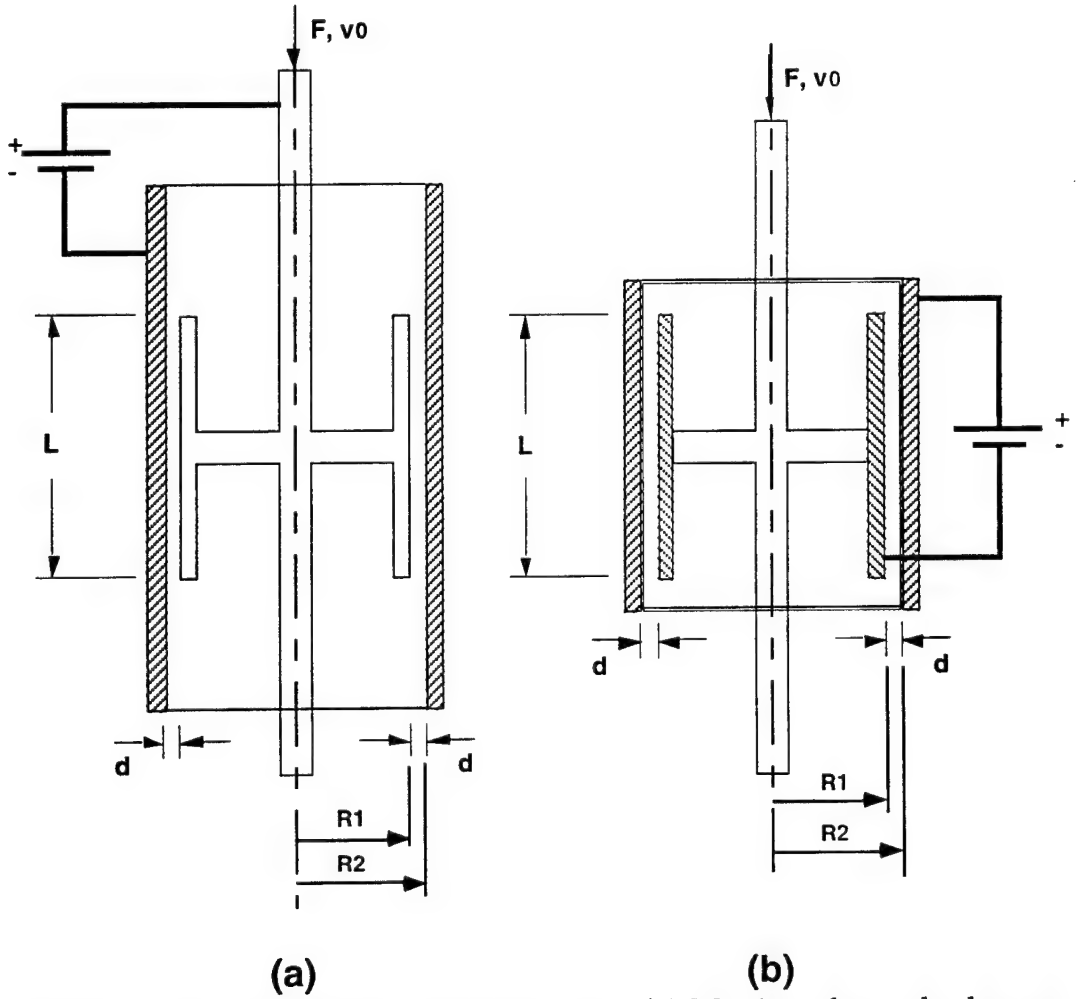

Figure 1: ER fluid damper configurations. (a) Moving electrode damper configuration. (b) Fixed electrode damper configuration

The viscous damping parameter, c, which is proprtional to the velocity is to be calculated for both of these configurations. These analyses are complete for both a Newtonian viscous shear law, and for a Bingham plastic shear law. In both of these cases, quasi-steady flow was assumed. In other words, the force applied to the damper was constant and neither oscillatory nor periodic, so that fluid inertia terms were ignored. The Newtonian viscous shear law was used to derive the damping parameter for both the moving and fixed electrode configurations. These results are available in detail in [Kam95a].

The Bingham plastic shear law was used to calculate the equivalent viscous damping for the fixed electrode. This result is shown in Figure 3 for two different loadings, 800 and 1500 N. Based on this calculation, an interesting conclusion is that increasing the force reduces the adaptability of the damping constant as the electric field is changed.

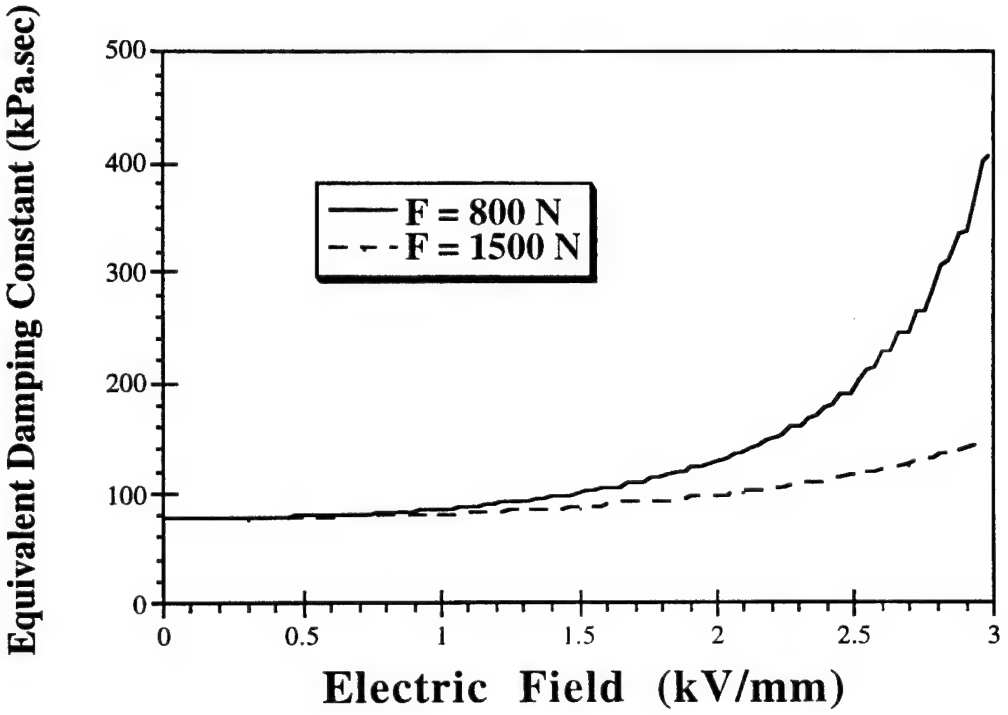

Figure 2: Equivalent damping parameter for varying field for the fixed electrode damper using a Bingham plastic shear law.

Future Work

Future work will seek to conclude the analysis for ER fluid-based dampers using a Bingham plastic shear law for both the fixed and moving electrode configurations, as well as other dampers. The same Bingham plastic models will be used to develop magneto-rheological fluid-based damper equations and analyses. ER and MR fluids

will be compared in terms of their performance for a lag damper application in a hingeless/bearingless rotor.

Publications

[Kam95a] G.M. Kamath and N.M. Wereley (1995). "Development of ER Fluid-Based Actuators for Rotorcraft Flexbeam Applications." 1995 SPIE Conf. on Smart Structures and Materials, Smart Structures and Integrated Systems, 26 February to 3 March 1995, San Diego, CA, SPIE Vol. 2443, pp. 120-135.

COMPUTATIONAL FLUID DYNAMICS AND AEROACOUSTICS

COMPUTATIONAL FLUID DYNAMICS AND AEROACOUSTICS

James D. Baeder

Overview

In order to extend the lead of the United States in rotorcraft computational fluid dynamics and aeroacoustics research and transfer the benefits to U.S. industry, the University of Maryland prepared graduate students with the proper foundation. Thus, during the course of this period numerous students took CFD I and CFD II. Furthermore, the desire for study in aeroacoustics has led to the development of a brand new graduate-level Aeroacoustics class to be taught for the first time in 1997. The research tasks described aimed at developing technology that is usable by industry in the short and long term for designing and building cheaper, faster, better, and quieter rotorcraft. The primary hurdle to greater acceptance of CFD in the rotorcraft industry has been the lack of close coupling of CFD with other disciplines, such as aeroacoustics, wake modeling and structural dynamics. Because of the lack of such close interdisciplinary coupling, the full capabilities of CFD to perform unsteady, compressible 3-D computations about complex geometries with possibly nonlinear acoustic propagation has been greatly diminished and dissipated. Thus, unfortunately many times the large computational requirements of CFD have not been fully justified because of the large simplifications made in the aeroacoustic, wake and structural dynamic modeling and coupling. The summarized research attempted to address some of these coupling issues.

The development of new CFD tools must provide new physical insight into problems and allow for the study of innovative concepts. Furthermore, through the proper choice of model problems, CFD simulations can form a numerical database that can be explored to improve simpler methods that can gain a more immediate impact on the design process. Thus, an important part of this research was the application to simple model problems that can result in the development of improved simpler methods and towards evaluating innovative concepts through some parametric studies.

The base CFD code upon which the research proposed below is based is the TURNS (Transonic Unsteady Rotor Navier-Stokes) code. It was originally developed by Dr. Srinivasan under ARO sponsorship and further modified by himself and colleagues at the Army Aeroflightdynamics Directorate. It was recognized to be a state of the art Navier-Stokes code with many applications to rotor problems. Details of the code have been published in an archive journal [Srinivasan, G.R., Baeder, J.D., Obayashi, S., and McCroskey, W.J., AIAA J., 30, (5), pp. 2371-2378.]. Prescribed vortices and/or gusts are handled without dissipation through the use of a perturbation method [Srinivasan, G.R., McCroskey, W.J. , and Baeder, J.D., AIAA J., 24, (10), pp. 1569-1576.]. This method is perfectly suitable for simple prescribed vortical flow fields. However,

a more general approach was developed within these tasks for the incorporation of general vortical systems for viscous and inviscid flow. The existence of such an excellent base code allowed for the success of these two tasks. Furthermore, several improvements to the base code have been implimented and are easily transferrable to the industry for incorporation in other codes. However, none of the described tasks required the use of multiple-block schemes. Fortunately, the advancement of graphical and computational workstation capabilities and the choice of as simplified model problems as possible enabled most of the research to be performed in-house on high-end workstations, rather than supercomputers or massively parallel machines. Thus, while maintaining a heavily research oriented program, the developments to be described should be widely deployabel to industry.

Task 5.1 Computational Aeroacoustics

Proposed Research (from CRER Augmentation proposal)

We propose to investigate the modeling of 3-D unsteady rotor blade noise through the use of a combination of CFD methods to calculate the near-field aerodynamic and acoustic fields with non-stationary Kirchhoff formulations to calculate the resulting far-field acoustics. Specifically, this method will be applied to the acoustics of high-speed-impulsive noise in forward flight as well as 3-D isolated blade-vortex interactions. Finally, the resulting methodology will be applied to innovative concepts for reducing BVI loading fluctuations, noise and vibration.

Introduction and Previous Work

Noise is a major limitation in expanding military and commercial applications. This is primarily because extreme operating conditions tend to generate impulsive noise. When it occurs, impulsive noise is unquestionably the loudest and most annoying source of noise. It is annoying because the ear is particularly sensitive to pressure changes that occur over a very short period of time. There are two types of impulsive noise: blade-vortex interaction noise (BVI), and high-speed impulsive noise (HSI). Unfortunately, methods currently used in industry have difficulty with predicting these noise sources because of the neglecting of nonlinear aerodynamics and propagation.

The application of Euler/Navier-Stokes codes to rotorcraft aeroacoustics was pioneered in the thesis of Dr. Baeder [Baeder, J.D., Ph.D Thesis, Stanford University, Sept. 1989.]. The model problem chosen was the 2-D interaction of an isolated vortex with an isolated airfoil. Although these calculations provided physical insight into the formation and initial propagation of the acoustic wave, the lack of experimental data for comparison limits the applicability of the method. Also, fundamental differences exist between 2-D acoustics from linearly moving sources and 3-D acoustics from rotating sources. Unfortunately, 3-D rotor calculations were deemed to be too expensive at the time. For these reasons the follow-on work was refocused towards examining the high-speed impulsive noise from non-lifting

rotors in hover and forward flight. Extensive experimental and theoretical work was applied to this problem in the late 70's and 80's. However, at the time the use of a purely CFD method to calculate the acoustics was deemed to be too expensive. Unfortunately, the theoretical work relied on experimental data or the results from numerical CFD simulations to provide input to the acoustic codes. Experimental data in the amount required for predictions was not available and thus the acoustic codes relied only on computational results. Because there was no way to check the accuracy of the computational results off of the blade and because the resulting acoustic predictions were sometimes off by a factor of two or more, it was impossible to pinpoint the source of error.

It was due to the failure of current methods to predict HSI noise that it was decided that perhaps a purely CFD method could be used that was not too expensive. The Euler equations were chosen since they correctly model nonlinear propagation as well as the convection of entropy and vorticity. Furthermore, algorithms for solving the Euler equations are well developed for handling flows with subsonic, transonic and supersonic regions. This is critical for maintaining stability and accuracy outboard off of the blade tip. One of the key concepts in reducing the computational requirements was the use of linear characteristic theory in deciding that the region of fine clustering of grid points off of the blade surface could be limited to the region in the vicinity of the linear characteristic curve [Baeder, J.D., 16th Euro. Rotorcraft Forum, Glasgow, 1990] and in only one-direction. Combined with an accurate, efficient and robust algorithm the first purely CFD computations were performed out past three rotor radii from the center of rotation. The agreement with experiment was excellent. Subsequent work has extended this method to forward flight [Baeder, J.D., AHS Spec. Meet. on Rotor. Acoustics and Fluid Dyn., 1991] and to modern rotors and out of the plane of the rotor [Baeder, J.D., Gallman, J.M., and Yu, Y.H., 49th AHS Forum , 1993]. The forward flight calculations were more expensive and the agreement with experiment for cases in which the flow was delocalized was only fair.

Because of the excellent agreement in hover between experiment and direct CFD calculations, some work on testing simpler acoustic methods has been initiated using the direct CFD solution in the vicinity of the rotor blade as input [Prieur, J., Costes, M., and Baeder, J.D., AHS Spec. Meet. on Rotor. Acoustics and Fluid Dyn., 1991]. The nonlinear acoustic analogy approach using the Euler solution input showed improvements over previous work [Prie91]. Unfortunately, the extension to forward flight is somewhat expensive. Therefore, a code using the stationary Kirchhoff formulation (KARENS) was written to use the near-field input from the TURNS code [2]. The agreement with the experimental data and the direct CFD approach was excellent.

Modifications to Proposed Research

(a) Kirchhoff Method Using CFD as input: The approach for this sub-task was eliminated from that contained in the proposal, due to the rapid development of non-rotating Kirchhoff methods at the U.S. Army Aeroflightdynamics Directorate

by Strawn, et. al. based upon the earlier work pioneered by Dr. Baeder described above.

(b) Acoustics of Isolated Blade-Vortex Interaction: The approach for this task was essentially unmodifiedfrom that contained in the proposal.

(c) BVI Noise and Vibration Alleviation: The approach for this task was essentially unmodifiedfrom that contained in the proposal.

Summary of Results

A couple of initial studies using, the perturbation approach, was performed to calculate the surface quantities as well as the acoustic near-field directly [1,5-7] for the case of an isolated blade-vortex interaction. The strength and location of the vortex, generated upstream by a wing at angle-of-attack, was chosen to correspond to that obtained in the experiments of Caradonna and Kitapliaglu et al. A photograph of the setup in the NASA Ames 80'x120' wind tunnel, along with a schematic of the experiment with the location of the near field microphones are shown.

Photograph of BVI Experiment in the NASA Ames 80' by 120' wind tunnel.

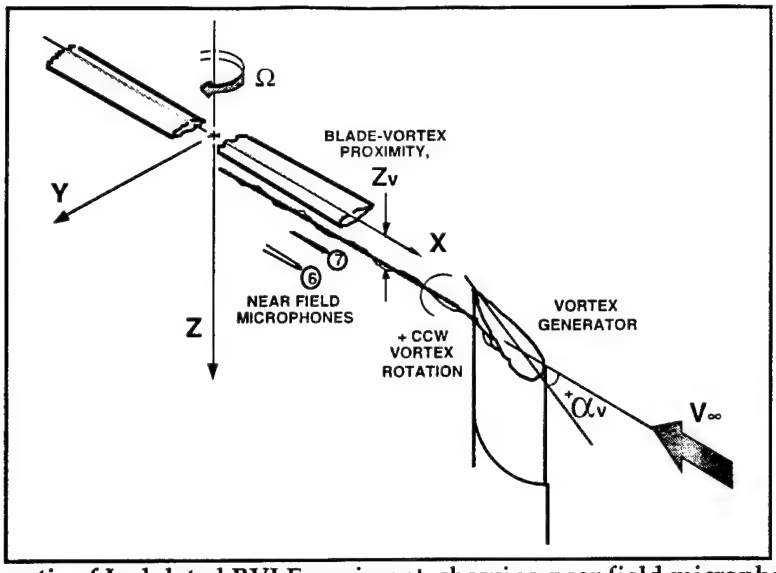

Schematic of Isololated BVI Experiment, showing near field microphones.

The initial study of Baeder and Srinivasan [5-6] demonstrated that a purely CFD method could be used to study the initial development and propagation of the BVI acoustic waves. Furthermore, the lift on the 3-D rotor was shown to be less than that for a 2-D interaction with the same dimensionless vortex parameters, due to the 3-D tip loss effects. In addition, the finite span seemed to caused a faster rise in the lift during the vortex interaction and a faster relaxtion of the flowfield after the vortex encounter. An examination of the contour plots of the pressure disturbance due to the fluctuating lift provided global details of the initial development and propagation of the acoustic waves. In addition, a cursory examination of time histories past the tip of the rotor seemed to indicate that the far-field is starting to be reached by the time that the acoustic wave reaches r/R=1.25.

Therefore, the next study expanded the examination to four different cases of vortex sign and miss-distance that were investigated at two different rotational Mach numbers in the study of McCluer and Baeder [1,7] to compare the direct CFD calculated near-field microphone pressure time histories with experiment.

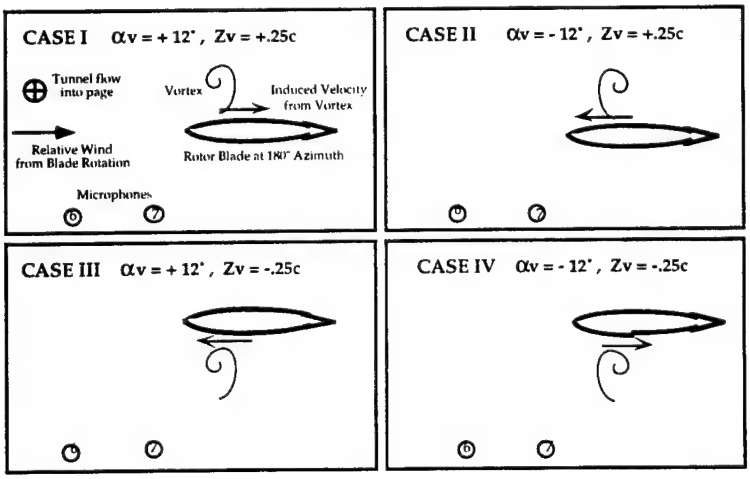

Illustration, looking downwind, of the rotor blade intersecting the line vortex for four cases.

All of the computed solutions using the TURNS code were run in Euler mode which neglects the viscous terms. Limiting was performed in the wrap-around direction to prevent numerical oscillations at shocks. No limiting was done in the normal and spanwise directions in order to better maintain the initial formation and propagation of the acoustics. The flowfield was discretized using 169 points in the wrap-around direction with 121 points on the blade surface, 45 points in the spanwise direction with 23 points on the blade surface and 57 points in the normal direction for a total of over 430,000 grid points. The results from the TURNS code correlatee well with the experimental pressure time histories in the near field. The results showed excellent qualitative comparison, but an overprediction in amplitude and a phase shift in some cases. The most likely cause for discrepancies were deficiencies in the vortex modeling used in the CFD computations.

Test Conditions				Peak to Peak Pressure Amplitude in Pascals				
Mtip = 0.6	**Mic**	**a_v**	**Zv**	**Expt.**	**CFD Γ = 0.406**	**Γ = 0.406 w/o thickness**	**Γ = 0.35 w/o thickness**	**Γ = 0.406 3 Sub-Iteration**
Case I	m6	12	0.25	786.12	964.08	916.60	781.03*	1053.30
Case II	m6	12	-0.25	549.73	851.88	899.34	766.32*	940.80
Case III	m6	-12	0.25	634.35	814.92	749.20	638.39*	864.15
Case IV	m6	-12	-0.25	575.83	861.85	910.59	775.91*	936.85
Case I	m7	12	0.25	708.58	925.48	971.51	827.82*	1026.07
Case II	m7	12	-0.25	722.66	962.81	921.13	784.89*	1073.32
Case III	m7	-12	0.25	575.51	845.10	897.74	764.96*	912.56
Case IV	m7	-12	-0.25	825.94	1078.72	1035.64	882.47*	1206.99
Mtip = 0.7	**Mic**	**a_v**	**Zv**	**Expt.**	**CFD Γ = 0.406**	**Γ = 0.406 w/o thickness**	**Γ = 0.35 w/o thickness**	**Γ = 0.406 3 Sub-Iteration**
Case I	m6	12	0.25	1661.05	1606.59	1544.06	1326.61	1717.33
Case II	m6	12	-0.25	965.43	1399.73	1462.25	1245.98*	1537.59
Case III	m6	-12	0.25	914.42	1191.72	1114.92	950.02*	1220.35
Case IV	m6	-12	-0.25	1028.70	1414.18	1486.71	1252.30	1500.05
Case I	m7	12	0.25	1372.30	1343.25	1450.07	1242.16	1457.26
Case II	m7	12	-0.25	1189.24	1427.71	1309.47	1115.80*	1565.80
Case III	m7	-12	0.25	761.50	1192.54	1305.80	1112.67*	1268.22
Case IV	m7	-12	-0.25	1422.35	1677.39	1571.31	1335.96	1809.56

Peak to peak pressure amplitude comparisons (* Value obtained by linear relation).

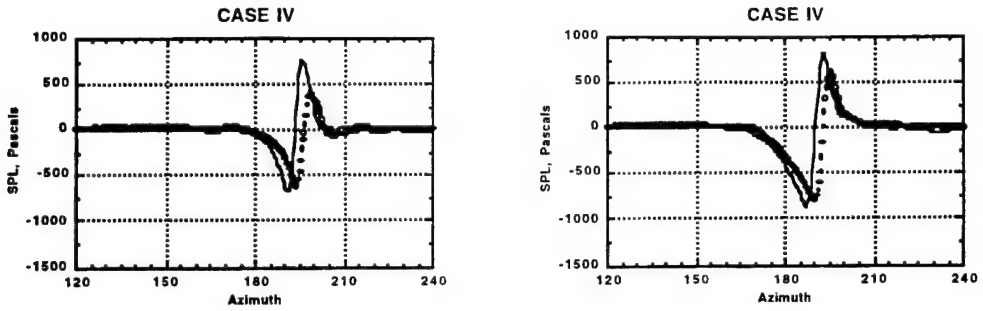

a) Microphone 6 b) Microphone 7

Pressure time histories for Mtip=0.7 and CASE IV, Comparison of Experiment and CFD.

A logical follow on for future work, based on the success of the near-field predictions, will be a future study of isolated BVI interaction far-field pressure time histories using the "field velocity" approach discussed in the following task coupled to a linear acoustic analogy code and/or nonlinear acoustic code

There have been several attempts at trying to reducing BVI noise. Broadly speaking, such methods fall into the following categories:

1: Incorporating flapping to enlarge the interaction distance.
2: Incorporating an oscillating trailing edge flap.
3: Incorporating suction/blowing on the airfoil surface.
4: Prescribed harmonic pitching.
5: Reshaping the blade tips to alter the strength and core size of the tip vortices.
6: Reducing the loading in the region of vortex generation.

As stated previously, 2-D airfoil-vortex interactions are not the best choice for studying BVI acoustics. However, they are a necessary first step and require dramatically less computational resources. Furthermore, the applicability to vibration and fluctuating loads is perfectly fine in two dimensions. Thus, initial attempts to model innovative concepts for BVI noise, vibration and fluctuating loads were performed in two dimensions. Since this 2-D modeling was performed with the TURNS code, future work can investigate the effects of three dimensionality and rotational effects.

This task examined an alternative approach to reducing BVI noise, using smart materials to dynamically vary the twist of the rotor blade, as shown in the figure. Specifically, sensors would monitor the sectional lift along the rotor blade. If large sudden changes in lift were detected during a particular blade passage, then the twist would be altered for subsequent passages in order to reduce the fluctuations in loading in such a manner as to reduce the resulting vibrations and acoustics. Within a few blade passages the procedure should stabilize to a pitching motion that varies little from blade passage to blade passage. Specifically, this phase of the study utilized computational fluid dynamics to examine a simplified model of an isolated airfoil-vortex interaction as shown in the other figure. The calculated loading is

used as the input to a simple aerodynamic model to determine the arbitrary pitching motion needed to reduce the fluctuating lift. The airfoil-vortex interaction is then recalculated with the airfoil undergoing the prescribed arbitrary pitching motion [4,6,8].

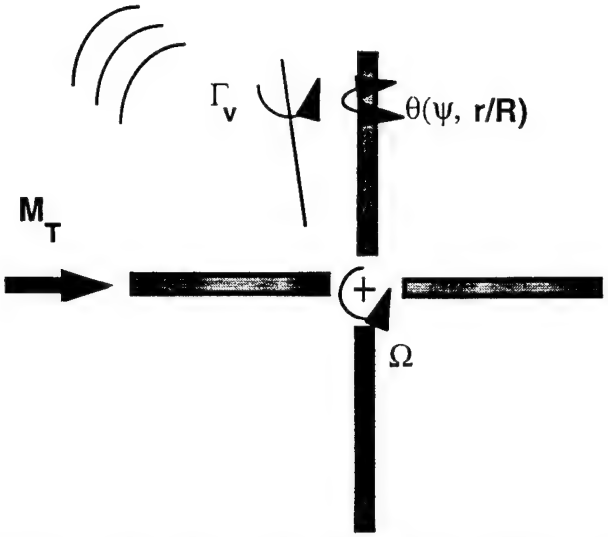

Schematic of BVI Noise Reduction Using Dynamic Twist.

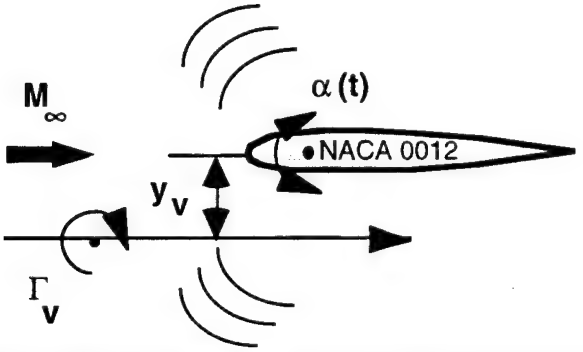

Schematic of 2-D Model Problem for Investigating BVI Noise Reduction Using Dynamic Twist.

The approach assumes that the aerodynamic loads on the airfoil, due to pitching, and due to the vortex are approximately independent. Thus, it is assumed that the unsteady lift fluctuation produced by the passage of a vortex can be canceled by pitching the airfoil. The vortex induces an equivalent angle of attack as seen by the airfoil. The time derivatives are most important when the vortex is close to the airfoil, and affect the loading significantly. To achieve reasonable cancellation of the noise, the time derivatives have to be modeled accurately.

Unsteady thin airfoil theory predicts that the loading on an airfoil undergoing pitching and flapping in inviscid incompressible flow is given by:

$$C_l = 2\pi C(k)\left[\alpha + \frac{b}{V}\dot{\alpha} + \frac{1}{V}\dot{h}\right] + \pi\left[\frac{b}{V}\dot{\alpha} + \frac{b}{V^2}\ddot{h} + \frac{b^2}{2V^2}\ddot{\alpha}\right]$$

where:

C_l = Lift coefficient on the airfoil
$C(k)$ = Theodorsen's function, based on reduced frequency, k
α = Angle of attack of the airfoil
h = Height of airfoil above a fixed reference
b = Semichord
V = Freestream velocity

This can be simplified by assuming quasi-steady flow, setting Theodorsen's function to one for all reduced frequencies and neglecting the noncirculatory terms. Furthermore, we decide to only apply a pitching motion at the quarter chord. For linearised compressible flow, the lift coefficient generated on a thin airfoil due to an arbitrarily pitching airfoil can then be written as:

$$C_l = \frac{2\pi}{\beta}\left[\alpha + \frac{b}{V}\dot{\alpha}\right]$$

where:

β = Prandtl-Glauert correction, $\sqrt{1-M^2}$

Note that the Duhamel integral from indicial theory could also be used similarly [8].

To cancel the vortex induced loading, we consider the variation of C_l with time to be known (as obtained from a previous vortex passage). Thus the above equation represents an ordinary differential equation of alpha in time, which can be solved either analytically or numerically, to give the variation of the equivalent angle of attack seen by the airfoil with time.

Typical results of the unsteady loading, pitching, moments, and time derivative of loading are shown for a typical BVI situation. It can be observed that the peak to peak lift for M_∞ = 0.65 is reduced by about a factor of 2.5 for one application of `quasisteady' pitch, about 3.5 for two applications of quasisteady pitch and about 6.2 for one application of `indicial' pitch. The reduction in maximum slope is 2.5 for one application of `quasisteady' pitch , 4.5 for two applications of `quasisteady' pitch and 10 for one application of `indicial' pitch. This would correspond to a reduction of approximately 8, 13 and 20 dB. Approximately a maximum of 1.5 degrees of pitching is required, however, it occurs over such a short period of time that relatively large pitching moments are obtained. The feasibility of such a method was further examined by Amerigo and Baeder [4].

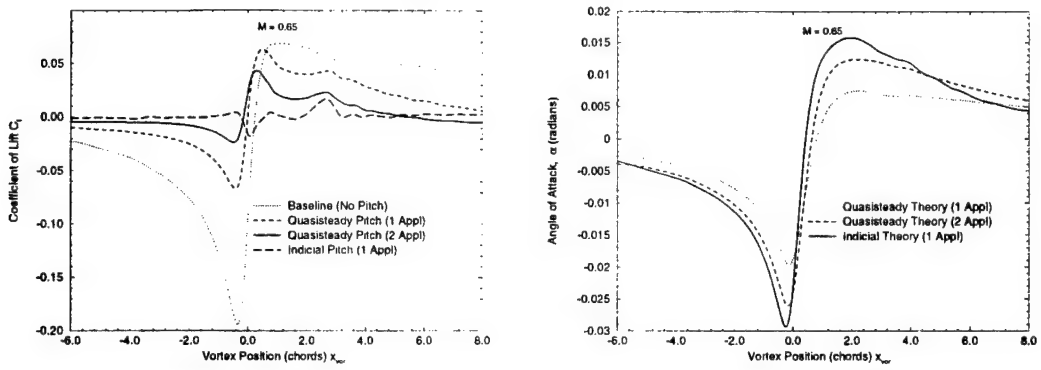

Unsteady Loading and Pitching Time Histories for typical 2-D BVI.

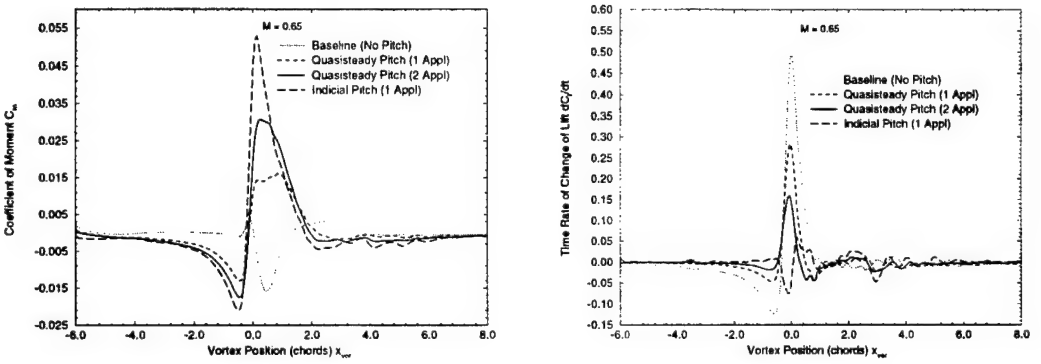

Unsteady Moment and Time Derivative of Loading (Proportional to noise in the far field) Time Histories for typical 2-D BVI.

The final part of this task focused on performing 2-D calculations on non-deformable airfoils in order to better understand compressibility effects on the fluctuating airloads in BVI. These calculations form the basis for improving simpler methods that rely on indicial methods [3].

Publications

1. McCluer, Megan, "Comparison of Experimental Helicopter Rotor Blade-Vortex Interaction Noise with Computational Fluid Dynamic Calculations", M.S. Thesis, May 1995.
2. Baeder, J.D., Gallman, J.M., and Yu, Y.H., "A Computational Study of the Aeroacoustics of Rotors in Hover", **Journal of the American Helicopter Society,** Vol. 42, No. 1, Jan. 1997, pp. 39-53.
3. Parameswaran, V., and Baeder, J.D.,"Indicial Aerodynamics in Compressible Flow - Direct Calculations," **AIAA Journal of Aircraft**, Vol. 34, No. 1, Jan.-Feb. 1997, pp. 131-133.
4. Amerigo, M., and Baeder, J.D., "Feasibility of Arbitrary Pitching Motion Controlled by Piezoceramic Actuators to reduce BVI noise", accepted to **AIAA Journal of Aircraft**. Also *Proceedings of the AHS 51st Annual Forum*, Fort Worth, TX, May 1995.

5. Baeder, J.D., and Srinivasan, G.R.,"Computational Aeroacoustic Study of Isolated Blade-Vortex Interaction Noise", *American Helicopter Society Aeromechanics Specialists Meeting*, San Francisco, CA, Jan. 1994.
6. Baeder, J.D., "The Role and Status of Euler Solvers in Impulsive Rotor Noise Computations", *Proceedings of the AGARD Symposium on Aerodynamics and Aeroacoustics of Rotorcraft*, Berlin, Germany, Oct. 1994.
7. McCluer, M., and Baeder, J.D., "Comparison of Experimental Blade Vortex Interaction Noise with Computational Fluid Dynamic Calculation", *Proceedings of the AHS 51st Annual Forum, Fort Worth*, TX, May 1995.
8. Parameswaran, V., and Baeder, J.D., "Reduction of Blade Vortex Interaction Noise Using Prescribed Pitching", *Proceedings of the 13th AIAA Applied Aerodynamics Conference*, San Diego, CA, June 1995.

Task 5.2 Rotor Blade Aerodynamics

Proposed Research (from CRER Augmentation proposal)

We propose to investigate the modeling of 3-D lifting rotor blade aerodynamics through the coupling of an Euler/Navier-Stokes code to calculate the near field aerodynamics with methods for predicting the wake, rigid body motion, structural deformation and trim. Unlike previous attempts, the rigid blade motion will be incorporated into the CFD solution through the movement of the computational grid.

Introduction and Previous Work

Due to the inherently interdisciplinary nature of rotorcraft, realistic calculations of the rotor aerodynamic flowfield requires the inclusion of the effects from the wake, rigid blade motion and structural deformation of the rotor blade. Furthermore, the rotor must be trimmed to insure that a periodic motion is indeed obtained. Comprehensive codes tend to rely on unsteady airfoil theory or lifting-line or lifting-surface theory to provide the individual blade aerodynamics. The 2-D airfoil characteristics are provided from experimental data. Due to the complexities of comprehensive codes, initial attempts to model the aerodynamics of rotors using CFD codes was limited to non-lifting rigid blades. This was essential at the time in order to remove ambiguities in the interpretation of discrepancies with experimental data and allow for the refinement of the CFD methods. Despite these limitations, important contributions to the advancement of the understanding of advancing blade compressibility effects were obtained.

It was only natural that the compressible CFD codes would be coupled to the nonaerodynamic portions of comprehensive codes in order to improve predictive capabilities. At the time, CFD codes primarily solved the transonic small disturbance equation. The inviscid boundary condition consists of flow tangency on

the rotor surface. The problem is greatly simplified if the angle of the oncoming flow and the tangent of the surface are assumed to be small. Then a small angle assumption allows the tangency boundary condition to be applied at the z=0 surface. This greatly simplifies the problem of mesh generation, since the mesh no longer needs to conform to the body geometry but rather can be a simple stretched Cartesian mesh. The simplest approach to couple comprehensive codes with CFD codes was to modify this surface tangency condition by allowing for a transpiration velocity. The surface transpiration velocity was chosen to account for the induced velocity of the wake, the rigid blade motion and the structural deformation of the blade. The comprehensive code was modified to allow for the spanwise thrust calculated by the comprehensive code to be replaced by the spanwise thrust from the CFD solution. Two main weakness were the incorrect handling of even moderate shocks and the frequent violation of the small angle assumption. In addition, often times the transpiration velocity was assumed to have a constant chordwise distribution. However, at the time, such an approach was indeed a breakthrough in allowing for the effects of 3-D unsteady compressible CFD results into comprehensive predictions of rotors operating in realistic conditions.

The next step in improving the aerodynamics of 3-D unsteady forward flight calculations was the replacement of the transonic small disturbance equation with the full potential equation. This allowed for better predictions of the shock strengths and speeds. Furthermore, the Cartesian mesh was replaced by a body conforming mesh, thus, removing the small angle assumption. Unfortunately, the coupling with comprehensive codes was still performed with a transpiration velocity to account for the effects of the wake, rigid blade motion and structural deformation. Since even the rigid blade motion is used for the transpiration velocity, the small angle assumption for the use of a transpiration velocity is often violated over a significant portion of the rotor disc. In addition, often the transpiration velocity was still assumed to be constant in the chordwise direction (the value at the aerodynamic center). Furthermore, attempts to couple the calculated spanwise power and moment distributions have had limited success, such that usually only the spanwise thrust is used to couple the CFD solution to the comprehensive code. Despite these limitations, improved comparisons with experiment were obtained. A comparison of various full potential methods indicate that the various implementations all give similar results when coupled to the same wake model. However, discrepancies still remain with airloads obtained in test flights. Many have blamed the discrepancies on deficiencies in wake modeling. This has led to a large increase in attention to methods that can more accurately describe and predict the wake. However, it is also possible that the coupling of the CFD codes with the wake, blade motion and structural deformation needs to be improved.

The TURNS code has been used to accurately predict the aerodynamics of non-lifting blades in both hover and forward flight. Furthermore, wake capturing in hover has been proven to be both feasible and as accurate as other methods. The next logical step in coupling CFD methods to comprehensive codes was to replace

the full potential equation solver with an Euler/Navier-Stokes solver such as TURNS and improve the coupling, especially for viscous flow.

Modifications to Proposed Research

(a) Coupling of CFD with Wake and Blade Motion: The approach for this task was modified slightly from that contained in the proposal, in order to concentrate on the coupling of the wake system from the Maryland Free Wake (MFW) code (described in Task 1) with the TURNS code for an isolated trimmed rigid rotor blade in hover.

(b) Application to Advanced Tip Shapes: The approach for this task was essentially unmodifiedfrom that contained in the proposal. The application was primarily to the effects of sweep, taper and thinning to HSI noise problems.

Summary of Results

A new coupled wake/ CFD methodology, using a new Field Velocity approach, was used to include realistic wake effects in CFD solutions for rotors in hover. A modified free-wake method was used to compute efficiently, in hover, the wake geometry. The free-wake method uses a psuedo implicit predictor to compute the wake geometry at any one azimuth (in hover) and uses the axisymetric nature of the wake to compute the free-wake geometry. The Field Velocity approach involves bringing in the vortex-wake effect by modifying the grid time-metrics. Consider the velocity, $\vec{V}_s$ at the surface of the blade. It can be written as:

$$\vec{V}_s = (u - x_\tau)\vec{i} + (v - y_\tau)\vec{j} + (w - z_\tau)\vec{k}$$

Then, the vortex wake effect can be considered equivalent to modifying the velocities along all three directions. Thus, on can write:

$$\vec{V}_s = (u - x_\tau - V_{wx})\vec{i} + (v - y_\tau - V_{wy})\vec{j} + (w - z_\tau - V_{wz})\vec{k}$$

where V_{wx}, V_{wy}, and V_{wz} represent the wake induced velocity field along the x, y and z directions respectively. This velocity correction is applied to all of the points in the flowfield, hence, the term Field Velocity approach. Thus, the idea is to modify all of the time metrics to include the velocity effects of the vortex wake system. The approach does not model the vortex pressure and density fields as in the prescribed or perturbation approach described previously. Fortunately, the velocity field is by far the dominant field regarding the effects of the surface loading and pressure distribution on the rotor surface. The suitability of the field velocity approach has been demonstrated on a wide variety of cases [1,3,5], both steady and unsteady. Furthermore, the method is suitable for both viscous and transonic flows, where the simpler transpiration methods tend to break down.

The coupled approach was validated for a small aspect ratio rotor blade. This demonstrated the importance of the inboard vortex sheet on the blade surface pressures. The computed pressure distributions compared well with experimental results. This coupled approach utilized approximately one-third the number of points aas for a conventional direct wake captured CFD solution and led to a much

faster drop in the residuals. Thus, the couple wake/ CFD solution can be carried out with substantial reduction in the CPU times. The resulting viscous solutions are only moderately more expensive than the surface transpiration approach but are much more accurate, especially for transonic and seperated flows. On the other hand, the Field Velocity approach is much simpler than the perturbation approach, which is too expensive and complicated for complete 3D vortex wake problems. Finally, the coupled approach was used to trim the rotor, using CFD, for a consistent tip vortex strength and free-wake geometry. The tip vortex strength and roll-up position can be computed from the CFD solution through the use of a contour integral near the blade of the tip. This eliminates the uncertainties in the assumptions commonly used in the comprehensive codes.

Future work in this area should be to extend the method to forward flight and to reduce the cost associated with the somewhat expensive Biot-Savart calculations used to determine the wake velocity field.

The second part of this subtask consisted of examining the effect of advanced tip shapes on the high-speed impulsive noise from non-lifting rotors in hover at large tip Mach numbers using an Euler/ Navier-Stokes solver. A parametric study was performed to systematically investigate the nonlinear effects of sweep, taper and thinning on high-speed impulsive noise in order to determine the key parameters for the design of a low noise rotor. An untwisted UH-1H rotor blade formed the baseline blade for this study [4]. Forward sweep was found to be more beneficial for noise reduction than rearward sweep. In fact, the maximum noise was generated for a slight amount of rearward sweep. Forward sweep moved the strongest portion of the shock inboard, reduced the shock strength outboard of the onset of sweep and curved the shock forward; effectively delaying delocalization.

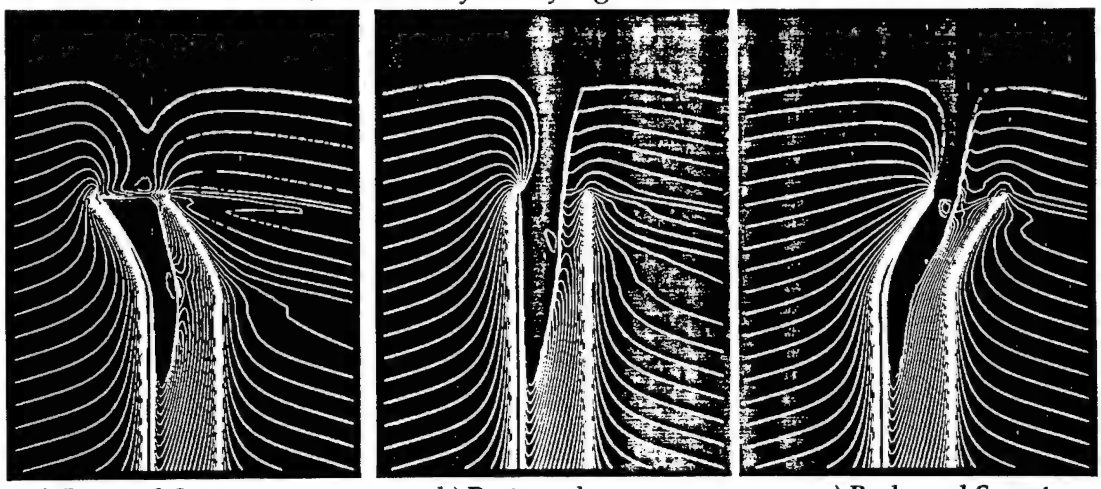

a) Forward Swept **b) Rectangular** **c) Backward Swept**

Mach contours in-plane for a hover tip Mach number of 0.90.

At lower tip speeds taper and thinning were more effective for reducing the in-plane noise. However, at high tip speeds phasing effects became more important and sweep became more effective at reducing high-speed impulsive noise.

Combinations of sweep, taper and thinning were also investigated. Furthermore, a dogleg planform, with backward sweep inboard of the forward swept tip, was included in order to place the aerodynamic center near the root quarter chord. In particular the Forward Aeroacoustically Swept Thin and Tapered (FASTT) blade was seen to delay delocalization well past a tip Mach number of 0.95 while providing at least 10 dB of noise reduction from the baseline untwisted UH-1H over the entire tip Mach number range investigated. The numerical results form a rich numerical data base for investigating the ability of simpler methods for predicting high-speed impulsive noise for more complex planforms.

Future work in this area should be to extend the method to forward flight to investigate the effects of planform on BVI noise production.

Publications

1. Khanna, Harsh, "Coupled Wake / CFD Solutions for Rotors in Hover", M.S. Thesis, Aug. 1996.
2. Wake, B.E., and Baeder, J.D., "Evaluation of a Navier-Stokes Analysis Method for Hover Performance", **Journal of the American Helicopter Society**, Jan. 1996, pp.7-17. Also *American Helicopter Society Aeromechanics Specialists Mee*ting, San Francisco, CA, Jan. 1994.
3. Singh, R., and Baeder, J.D., "The Direct Calculation of Indicial Lift Response of a Wing Using Computational Fluid Dynamics", **AIAA Journal of Aircraft**, Vol. 35, No. 4, July-Aug. 1997, pp.465-471. Also *Proceedings of the 14th AIAA Applied Aerodynamics Conference*, New Orleans, LA, June 1996.
4. Baeder, J.D., "Passive Design for Reduction of High-Speed Impulsive Rotor Noise", accepted to **Journal of the American Helicopter Society**. Also *Proceedings of the AHS 52nd Annual Forum*, Washington, D.C., June 1996.
5. Khanna, H. and Baeder, J.D., "Coupled Wake /CFD Solutions for Rotors in Hover", *Proceedings of the AHS 52nd Annual Forum*, Washington, D.C., June 1996.

ABSTRACTS OF PUBLICATIONS AND PRESENTATIONS

A Computational Study of the Aeroacoustics of Rotors in Hover

James D. Baeder, Judith M. Gallman and Yung H. Yu

Journal of the American Helicopter Society
January 1997

The noise from low-thrusting rotors in hover is examined for a wide range of tip Mach numbers for various blade planforms using several different methods. The first approach is to use an Euler/Navier-Stokes code to calculate the acoustic field without using any acoustic analogy to examine the wavefront formation process and acoustic propagation through a nonlinear flow-field. Furthermore, the near field solutions from the CFD code are used as input to two different methods: a code based on the linear stationary Kirchhoff formulation and a code based on the linear acoustic analogy approach. The results from the CFD code compare very well with the experimental acoustic data available, as do the results from the Kirchhoff code. However, the lack of quadrupole terms in the linear acoustic analogy approach causes the negative peak pressure to be underpredicted by a factor of two in-plane at high tip speeds. This underprediction decreases as an observer moves out-of-plane. Finally, the CFD code is used to study the acoustic field for five different rotor blades. This study provides useful insight into the noise generating mechanisms of various blade planform shapes and near field wavefront formations near the blade.

High-Order State Space Simulation Models of Helicopter Flight Mechanics

Frederick D. Kim, Roberto Celi and Mark B. Tischler

Journal of the American Helicopter Society
October 1993

This paper describes the formulation and validation of a high-order linearized mathematical model of helicopter flight mechanics, which includes rotor flap and lag degrees of freedom as well as inflow dynamics. The model is extracted numerically from an existing nonlinear, blade element, real-time simulation model. Extensive modifications in the formulation and solution process of the nonlinear model, required for a theoretically rigorous linearization, are described in detail. The validation results show that the linearized model successfully captures the coupled rotor-fuselage dynamics in the frequency band most critical for the design of advanced flight control systems. Additional results quantify the extent to which the order of the model can be reduced without loss of fidelity.

Effects of Higher Order Dynamics on Helicopter Flight Control Law Design

Steven J. Ingle and Roberto Celi

Journal of the American Helicopter Society
July 1994

The main objective of the study is to assess the effects of incorporating higher order dynamics such as rotor and inflow dynamics when designing a flight control system to satisfy handling qualities specifications such as ADS-33C. The control methodologies examined are Linear Quadratic Gaussian (LQG), Eigenstructure Assignment (EA), and H_∞. The UH-60 in hover is used as a test case to which a representative subset of the ADS-33C requirements, for a Rate Command Attitude Hold response type, is applied. The results indicate that acceptable controllers can be designed using EA with a rigid body model of the helicopter; however the control activity is high and the controller is not robust. An H_∞ design requires the modeling of higher order dynamics; the resulting controller is higher order but more robust, and the control activity is lower. It was not possible to determine a suitable LQG based controller that would satisfy all the requirements.

Coupled Rotor-Fuselage Dynamics and Aeroelasticity in Turning Flight

Anne Marie Spence and Roberto Celi

Journal of the American Helicopter Society
January 1995

This paper describes the results of a numerical study of the aeromechanic stability of a soft-in-plane, hingeless rotor helicopter undergoing a coordinated steady turn. The mathematical model of the blade includes nonlinearities due to moderately large elastic deflections. The rigid body dynamics of the aircraft is described by nonlinear Euler equations valid for large fuselage attitudes and rates. The combined effects of turn rate, aircraft speed, and flight path angle are discussed. The results indicate that steady level turns tend to stabilize the lag mode. Descending turns are destabilizing and may limit the maneuver envelope of the helicopter. Judicious choice of flap and lag fundamental frequencies is necessary to insure stability of the lag mode in descending flight.

Modeling of Flexible Rotor Blades for Helicopter Flight Dynamics Applications

Stephen R. Turnour and Roberto Celi

Journal of the American Helicopter Society
July 1996

This paper describes a methodology for the treatment of rotor blade flexibility for helicopter flight dynamics applications. A coupled flap-lag-torsion elastic rotor model, previously used in aeroelasticity studies, is coupled with a blade-element-type flight dynamic simulation model. The methodology reduces the amount of symbolic manipulation and reduces the effort required for computer implementations. The treatment of selected terms of the equations of motion is presented in detail. The mathematical structure of flight dynamics equations is also discussed. Results are presented for the frequency response to pilot inputs of a UH-60 Blackhawk in hover and forward flight, including comparisons with flight test data. The effects of blade flexibility are generally modest, at least for the articulated rotor configuration used in the illustrative examples.

The Natural Frequencies of Rotating Composite Beams With Tip Sweep

Jeanette J. Epps and Ramesh Chandra

Journal of the American Helicopter Society
January 1996

This paper presents an experimental-theoretical investigation of the influence of tip sweep on the natural frequencies of rotating aluminum and composite solit-section beams. An in-vacuo rotor test facility was used to test the beams for their vibration characteristics. Induced-strain actuation via piezoceramic elements was used to excite the beams, and strain gauges were used to measure the response of the beams. The theoretical frequencies were calculated using a finite-element structural model in which the beam had one elastic axis for the straight portion and another elastic axis for the swept portion. Nonlinear transformation relations were used to connect the elastic axes of the straight and swept segments of the beam. Natural frequencies of the beams were obtained by carrying out linearized free vibration analysis about their deformed states. For better accuracy in the prediction of these frequencies, graded finite-element mesh with finer mesh at the junction of straight and swept segments of the beam was used. Good correlation between experiment and theory was achieved for these beams. Modeling the sweep as an offset of the center of gravity from the assumed straight elastic axis was found to be inadequate for predicting the natural frequencies of swept tip beams.

Aeroelastic Optimization of a Helicopter Rotor to Reduce Vibration and Dynamic Stress

Ranjan Ganguli and Inderjit Chopra

Journal of Aircraft, Vol. 12, No. 4, July-August 1996

Optimization studies are carried out for a four-bladed, soft in-plane hingeless rotor consisting of a two-cell composite box-beam spar. The design variables are the ply angles of the box-beam walls. The objective functions are the vibratory hub loads and the fibratory blade bending moments; constraints are imposed on blade rotating frequencies and aeroelastic stability. The objective functions are first minimized individually, and then a combined optimization is performed to minimize both the objectives simultaneously. As compared to the starting design, the optimum solution results in a 15-60% reduction of the 4/rev hub loads as well as a reduction in the peak-to-peak flap and lag bending moments of 11 and 14%, respectively. Starting from an initially infeasible starting design with a 3% requirement on lag mode damping, the optimum solution with composite chordwise bending-torsion coupling results in an increase in lag mode damping of over 200% compared to the starting design.

Aeroelastic Optimization of a Helicopter Rotor with Composite Coupling

Ranjan Ganguli and Inderjit Chopra

Journal of Aircraft, Vol. 32, No. 6, November-December 1995

Sensitivity derivatives of blade loads and aeroelastic stability of a composite helicopter rotor in forward flight are calculated as an integral part of an aeroelastic analysis using an analytical approach. Design variables are the ply angles of the laminated walls of the box-beam spar used to model the composite rotor blade. By means of a parametric study, the influence of the ply angles on the blade elastic stiffness, vibratory hub loads, and aeroelastic stability are examined for a four-bladed, soft in-plane, hingeless rotor. Aeroelastic and sensitivity analysis of the rotor, based on a finite element in space and time, are linked with an automated optimization algorithm. For the optimization, the objective function is a combination of all six vibratory hub loads and the constraints are imposed on frequency placement and aeroelastic stability in forward flight. The optimization procedure is used to tailor composite coupling for minimizing vibratory loads and enhancing aeroelastic stability of the blade in forward flight. The influence of composite coupling on the vibratory hub loads corresponding to the optimum solutions is relatively small with reductions in the objective function of about 10%. The effect of lag bending-torsion coupling in stabilizing the lag mode is significant. Starting from an initially infeasible design, the optimum design solution for a box-

beam configuration with lag bending-torsion coupling shows an increase in lag damping of over 200%.

Aeroelastic Optimization of a Helicopter Rotor with Two-Cell Composite Blades

Ranjan Ganguli and Inderjit Chopra

AIAA Journal, Vol. 34, No. 7, July 1996

Aeroelastic and sensitivity analyses of the rotor based on a finite element in space and time are linked to an automated optimization algorithm to perform optimization studies for a four-bladed, soft in-plane composite rotor consisting of a two-cell thin-walled beam. The design variables used in this study are the ply angles of the laminated walls of the composite beam. The objective function minimizes the 4/rev hub loads, with constraints on blade frequencies and aeroelastic stability in forward flight. Optimum design solutions show a reduction in the objective function of about 20% due to elastic stiffnesses and an additional 13% due to composite couplings. Starting from an initially infeasible design, the optimum design solution with negative lag bending-torsion coupling results in an increase in lag mode damping of about 140% compared to the baseline layup.

Aeroelastic Optimization of an Advanced Geometry Helicopter Rotor

Ranjan Ganguli and Inderjit Chopra

Journal of the American Helicopter Society
January 1996

Sensitivity derivatives of blade loads and stability in forward flight are calculated as an integral part of the basic aeroelastic analysis using a computationally efficient analytical approach. Design variables include nonstructural mass and its placement, blade bending stiffness (flap, lag, torsion), and blade geometry (sweep, anhedral and planform taper). Aeroelastic and sensitivity analyses of the rotor based on a finite element method in space and time are linked with automated optimization algorithms to perform optimization of rotor blades. The objective function constitutes minimization of oscillatory hub loads including constraints on frequency placement, autorotational inertia and aeroelastic stability of the blade in forward flight. Optimum design solutions are calculated for a four-bladed, soft-inplane hingeless rotor. Analytical predictions show a 25 to 60 percent reduction in all the 4/rev loads, compared to the starting design. The optimum design is swept back. drooped down and tapered along the blade span, with nonstructural mass distributed behind the elastic axis along the outer 60 percent of the blade.

Formulation of a Helicopter Rotor System Damage Detection Methodology

Ranjan Ganguli, Inderjit Chopra and David J. Haas

Journal of the American Helicopter Society
October 1996

A helicopter rotor-system damage detection methodology is formulated for an articulated rotor in hover, and in forward flight. Damages modeled are moisture absorption, loss of trim mass, misadjusted pitch-link, damaged trailing-edge flap, damaged pitch-control system and inoperative lag damper. These damages are represented by changes in mass, stiffness, damping and aerodynamic properties of the rotor blade. A rotor aeroelastic analysis based on finite element discretization in space and time, and capable of modeling dissimilar blades, is used to simulate the undamaged and the damaged rotor. Changes in rotor system behavior are identified for the selected faults and tables of rotor system diagnostics are compiled. Rotor faults detectable from blade tip response include moisture absorption, misadjusted pitch-link, damaged trailing-edge flap and damaged pitch-control system. Rotor faults detectable from vibratory hub forces include moisture absorption, loss of trim mass, damaged pitch-control system and damaged lag damper. Finally, rotor faults detectable from vibratory hub moments include misadjusted pitch-link, damaged trailing-edge flap and damaged pitch-control system.

Air Resonance of Hingeless Rotor Helicopters in Trimmed Forward Flight

Judah H. Milgram and Inderjit Chopra

Journal of the American Helicopter Society
October 1994

Air resonance of a soft inplane hingeless rotor helicopter is examined in hover and forward flight using a simple model combining a rigid blade flap-lag model with body pitch and roll motions. Stability is calculated about a coupled rotor/body trim condition obtained using a finite element in-time approach for blade response and a force-summation method for hub loads. The linearized rotor-body stability equations are expressed in the fixed system using a multiblade coordinate transformation and solved via Floquet analysis. Predicted stability results correlate well with experimental data. Both shaft fixed flap-lag stability and air resonance stability improve in forward flight above an advance ratio of approximately 0.2. This is largely the result of changes in the vehicle trim solution. The effects of variations of several design parameters are investigated. For the configuration examined, air resonance stability varied with body roll inertia but was insensitive to pitch inertia. Variations in blade lag frequency had a considerable effect on stability, while the blade flap frequency had relatively less influence. Increasing Lock number decreased hover stability but had a strong stabilizing effect in forward flight.

An Analytical Model for a Nonlinear Elastomeric Lag Damper and Its Effect on Aeromechanical Stability in Hover

Farhan Gandhi and Inderjit Chopra

Journal of the American Helicopter Society
October 1994

A new nonlinear elastomeric damper model, based on a combination of linear and nonlinear springs and dashpots, is developed. The damper is characterized completely by a nonlinear constitutive differential equation. Since this "differential equation approach" is not based on the frequency- and amplitude-dependent complex modulus components, it can conveniently be used in a variety of operating conditions, including multi-frequency excitations, varying rotor speeds, and different steady-lag angles. A methodology is developed for the inclusion of such a damper model into a rotor analysis scheme. For aeromechanical stability analysis, the damper perturbation equation is solved along with the blade and fuselage equations, with damper-force appearing as an independent state. The elastomeric damper has a stabilizing influence on ground resonance and hover air resonance regressive lag modes. The eigensolution damping estimates overpredict the damping when the system is subjected to larger perturbations. Steady lag angle has a significant influence on the elastomeric damper behavior and can change the regressive lag mode damping by 50% for ground resonance and 80% for air resonance in hover.

Air and Ground Resonance of Helicopters with Elastically Tailored Composite Rotor Blades

Edward C. Smith and Inderjit Chopra

Journal of the American Helicopter Society
October 1993

The aeromechanical stability, including air resonance in hover, air resonance in forward flight, and ground resonance, of a helicopter with elastically tailored composite rotor blades is investigated. Five soft-inplane hingeless rotor configurations, featuring elastic pitch-lag, pitch-flap and extension-torsion couplings, are analyzed. Elastic couplings introduced through tailored composite blade spars can have a powerful effect on both air and ground resonance behavior. Elastic pitch-flap couplings (positive and negative) strongly affect body, rotor and dynamic inflow modes. Air resonance stability is diminished by elastic pitch-flap couplings in hover and forward flight. Negative pitch-lag elastic coupling has a stabilizing effect on the regressive lag mode in hover and forward flight. The

negative pitch-lag coupling has a detrimental effect on ground resonance stability. Extension-torsion elastic coupling (blade pitch decreases due to tension) decreases regressive lag mode stability in both airborne and ground contact conditions. Increasing thrust levels has a beneficial influence on ground resonance stability for rotors with pitch-flap and extension-torsion coupling and is only marginally effective in improving stability of rotors with pitch-lag coupling.

Modeling and Validation of Induced Strain Actuation of Composite Coupled Plates

Chang-Ho Hong and Inderjit Chopra

Presented to the 38th Structures, Structural Dynamics and Materials Conference, and Adaptive Structures Forum, Kissimmee, Florida, April 9-10, 1997

A consistent plate finite element analysis is developed for coupled composite plates with induced strain actuation, and validated it with test data obtained from cantilevered isotropic and anisotropic plates. Actuators are assumed as additional plies fully integrated into substrate laminae, and formulation is based on modified thin classical laminated plate theory. The analysis is formulated for a generic anisotropic plate with a number of piezo actuators of arbitrary size, surface-bonded or embedded at arbitrary locations. Composite plates are designed to produce extension-twist and bending-twist couplings. Two rows of piezoceramic elements are surface mounted on both top and bottom surfaces near the root. Static tests are carried out using induced strain actuation, and mechanical loading and measured data are correlated with predictions for bending and twist distributions. For an extension-twist coupled plate, the agreement between predicted and measured induced twist due to extensional strain with piezo actuation is excellent. For a bending-twist coupled composite plate, the predicted induced twist due to bending strain with piezo actuation agrees extremely well in trends, but magnitudes are underpredicted by a maximum of 25% from measured values.

Prediction of Tail Rotor Thrust and Yaw Control Effectiveness

Venkataraman Srinivas, Inderjit Chopra, David Haas and Kelly McCool

Journal of the American Helicopter Society
October 1995

A comprehensive tail rotor model capable of predicting the tail rotor thrust under a combination of axial and edgewise flow is developed. The predicted tail rotor thrust is correlated in hover and in low speed flight at different azimuth ngles. An

empirical tail rotor/vertical fin interaction model is developed from wind tunnel data. Predictions of the SH-2 trim pedal position with the isolated tail rotor alone as well as including the main rotor wake and tail rotor'fin interactions are obtained and correlated with flight test data. The isolated main rotor wake induces considerable velocities at the tail rotor location and, when included in the analysis, has a significant effect on the predictions of pedal position. The tail rotor/fin interactions affect the predictions of pedal position considerably in right sideward flight, particularly at speeds above 25 knots.

Aeroelastic Analysis of a Composite Bearingless Rotor in Forward Flight with Improved Warping Modeling

(Presented at the 1994 AHS Aeromechanics Specialists Conference, San Francisco, January 1994)

Anita L. Tracy and Inderjit Chopra

Abstract

The aeromechanical stability of a helicopter with an elastically coupled composite bearingless rotor in forward flight is investigated. A finite element based structural analysis including the effects of transverse shear, torsion related out-of-plane warping, and warping restraint is incorporated into the University of Maryland Advanced Rotorcraft Code (UMARC). The out-of-plane warping model is developed using a fourth order polynomial over the cross section area. The effects of restrained warping are incorporated by modifying the torsion stiffness distribution along the blade. Three soft in-plane bearingless rotor configurations, including bending-torsion structural couplings are analyzed. The analysis covered free flight propulsive trim, blade steady periodic response, and stability of the perturbed rotor-body system. Elastic pitch-lag couplings caused by the ply layup of the flexbeam have a significant effect on the vibratory response, hub loads, and aeroelastic stability of a bearingless rotor. Negative pitch-lag elastic couplings have a stabilizing effect on the regressive lag mode in hover and forward flight. The stability margin is increased by as much as 130 percent.

Aeroelastic Analysis of a Composite Bearingless Rotor in Forward Flight Using an Improved Warping Model

Anita L. Tracy and Inderjit Chopra

Journal of the American Helicopter Society
July 1995

The aeromechanical stability of a helicopter with an elastically coupled composite bearingless rotor in forward flight is investigated. A finite element based structural

analysis including the effects of transverse shear, torsion related out-of-plane warping, and warping restraint is incorporated into the University of Maryland Advanced Rotorcraft Code (UMARC). The out-of-plane warping model is developed using a fourth order polynomial over the cross section area. The effects of restrained warping are incoporated by modifying the torsional stiffness distribution along the blade. Three soft in-plane bearingless rotor configurations, including bending-torsion structural couplings are analyzed. The analysis covered free flight propulsive trim, blade steady periodic response, and stability of the perturbed rotor-body system. Elastic pitch-lag couplings caused by the ply layup of the flexbeam have a significant effect on the vibratory response, hub loads, and aeroelastic stability of a bearingless rotor. Negative pitch-lag elastic couplings have a stabilizing effect on the regressive lag mode in hover and forward flight. The stability margin is increased by as much as 250 percent.

An Analytical Model For Nonlinear Elastomeric Lag Dampers, And Its Effect On Bearingless Rotor Dynamics And Aeroelasticity

Farhan Gandhi
PhD Dissertation, 1995

An analytical model for an elastomeric lag damper is developed, as a combination of linear and nonlinear springs and dashpots. Its behavior is described in the time-domain by a nonlinear differential equation. This representation is independent of frequency- and amplitude-dependent complex modulus components (G' and G''), and can be used directly to predict damper behavior under various operating conditions such as large amplitude or multi-frequency excitations, and various equilibrium conditions. A methodology is developed for the integration of the elastomeric damper model into rotorcraft aeromechanical analyses, wherein the damper differential equation is solved simultaneously with the rotor blade flap-lag-torsion equations, with damper force appearing as an independent state. An examination of damper effects on simplified rigid blade analyses reveals that the lag mode damping is strongly dependent on the damper equilibrium condition. In forward flight, shaft-fixed stability was found to depend on both the steady as well as the periodic (cyclic) components of damper equilibrium response. If appropriate nonlinear springs are used to model degradation in damping at very small excitation amplitudes, the occurrence of limit cycle oscillations can be analytically predicted when the damper is integrated into an aeromechanically unstable rotor system.

A methodology is developed for the aeroelastic analysis of bearingless main rotor helicopters in forward flight. The large elastic twisting in the flexbeam due to pitch control is independently evaluated as the structural response to a prescribed swashplate motion (in vacuum), and its inclusion in the calculation of strain energy, results in modified nonlinear equations for aeroelastic analysis. Since the large elastic control deformations are purged from the total elastic deformations,

normal modes can be used for the aeroelastic analysis in forward flight. The present analysis has good convergence behavior in evaluation of blade periodic response.Introducing an elastomeric damper between the flexbeam and torque tube results in an increase in equilibrium lag displacement as the damper stiffness increases the lag frequency and brings it closer to resonance with the forcing frequency ($1/rev$). Using normal modes which consider elastomeric damper impedance in the calculation of blade modal matrices and load vector, results in better convergence behavior for the calculation of rotor-fuselage-damper trim (equilibrium) response. For a larger (stronger) damper, the lag mode stability decreases with increasing forward flight velocity, due to the reduced damping of the elastomer at higher amplitudes of excitation. For a smaller (weaker) damper, the lag mode stability may increase slightly at higher forward flight speeds due to increased aerodynamic damping.

Free-Wake Analysis of Tandem, Tilt-Rotor and Coaxial Rotor Configurations

Ashish Bagai and J. Gordon Leishman

Journal of the American Helicopter Society
July 1996

A free-wake model has been developed to predict the wake geometries of tandem, tilt-rotor and coaxial twin-rotor systems. The basic formulation is based on a pseudo-implicit, predictor-corrector, relaxation scheme with five-point central differencing and velocity averaging in space. Results are presented for three rotor configurations for several advance ratios ranging from relatively low speed to moderately high speed forward flight conditions. Comparisons have been made between computed and measured tip vortex geometries for the coaxial configuration, with good overall agreement.

On the Influence of Time-Varying Flow Velocity on Unsteady Aerodynamics

B.G. van der Wall and J.G. Leishmen

Journal of the American Helicopter Society, October 1994

The effects of a periodic free-stream velocity on the unsteady aerodynamics of an airfoil in incompressible flow are examined. Existing theories are reviewed, and their simplifications and limitations are properly identified. A new general aerodynamic theory for an airfoil undergoing a combination of harmonic pitching, plunging and fore-aft motion is presented. An extension to arbitrary free-stream velocity variations and arbitrary airfoil motion is also given. The theoretical results are validated against numerical predictions made by a modern Euler code.

Analysis of Pitch and Plunge Effects on Unsteady Airfoil Behavior

Joseph C. Tyler and J. Gordon Leishman

Journal of the American Helicopter Society
July 1992

An analysis was conducted into the effects of pitch versus plunge forcing on unsteady airfoil behavior. Experimental measurements of unsteady airloads were analyzed on conjunction with classical unsteady airfoil theory and a semi-empirical model for dynamic stall. The separate contributions to the unsteady airloads due to angle of attack and pitch rate are shown to be the key variables governing aerodynamic damping, the onset of leading edge separation, and dynamic stall.

Improved Wide-Field Shadowgraph Set-up for Rotor Wake Visualization

A. Bagai and J.G. Leishman

Journal of the American Helicopter Society

July 1992, pp. 86-92

The development of an improved wide-field shadowgraph set-up for rotor wake visualization is described. The improved system makes use of one or more beam splitters, and provides several significant advantages over previously used wide-field shadowgraph set-ups. The primary advantage is that the technique can be used to effectively collocate the point light source and the recording camera on the optical axis. This eliminates various optical deficiencies of previous systems, such as ghost and/or blurred images, contrast gradients, and reduced reflected light intensity at the camera optics. A secondary advantage is that the system can be arranged to permit simultaneous viewing by two separate cameras, such as a still and a video. Typical results are shown, which demonstrate the higher quality of rotor wake shadowgraphs possible with the improved set-up.

Developments in the Visualization of Rotor Wakes Using the Wide-Field Shadowgraph Method

Ashish Bagai, Erwin P. Moedersheim and J. Gordon Leishman

Journal of Flow Visualization and Image Processing, vol. 1, pp. 211-233, 1993

Some techniques are discussed that aid in the flow visualization of rotor tip vortices using wide-field shadowgraphy. The use of a beam splitter is shown to provide a

particularly important enhancement to the method when large fields or angles of view are required. The optical characteristics of the stobe, observation screen, and recording film are also shown to be important for maximizing the shadowgraph contrast. Finally, theoretical predictions of the shadowgraph contrast for a series of compressible vortices are compared to experimental contrast results with a view to estimating the general velocity profile, viscous core radius, and viscous diffusion rate of the tip vortices.

Measurements of Rotor Tip Vortices Using Three-Component Laser Doppler Velocimetry

J. Gordon Leishman, Andrew Baker and Alan Coyne

Journal of the American Helicopter Society
October 1996

Phase-resolved laser Doppler measurements were made of the three-dimensional velocity field and tip vortex structure in the wake of a hovering rotor. A one-bladed rotor was used to generate a single and nominally helical shaped vortex filament in the rotor flow field. The measurements were analyzed to establish the detailed structure of the tip vortex, such as the tangential and axial velocity profiles, circulation profiles, and viscous core growth with vortex age.

Flow Visualization of Compressible Vortex Structures using Density Gradient Techniques

Ashish Bagai and J. Gordon Leishman

Experiments in Fluids 15, 431-442 (1993)

Mathematical results are derived for the schlieren and shadowgraph contrast variation due to the refraction of light rays passing through two-dimensional compressible vortices with viscous cores. Both standard and small-disturbance solutions are obtained. It is shown that schlieren and shadowgraph produce substantially different contrast profiles. Further, the shadowgraph contrast variation is shown to be very sensitive to the vortex velocity profile and is also dependent on the location of the peak peripheral velocity (viscous core radius). The computed results are compared to actual contrast measurements made for rotor tip vortices using the shadowgraph flow visualization technique. The work helps to clarify the relationships between the observed contrast and the structure of vortical structures in density gradient based flow visualization experiments.

Rotor Free-Wake Modeling using a Pseudo-Implicit Technique - Including Comparisons with Experimental Data

Ashish Bagai and J. Gordon Leishman

Journal of the American Helicopter Society
July 1995

A pseudo-implicit predictor-corrector method with five-point central differencing in space has been developed for the solution of the governing differential equations of the rotor free-wake problem. It is shown that a relaxation implementation of this method exhibits good convergence characteristics for the rotor tip vortex locations. The method is also generalized to allow unequal azimuth and trailed vortex segment angles, which for some applications, help retain the fidelity of the results, while keeping computational requirements to a minimum. The results are compared with experimental measurements of the rotor tip vortex geometries and flow field velocities in hover and forward flight with good agreement.

Rotor Free-Wake Modeling Using a Pseudoimplicit Relaxation Algorithm

Ashish Bagai and J. Gordon Leishman

Journal of Aircraft, Vol. 32, No. 6, November-December 1995

A pseudoimplicit predictor-corrector relaxation algorithm with five-point central differencing in space has been developed for the solution of the governing differential equations of the helicopter rotor free-wake problem. This new approach is compared and contrasted with more conventional explicit-type free-wake algorithms. A convergence analysis shows that the new algorithm provides for much more rapid convergence characteristics compared to explicit methods, with improvements in numerical efficiency and predictive accuracy.

Parametric Studies for Tiltrotor Aeroelastic Stability in Highspeed Flight

Mark W. Nixon

Journal of the American Helicopter Society
October 1993

The influence of several system design parameters on tiltrotor aeroelastic stability is examined for the high-speed (axial) flight mode. The results are based on a math model in which the wing is assumed to be cantilevered and is represented by beam finite elements having vertical bending, chordwise bending and torsional degrees of freedom. A quasi-steady aerodynamic model is used for both the wing and rotor

system. Coupling of the rotor flapping modes with the wing elastic modes produces a whirl motion, typical of tiltrotors, that can become unstable at high speeds. The sensitivity of this instability with respect to rotor frequencies, wing stiffnesses and forward wing sweep is examined. Some important new trends are identified regarding the role of blade lag dynamics and forward wing sweep in tiltrotor aeroelastic stability. Two important conclusions based on these trend studies are that the blade lag frequency may be tuned to improve tiltrotor stability, and forward wing sweep is destabilizing because of changes in rotor force components associated with the sweep.

Delamination of Ply-Drop Configurations

J.C. Fish and A.J. Vizzini

Composite Materials: Testing and Design---Eleventh Volume,
ASTM STP 1206,
E.T. Camponeschi, Jr., Ed.
American Society for Testing and Materials, Philadelphia, PA 1993,
pp. 323-332

Unidirectional glass/epoxy tapered specimens were manufactured and tested under static tension and tension-tension fatigue. Four different ply-dropped configurations are studied with either grouped or dispersed plies and either staircased or overlapped dropped plies. At damage events in the static tests and at prescribed numbers of cycles in the fatigue tests, the specimens were placed in a cantilever fixture to determine their bending stiffnesses. The static tests indicated that the staircased-grouped and dispersed-overlapped specimens exhibited preferred structural performance by retaining their bending stiffness up to failure. The dispersed-overlapped specimen exhibited stable delamination growth. In addition, the fatigue tests indicated slow growth in the dispersed-overlapped with corresponding losses in the bending stiffness.

Influence of Realistic Ply-Drop Geometries on Interlaminar Stresses in Tapered Laminates

A.J. Vizzini

Composite Materials: Fatigue and Fracture---Fifth Volume
ASTM STP 1230
R.H. Martin, Ed.
American Society for Testing and Materials, Philadelphia, PA, 1995
pp. 467-485

A finite element model of a tapered specimen was developed that incorporates naturally occurring realistic geometries such as ill-formed resin pockets, unsymmetric and offset ply-drop locations, varying ply thickness, and voids. Parametric studies were performed to determine the effects of these geometries, which occur naturally in a manufactured specimen. Ill-formed resin pockets increase the effective taper angle at the ply drop and cause a corresponding increase in the interlaminar stresses. In addition, the onset of damage location is dependent on the geometry of the ill-formed pocket. The effect of ply drops occurring unsymmetrically about the midplane is significant for offset values that occur as a result of the manufacturing process. Again the location for damage onset is dependent on the amount of the offset of the resin pocket. Voids or fracture within the resin pockets significantly increase the interlaminar stress at the ply drop and thus decrease the damage onset load within the tapered element.

Tapered Geometries for Improved Crashworthiness under Side Loads

D.C. Fleming and A.J. Vizzini

Journal of the American Helicopter Society
Vol. 38, No. 1, January 1993, pp. 38-44

Truncated cones of varying degrees of taper are manufactured from unidirectional AS4/3501--6 graphite/epoxy preimpregnated tape and are loaded in compression. Different amounts of side loads are introduced by orienting the loading axis away from the central axis of the cone. The energy absorption properties of the cones are measured under quasi-static conditions. The failure modes are determined around the circumference as a function of the loading and taper angles, and the energy absorbency is correlated to the observed failure modes. Constant cross-section specimens suffer significant losses in energy absorption in the presence of side loads; however, tapered specimens are less sensitive and do not suffer such significant losses. In fact tapered geometries provide greater energy absorption than constant cross-section geometries at moderate levels of side loads.

Damage Analysis of Composite Tapered Beams

A.J. Vizzini and S.W. Lee

Journal of the American Helicopter Society
Vol. 40, No. 2, April 1995, pp. 43-49

The stress state and the resulting failure mechanisms of composite tapered components are investigated. Finite-element modeling and experimental evidence summarized from previous and present efforts are used to determine the location of the damage initiation, the interaction between the free edge and the taper discontinuities, the effect of realistic geometries, the extent and mode of damage growth, and the ability of simple physical models to explain the occurrence of the interlaminar stress state.

Bonded Repair of Minimum-Gage Composite Sandwich Structures

J. H. Ruddy and A. J. Vizzini

Journal of the American Helicopter Society,
Vol.41, No.3, July 1996, pp.232-238

The bonded repair of minimum-gage sandwich structures is investigated both experimentally and analytically. The experimental study focuses on the amount of strength recovery and failure mode of repairs with various numbers of plies in the patch. A three-dimensional finite element model was developed to determine the stress and strain states in the patch, adhesive layer, and face sheets. The repair is modeled on a ply-by-ply basis and includes resin-rich areas between the patch plies, and adhesive pockets at the ply drop locations. The model is correlated with experimental data and a phenomenological failure model is developed that predicts the onset of damage and the failure mode.

Off-Axis Energy Absorption Characterization of Composites for Crashworthy Rotorcraft Design

D. C. Fleming and A. J. Vizzini

Journal of the American Helicopter Society,
Vol.41, No.3, July 1996, pp. 239-246

The characterization of the off-axis crushing of composite materials is investigated experimentally and analytically. A fixture for crushing plate specimens against an adjustable inclined plane is reviewed. A phenomenological finite element model is

developed based upon results from tests of flat plate specimens crushed in the fixture. The model is based upon quasistatic crack growth along ply interfaces, and results in a one-parameter representation to predict the failure mode for a given crushing angle; however, no quantitative performance estimation is provided by the model. The model and the experimental results combine to produce a hybrid model whereby the crushing performance may be predicted for a given loading condition.

The Effect of Ply-Drop Configuration on the Delamination Strength of Tapered Composite Structures

A. D. Botting, A. J. Vizzini, and S. W. Lee

AIAA Journal
Vol. 34, No. 8, August 1996, pp.1650-1656

Delamination suppression by altering the sequence of ply drops is evaluated for tapered glass/epoxy laminates. Two different stacking sequences with thin section layups of [04/452]S and [452/04]S containing drops of three sets of 45 plies are investigated. A finite element model using three-dimensional solid elements is constructed to evaluate the state of interlaminar stress in and around the ply drops. The effect of the stress-free edge is considered by providing a mesh refinement near the free edge. Tapered specimens are manufactured and tested under quasistatic uniaxial tension. For specimens of [04/452]S stacking sequence, delamination strength is dependent on the ply drop sequence; and structural tailoring of the ply drop region results in a reduced interlaminar stress state and an associated increase in delamination strength. Structural tailoring, however, appears to be ineffective in the [452/04]S specimens. The measured delamination strengths are insensitive to the ply drop sequence, although the finite element model indicates a stronger sensitivity. In general, the finite element model correlates well with the data. The measured differences in strength among the [04/452]S specimens and the overall strength difference between the [04/452]S and the [452/04]S specimens are predicted by the finite element model using strength criteria on the stress state in the interply resin region.

The Energy Absorption of Composite Plates under Off-Axis Loads

D. C. Fleming and A. J. Vizzini

Journal of Composite Materials
Vol.30, No. 18, 1996, pp.1977-1995

Graphite/epoxy plates are crushed against an adjustable inclined plane surface and the energy absorbency is measured. The plates are stabilized in a testing fixture that

provides a simply-supported boundary condition on the sides of the specimen to prevent global buckling. Consistent test data is obtained that are similar to those obtained using different specimen geometries, indicating the acceptability of the test method. Under multiaxial loads, the energy absorbency of a specimen is dependent upon the failure mode experienced, but not directly on the orientation of the applied load. However, which failure mode occurs depends on the load orientation.

Shear-Lag Analysis about an Internally-Dropped Ply

A. J. Vizzini

to appear in *Journal of Reinforced Plastics and Composites.*

The region around a terminated ply is modeled as several elastic layers separated by shear regions. A shear-lag analysis is then performed allowing for the thickness of the elastic and shear layers to vary. Boundary conditions, away from the ply drop, are based on the deflections determined by a finite element model. The interlaminar stresses are compared against those generated by the finite element model for tapered laminates under pure extension, pure bending, and extension-bending coupling. The shear-lag analysis predicts the interlaminar shear at and near the ply drop for pure extension and in cases involving bending if the deflections due to bending are removed. The interlaminar shear stress and force equilibrium are used to determine the interlaminar normal stress. The trends in the interlaminar normal stress shown by the finite element model are partially captured by the shear-lag analysis. This simple analysis indicates that the mechanism for load transfer about a ply drop is primarily due to shear transfer through the resin rich areas.

Correlation of Energy Absorption of Composite Tubes and Plates

D. D. Dubey and A. J. Vizzini

reviewed by *Journal of Composite Materials,* January 1997.

A total of 28 graphite/epoxy flat-plate specimens and six graphite/epoxy tube specimens were crushed under quasi-static conditions to provide a basis for comparison of the measured energy absorbency of these two geometries. The energy absorbency of each specimen was measured, and the specific sustained crushing stress (SSCS) was determined. All plate and tube specimens were manufactured from AS4/3501-6 graphite/epoxy with the same layup and thickness, thus providing a common laminate for comparison. Flat-plate specimens of two different widths were tested to determine the effect of the testing fixture on the observed energy absorbency. The flat-plate results indicate that the specific energy absorbency per unit thickness is nearly independent of the specimen width, with a small contribution to the energy absorbency by the testing fixture. However, this calculated value of

measured energy absorption due to the test fixture is within the scatter of the data. The results also indicate that specimen geometry affects specimen stability and therefore the failure modes exhibited by the specimen during crushing. Similar failure modes were observed in the tube and flat-plate specimens with the flat-plates absorbing 12% less energy per unit mass. Consequently, flat-plate specimens can be used as a lower-cost alternative to tube specimens or in test programs requiring simpler geometries.

Structural Integrity of Composite Flexbeams

A. J. Vizzini and S. W. Lee

Proceedings of the American Helicopter Society 49th Annual Forum and Technology Display, St. Louis, MO, May 1993, pp.103-114

The structural integrity of composite tapered components is investigated. Several uncertainties within the research community are discussed. Finite element modeling and experimental evidence summarized from previous and present efforts are correlated to determine the location of the damage initiation, the interaction between the free edge and the taper discontinuities, the effect of realistic geometries, the extent and mode of damage growth, and the ability of simple physical models to explain the occurrence of the interlaminar stress state.

The Energy Absorption of Composite Plates under Combined Loads

D. C. Fleming and A. J. Vizzini

Proceedings of the American Society for Composites Eighth Technical Conference on Composite Materials, October 1993, Cleveland, OH, pp.650-659

Graphite/epoxy plates are crushed against an adjustable inclined plane surface and the energy absorbency is measured. The plates are stabilized in a testing fixture which provided a simply-supported boundary condition on the sides of the specimen to prevent global buckling. The failure modes observed are similar to failure modes obtained in previous research, indicating the acceptability of the test method. The energy absorbency of a specimen is dependent upon the failure mode experienced, but not directly on the load inclination angle. However, which failure mode occurs is dependent upon the load inclination angle.

Energy Absorption of Truncated Kevlar/Epoxy Cones under Side Loads

J. Knack and A. J. Vizzini

Proceedings of the AIAA/ASME/ASCE/AHS/ASC 35th Structures, Structural Dynamics and Materials Conference, Hilton Head, SC, April 1994, pp.2831-2837

A total of 27 Kevlar/epoxy truncated cones were manufactured and crushed under various angles of load inclination. Side loads were introduced by cutting the cones at angles relative to their central axes. The failure modes were observed and the specific sustained crushing stresses were determined and compared against graphite/epoxy cones of the same layup and similar geometry. The Kevlar/epoxy cones exhibited significantly different failure modes than the graphite/epoxy cones. Specifically, the cones did not experience brittle fracture, and thus maintained structural integrity after crushing. The role of specimen taper and load inclination is different than that for graphite/epoxy cones. In particular, 10 tapered cones overall had the best performance even under uniaxial loading conditions.

Failure of Sandwich to Laminate Tapered Composite Structures

S. K. Kuczma and A. J. Vizzini

Proceedings of the AIAA/ASME/ASCE/AHS/ASC 36th Structures, Structural Dynamics and Materials Conference, New Orleans, LA, April 1995, AIAA 95-1389

Failure modes and load distributions in tapered, minimum-gage composite sandwich structures are investigated. A total of 38 unidirectional graphite epoxy / Rohacell foam core structures were manufactured with varying taper angles and core thicknesses. The specimens were subjected to tensile, compressive, and bending loads. Experimental data is correlated with a three-dimensional finite-element model developed to determine the stress and strain state within a tapered sandwich structure. Emphasis is placed on the root of the taper where experimental observations suggest damage initiation. Nonlinearities result in significant load redistribution.

Bonded Repair of Sandwich Structures

J. H. Ruddy and A. J. Vizzini

Proceedings of the American Helicopter Society 51st Annual Forum and Technology Display, Ft Worth, TX, May 1995, pp.1604-1615

The bonded repair of minimum-gage sandwich structures is investigated both experimentally and analytically. The experimental study focuses on the amount of strength recovery and failure mode of repairs with various numbers of plies in the patch. A three-dimensional finite element model was developed to determine the stress and strain states in the patch, adhesive layer, and facesheets. The repair is modeled on a ply by ply basis and includes resin-rich areas between the patch plies and adhesive pockets at the ply drop locations. The model is correlated with experimental data and a phenomenological failure model is developed that predicts the onset of damage and the failure mode.

Shear-Lag Analysis about an Internally-Dropped Ply

A. J. Vizzini

Proceedings of the American Society for Composites Tenth Technical Conference on Composite Materials, Santa Monica, CA, October 1995, pp. 473-482

The region around a terminated ply is modeled as several elastic layers separated by shear regions. A shear-lag analysis is then performed allowing for the thickness of the elastic and shear layers to vary. Boundary conditions, away for the ply drop, are based on the deflections determined by a finite element model. The interlaminar stresses are compared against those generated by the finite element model for tapered laminates under pure extension, pure bending, and extension-bending coupling. The shear-lag analysis predicts the interlaminar shear at and near the ply drop for pure extension and in cases involving bending if the deflections due to bending are removed. The interlaminar shear stress and force equilibrium are used to determine the interlaminar normal stress. The trends in the interlaminar normal stress shown by the finite element model are partially captured by the shear-lag analysis. This simple analysis indicates that the mechanism for load transfer about a ply drop is primarily due to shear transfer through the resin rich areas.

Off-Axis Absorption Characterization of Composites for Crashworthy Rotorcraft Design

D. C. Fleming and A. J. Vizzini

Proceedings of the AHS Technical Specialists' Meeting, Williamsburg, VA, October 1995

The characterization of the off-axis crushing of composite materials is investigated experimentally and analytically. A fixture for crushing plate specimens against an adjustable inclined plane is reviewed. A phenomenological finite element model is developed based upon results from the flat plate crushing fixture. The model is based upon quasistatic crack growth along ply interfaces, and results in a one-parameter representation to predict the failure mode for a given crushing angle; however, no quantitative performance estimation is provided by the model. The model and the experimental results combine to produce a hybrid model whereby the crushing performance may be predicted for a given loading condition.

Energy Absorption of Composite Tubes and Plates

D. D. Dubey and A. J. Vizzini

Proceedings of the AIAA/ASME/ASCE/AHS/ASC 37th Structures, Structural Dynamics and Materials Conference, Salt Lake City, Utah, April 1996, pp. 419-426

A total of 14 flat-plate specimens and 6 tubes were crushed under quasi-static conditions. The energy absorbency of each specimen was measured resulting in a value of the specific sustained crushing stress (SSCS). The plates and tubes were all manufactured from AS4/3501-6 graphite/epoxy and had the same layup providing a common laminate for comparison. In addition, the data were also compared with existing data from flat-plate and truncated-cone specimens. Two different widths of flat plates were tested to determine the effect of the end conditions of the testing fixture on the observed energy absorbency. The flat-plate results indicate that the energy absorbency per unit width is independent of the specimen width indicating no significant contribution to the energy absorbency by the edges of the testing fixture. Furthermore, the results indicate that the tube geometry provides a higher amount of energy absorbency, although the values are comparable to the results of the flat-plate specimens.

Frequency Domain System Identification of Helicopter Blades with Trailing Edge Flaps

Sunghwan Hwang
Norman M. Wereley

Citation: Presented at the AIAA/ASME Adaptive Structures Forum, 18-19 April, 1996, Salt Lake City, UT. Paper No. AIAA-96-1271

In forward flight, the dynamics of a rigid flapping rotor blade, with and without a trailing edge flap, are represented by an ordinary differential equation with periodically time varying coefficients. Existing frequency domain system identification techniques were developed only for linear time invariant systems. A linear time periodic system, such as the rigid helicopter blade with a piezo-actuated flap, cannot be identified using these existing linear time invariant techniques, because the sinusoidal test input signal is not appropriate for linear time periodic systems. Thus, a new frequency domain system identification methodology for linear time periodic systems is introduced. The linear time periodic system identification theory is based on a new test input signal, which is the Fourier series of a periodic signal modulated by a sinusoid. Applying what is essentially harmonic balance, a linear time periodic state space model in the time domain can be transformed to an infinite dimensional linear time invariant harmonic balance state space model. In addition, the harmonic state space model leads to the concept of a harmonic transfer function in the frequency domain. A spectral theory for linear time periodic systems, which is analogous to that for linear time invariant systems, is then developed using a sinusoidally modulated complex Fourier series expansion, and is advantageous because it leads to a Fourier transformation that reproduces the harmonic balance state space model. The flapping helicopter blade model contains several parameters that may not be certain *a priori*, for example, the Lock number, and advance ratio. A procedure is developed to identify these uncertain parameters when the structure of the underlying helicopter dynamics is well understood. The system identification and parameter optimization procedures are validated using computer models of a helicopter rigid blade flapping in forward flight.

Frequency Domain System Identification of Helicopter Rotor Dynamics Incorporating Models with Time Periodic Coefficients

Sunghwan Hwang

Citation: Ph. D Thesis, Department of Aerospace Engineering, University of Maryland at College Park, January 1997

One of the most prominent features of helicopter rotor dynamics in forward flight is the periodic coefficients in the equations of motion introduced by the rotor rotation. The frequency response characteristics of such a linear time periodic system exhibits sideband behavior, which is not the case for linear time invariant systems. Therefore, a frequency domain identification methodology for linear systems with time periodic coefficients was developed, because the linear time invariant theory cannot account for sideband behavior.

The modulated complex Fourier series was introduced to eliminate the smearing effect of Fourier series expansions of exponentially modulated periodic signals. A system identification theory was then developed using modulated complex Fourier series expansion. Correlation and spectral density functions were derived using the modulated complex Fourier series expansion for linear time periodic systems. Expressions of the identified harmonic transfer function were then formulated using the spectral density functions both with and without additive noise processes at input and/or output. A procedure was developed to identify parameters of a model to match the frequency response characteristics between measured and estimated harmonic transfer functions by minimizing an objective function defined in term of the trace of the squared frequency response error matrix. Feasibility was demonstrated by the identification of the harmonic transfer function and parameters for helicopter rigid blade flapping dynamics in forward flight. This technique is envisioned to satisfy the needs of system identification in the rotating frame, especially in the context of individual blade control. The technique was applied to the coupled flap-lag-inflow dynamics of a rigid blade excited by an active pitch link. The linear time periodic technique results were compared with the linear time invariant technique results. Also, the effect of noise processes and initial parameter guess on the identification procedure were investigated. To study the effect of elastic modes, a rigid blade with a trailing edge flap excited by a smart actuator was selected and system parameters were successfully identified, but with some expense of computational storage and time.

Conclusively, the linear time periodic technique substantially improved the identified parameter accuracy compared to the linear time invariant technique. Also, the linear time periodic technique was robust to noises and initial guess of parameters. However, an elastic mode of higher frequency relative to the system

pumping frequency tends to increase the computer storage requirement and computing time.

Modeling the Damping Mechanism in Electro-rheological Fluid-based Dampers

Gopalakrishna M. Kamath, Graduate Research Assistant
Norman M. Wereley, Assistant Professor

M3DIII: Mechanics and Mechanisms of Material Damping, American Society of Testing and Materials, ASTM STP 1304, A. Wolfenden and V.K. Kinra, Eds., American Society for Testing and Materials, 1997, pp. 331-348.

Electro-rheological (ER) material behavior exhibits a transition from viscoelastic properties in the pre-yield region to viscous properties in the post-yield region. A nonlinear dynamic model based on linear shear flow mechanisms is proposed to describe ER fluid behavior. The nonlinear model combines a 3-parameter fluid element and a viscous (dashpot) element using sigmoidal weighting functions. The weighting functions are dependent on the strain rate and serve to enforce the transition between the viscoelastic and the viscous characteristics. The model is then extended to characterize a damper based on ER fluids. An SDOF system incorporating an ER fluid damper is considered and its dynamics studied via numerical simulations. The results of the simulations show that, as the applied electric field is increased, a significant attenuation in the amplitude can be achieved, while the response changes significantly. A system identification methodology is suggested to determine the model parameters from simple vibration experiments. An important issue of the amplitude dependence of the material behavior is addressed and modifications to the model suggested so as to incorporate these effects.

Transient Analysis for Damping Identification in Rotating Composite Beams with Integral Damping Layers

Clifford B. Smith, Graduate Research Assistant
Norman M. Wereley, Assistant Professor

Smart Structures Laboratory, Alfred Gessow Rotorcraft Center,
Department of Aerospace Engineering
Smart Materials and Structures, Vol. 5, No. 5, October 1996, pp 540-550.

The first objective is to evaluate the performance of damping identification algorithms. The second objective is to determine the feasibility of damping augmentation in rotating composite beams via passive constrained layer damping (PCLD). Damping identification schemes were applied to four rectangular cross-section laminated composite beams with cocured integral damping layers over the

span of the beam. The cocured beam consisted of a twenty ply balanced and symmetric cross-ply Gr/Ep composite host structure, a top and bottom damping layer of viscoelastic material (VEM), and a 2 ply Gr/Ep constraining layer sandwiching the viscoelastic material to the host structure. Four VEM thicknesses were considered: 0, 5, 10, and 15 mils. The cantilevered beams were tested at rotational speeds ranging from 0 to 900 RPM in a vacuum chamber. Excitation in bending was provided using piezo actuators, and the bending response was measured using full strain gage bridges. Transient data was analyzed using logarithmic decrement, a new Hilbert transform technique, and an FFT-based moving block analysis. When compared to the beam with no VEM, a 19.2% volume fraction (15 mil layer) of viscoelastic in the beam produced a 400% increase in damping ratio in the non-rotating case, while at 900 RPM, the damping ratio increased only 360%. Overall structural damping was reduced as a function of RPM, due to centrifugal stiffening.

Analysis and Testing of Bingham Plastic Behavior in Semi-Active Electrorheological Fluid Dampers

Gopalakrishna M. Kamath, Graduate Research Assistant
Melanie K. Hurt, Graduate Research Assistant
Norman M. Wereley, Assistant Professor

Smart Materials and Structures, Vol. 5, No. 5, October 1996, pp 576-590.

Electrorheological (ER) fluid-based dashpot dampers have smart capabilities because ER fluids undergo large changes in yield stress as electric field is applied. Our objective is the development and experimental validation of quasi-steady dashpot damper models, based on an idealized nonlinear Bingham plastic shear flow mechanism, for purposes of preliminary design and performance predictions. The data required for the Bingham plastic model is normally supplied by ER fluid suppliers, that is, plastic viscosity and dynamic yield stress as a function of applied field, as determined from a shear stress versus shear strain rate diagram. As force is applied to the dashpot damper, the ER fluid flows through an annulus between the concentric inner and outer electrodes. The idealized Bingham plastic shear flow mechanism predicts that three annular flow regions develop as a function of the local shear stress. In the central pre-yield or plug region, the local shear stress is less than the dynamic yield stress, so that the plug behaves like a rigid solid. The remaining two annular regions, adjacent to the electrodes, are in the post-yield condition and correspond to the shear stress exceeding the dynamic yield stress, so that the material flows. Equivalent viscous damping performance of an ER fluid dashpot damper is strongly coupled with the plug behavior. For a constant force, as the applied field increases, so does the plug thickness and equivalent viscous damping. For a constant applied field, as the force increases, the plug thickness and equivalent viscous damping both decrease. The passive and active or field

dependent damping behavior of an ER fluid-based dashpot damper can be designed for a specific application using these quasi-steady Bingham plastic models.